Electrochemical Studies of Coating Degradation

A.T.A. Jenkins

Thesis submitted to the University of Newcastle upon Tyne for
the degree of Doctor of Philosophy

October 1995

Abstract

The polymer coatings considered in this thesis work principally by creating a barrier, in order to prevent a corroding medium such as water and / or oxygen from contacting the surface of the underlying metal. Such coatings are subject to attack from the environment in which they are placed. This attack can lead to failure of the coating and corrosion of the underlying metal.

In this thesis, three principle means of coating degradation, leading to subsequent corrosion of the substrate have been considered: Mechanical damage of the coating, the effect of ultra-violet light weathering and filiform corrosion. Electrochemical measurements have been made in order to attempt to quantify both the degree of coating breakdown and the extent of corrosion of the substrate.

The principle method for measuring coating breakdown and substrate corrosion utilised in the work for this thesis was Electrochemical Impedance Spectroscopy (EIS). EIS, in principle, allows both changes in coating porosity resulting from coating breakdown, and the extent of corrosion of the substrate to be measured.

The extent of delamination under polymer coatings on defects of different sizes and on different substrates has been measured. The effect of ultra-violet light weathering of polymer coatings was measured using EIS and correlated with measurements of light reflection of the coating. Filiform corrosion was induced on two different substrates, coated with various coatings. The effect of substrate and coating on filiform corrosion growth rate and mechanism has been considered.

To Angela and my Family

Preface

The work reported in this thesis was carried out between October 1992 and September 1995 in the Department of Chemistry, University of Newcastle upon Tyne and at International Paints, Stoneygate Lane Felling under the supervision of Prof. R.D. Armstrong and Dr. B.W. Johnson. No part of this work has previously been submitted for a degree at this, or any other University.

Extracts from this work have been reported in *Corrosion Science,* **37**, 1615, (1995), *Corrosion Science* (accepted for publication, November 1995), in the *Proceedings of the Conference on Corrosion Prevention by Organic Coatings,* Cambridge 1994. and *J. Applied Electrochem.* (in press). Results have been presented at the Cambridge Conference on *Corrosion Prevention by Organic Coatings,* September 1994 and at Trondheim Institute of Technology, Norway in December 1994.

Acknowledgements

I would like to thank my supervisor, Prof. Ron Armstrong for his guidance and help over the last three years and for making the work for my Ph.D. enjoyable. In addition I would like to thank Dr. Brian Johnson of International Paints who has helped with access to materials, and training on specialised equipment. Also for his moral support and the odd pint of beer! Also Courtaulds Coatings Ltd. for sponsoring the project and the U.K. tax payer for paying for most of it.

Various members of my group, both past and present have all contributed to the Ph.D. 'experience': Lee, Hazel, Mark, Dale, Wang, Vicky, Bill, Angela, Steffi, On, Caroline, Gareth, Martin and Simon (Mr. C.).

I would also like to thank the following members of the department for their technical support and help: Lance and Martin in electronics, George the electrical chap, Roland, Bruce, Alan and Gary in the mechanical workshops, John the Glassblower, Doug and Peter Oakes.

I would also like to thank Dr. Ben Horrocks for proof reading this thesis for me.

I am especially grateful to my family for their support, Mum, Dad, Daniel, Sarah and Katie, for their support of the many years now have been a student, and trying to show interest in my work!

Last of all, I would like to thank Angela, my fiancée for putting up with me as I wrote this thesis, and her love and encouragement over the last few years.

' What is the use of a book,' thought Alice, 'without pictures or conversations?' [1]

---

[1] Lewis Carroll, *Alice in Wonderland*, Ch. 1.

Nomenclature

E^o	Standard Potential
$E_{corr,}$ E_c	Corrosion Potential
ΔE	AC Potential Amplitude Maximum
Δi	AC Current Amplitude Maximum
$i_{corr,}$ i_c, I_{corr}	Corrosion Current
i_L	Diffusion Limited Current
ΔE / Δi	Polarisation Resistance
R_p	Polarisation Resistance
R_{ct}	Charge Transfer Resistance
R_{cto}	Bare Electrode Charge Transfer Resistance
R_u, R_Ω	Electrolyte Resistance
R_b	Bulk (Coating) Resistance
R_{bt}	Theoretical Bulk Resistance
R_{ox}	Oxide Film Resistance
Z	Impedance
Z'	Real Component of Impedance
Z''	Imaginary Component of Impedance
C	Capacitance
C_{dl}	Double Layer Capacitance
C_{dlo}	Double Layer Capacitance of Bare Electrode
C_{ox}	Oxide Film Capacitance
C_g	Geometric (Coating) Capacitance
q	Charge
t	Time
ε_o	Permitivity of Free Space
ε_r	Dielectric Constant
j	$\sqrt{}$ -1
ϕ	Phase Difference Between Current and Potential
f	frequency
ρ	Restivity of Electrolyte
κ	Conductivity of Electrolyte
D	Diffusion Coefficient
SHE	Standard Hydrogen Reference Electrode
SCE	Saturated Calomel Reference Electrode
R	Gas Constant *or* Resistance

F	Faraday's Constant
n	Number of Electrons Involved in Overall Electrode Reaction
A	Electrode Area
a_{ox}	Activity of Oxidised Species
a_{red}	Activity of reduced Species
α_a , α_c	Transfer Coefficient (Anodic and Cathodic)
β_a , β_c	Tafel Gradients (Anodic and Cathodic)
N	Number of Pores (in a coating)
a	Average Area of Pore
d	Thickness of Coating
$P(O_2)$	Pressure of Oxygen
T	Temperature / K

Contents

Chapter 3: Measurements of Mechanically Damaged Coatings

Chapter 1

1.1 Introduction

In this chapter there are two principle sections. First, the mechanism of corrosion control of metals is considered. Secondly, the specific corrosion problems looked at in this thesis, of underfilm corrosion caused by coating degradation from mechanical damage, UV light and filiform corrosion are considered together with the instrumentation used to analyse corrosion.

1.2 Corrosion

In this section, references have been taken from Shrier [1], Wranglen [2], Fontana [3], Scully [4], Evans [5].

1.2.1 Definition

Definitions of corrosion are various. Some authorities [6] regard metallic corrosion as the interaction between a metal and its environment regardless of whether this interaction is detrimental to the metal, or not. This is a rather broad definition, a more specific definition based on the detrimental effects of the metals interaction with its environment is given by the Corrosion Education Manual of the European Federation of Corrosion [7]:

" Corrosion: Attack on a material by the environment with a consequential deterioration in properties. When no reference is made to the material it is normally understood that a metal is involved, and that the valency of the metal is increased; an exception is the dissolution of a metal in a liquid metal or a fused salt. The term corrosion may refer either to the process or the damage caused. Implicit in the concept of corrosion as a process is the rate per unit area of the corrosion reaction; implicit in the damage caused is the extent and nature of the damage in relation to the function of the component concerned ".

This definition regards corrosion as a chemical process, and excludes mechanical degradation of the metal such as wear, abrasion and erosion. The term corrosion is becoming more extensive than just referring to metals. The reactions of glasses, polymeric solids, ionic solids and composites as well as metals have been considered as corrosion processes.

Corrosion can proceed at various rates, dependent on the nature of the corroding material and its environment. An example of rapid corrosion is the almost complete destruction of a 18/8 stainless steel pipeline carrying 1% mineral acids at 100°C, where the pipe thickness decreased from 4.5 mm to almost zero in the space of just a year [2]. In contrast is the wrought iron pillar in Delphi, India that has stood for the last 1600 years [2].

1.3 Cost of Corrosion

The cost of corrosion to industry, and therefore most of society is enormous. It has been estimated that the U.S. Airforce spends $6 billion a year on corrosion prevention and treatment of their aircraft [8]. It is estimated that the annual cost of corrosion in the US is between $8 billion and $126 billion dollars [3]. In fact the cost may be higher still due to the secondary costs of industrial plant damage and damage from pipeline failure *etc.*

Corrosion, in addition causes a depletion of natural resources by causing the need for frequent renewal of manufactured materials - for example cars, pipelines *etc.* This then leads to greater energy consumption and hence greater pollution.

1.4 Thermodynamics of Corrosion

1.4.1 Introduction

Thermodynamics can tell us which metals will corrode under particular conditions. In addition thermodynamics will give information on the potentials and pH where metals are immune to corrosion, where they will form a passive oxide film and where they will corrode.

Corrosion takes place because the metal in its unoxidised pure state is less thermodynamically stable than its oxide or its metal ions in solution. Most metals are extracted from the earth in their oxidised form - for example iron, aluminium and only by a process of reduction are converted to the metallic elements.

The tendency of a metal to oxidise to the corresponding metal ions *i.e.* to lose electrons is given by its electrode potential, E°. E° is obtained by measuring the potential of an oxidation/reduction reaction versus a reference electrode, which is itself related to the Standard Hydrogen Electrode (SHE), arbitrarily given the potential 0.00V.

A corrosion reaction is the product of two separate reactions, the oxidation or *anodic* dissolution of the metal, and the reduction of another species the *cathodic* reaction.

For example, corrosion of iron in deaerated acid:

$$Fe + 2H^+ \rightarrow Fe^{2+} + H_2$$

$$Fe \rightarrow Fe^{2+} + 2e^- \qquad \textit{Anodic reaction}$$

$$2H^+ + 2e^- \rightarrow H_2 \qquad \textit{Cathodic reaction}$$

For a reaction to proceed, the E° value of the cathodic reaction must be more positive than the E° value of the anodic reaction. The following table shows the Standard Electrode Potentials of some metals in 1 mol dm^{-3} H^+ at 25° C.

	E° vs. SHE
$Ag = Ag^+ + e^-$	$E^\circ = 0.8$ V
$Cu = Cu^{2+} + 2e^-$	$E^\circ = 0.34$ V
$\frac{1}{2}H_2 = H^+ + e^-$	$E^\circ = 0.00$ V
$Ni = Ni^{2+} + 2e^-$	$E^\circ = -0.25$ V
$Fe = Fe^{2+} + 2e^-$	$E^\circ = -0.44$ V
$Al = Al^{3+} + 3e^-$	$E^\circ = -1.67$ V

Since silver and copper are positive (noble) of H_2/H^+ they will not dissolve in deaerated 1M acid, while nickel and iron and bare aluminium all will, as they have a more negative E° than H_2/H^+. In summary, a metal has to be able to supply electrons to the species oxidising it in order to react. Thermodynamics gives no information on the rate of reaction. Aluminium will react relatively slowly as it is covered with an oxide film (Al_2O_3).

1.4.2 The Nernst Equation

The Nernst equation describes how electrode or cell potentials depend on the activities of the species involved. The reaction potential values given in the previous table are only correct for unit activities of the ions.

Metal Dissolution

The metal dissolution reaction potential can vary with change in the activity (concentration) of the dissolved cation. This can happen where the dissolved cation diffuses slowly away from the surface or the reaction takes place in a limited volume of electrolyte. The change in potential of the anodic metal dissolution reaction is given by:

$$E = E^o + \frac{2.3RT}{nF}\log(a_{M^{n+}}) \text{.......................................}(1)$$

Hydrogen Evolution

In a corrosion reaction, that has hydrogen evolution as the principle cathodic reaction it can be seen that the potential of the hydrogen evolution reaction will vary with changes in pH by:

$$E = E^o + \frac{2.3RT}{nF}\log\left(\frac{a_{ox}}{a_{red}}\right) \text{.......................................}(2)$$

so for the cathodic hydrogen evolution reaction:

$$E = 0.00 + 0.059\log a(H^+)$$

So it can be seen that for every unit change in pH the potential of the reversible H_2/H^+ potential changes by 59 mV.

Therefore at 298K, the Nernst equation for the hydrogen evolution reaction simplifies to:

$$E = E^o - 0.059pH$$

Oxygen Reduction

In solutions containing oxygen, the oxygen reduction reaction can act as the cathodic part of a corrosion reaction.
In alkaline electrolyte at pH 14:

$$O_2 + 2H_2O + 4e^- \rightarrow 4OH^- \qquad E^\circ = +0.401\text{V}$$

Where $[OH^-] = 1 \text{ mol dm}^{-3}$.

($E^\circ = +1.23$ V when $[OH^-] = 10^{-14}$)

The Nernst equation for this is:

$$E = E^o + \frac{2.3RT}{4F}\log\left(\frac{p(O_2)}{a(OH^-)^4}\right) \ldots\ldots\ldots\ldots\ldots (3)$$

$$E = 0.401 + \left(\frac{0.059}{4}\right)\log p(O_2) - 0.059\log a(OH^-)$$

Which simplifies to:

$$E = 0.401 + \left(\frac{0.059}{4}\right)\log p(O_2) - 0.059(pH - 14)$$

The partial pressure of oxygen ($p(O_2)$) is approximately 0.2 atm. for a neutral solution. This changes the oxygen reduction potential to 0.814V. There is a pH dependence of 59mV / pH unit.

1.4.3 Pourbaix Diagrams

Pourbaix diagrams are isothermal potential - pH diagrams that show which electrochemical reactions a metal will undergo at different potentials and pH values. Pourbaix diagrams are constructed from thermodynamic data, solubility data on the metal oxides and hydroxides and the Nernst equation. From such diagrams it can easily be seen at which potentials and pH values a metal will corrode, passivate or be immune to corrosion. An example is given in Figure 1.0. This shows iron, with a concentration of iron cations of 10^{-6} M dm^{-3} at 25° C [9]. At concentrations lower than this corrosion is said not to have taken place .

The sloping dashed straight lines in the diagrams show the redox potentials of solutions in equilibrium with oxygen and hydrogen. Both lines have a gradient of 59 mV / pH unit for reasons discussed in section 1.4.2. In the diagrams, in general sloping lines relate to pH dependent redox equilibria, horizontal lines to none pH dependent redox equilibria and vertical lines correspond to equilibria that does not change with change in valency of the ion, for example Fe^{3+} / Fe_2O_3. Immunity refers to potentials and pHs where a metal is thermodynamically unable to corrode. Passivity refers to where a sparingly soluble film, often an oxide is deposited on the metal surface. Such a film affects the kinetics of the corrosion process.

Characteristics of the iron Pourbaix diagram

Figure 1.0 shows that the redox potential line of the H^+/H_2 line is above the immunity region of the iron at all values of pH. Therefore iron will dissolve in aqueous solutions of any pH value. However at pH values between 9.4 and 12.5 a passivating layer of $Fe(OH)_2$ is predicted by the diagram:

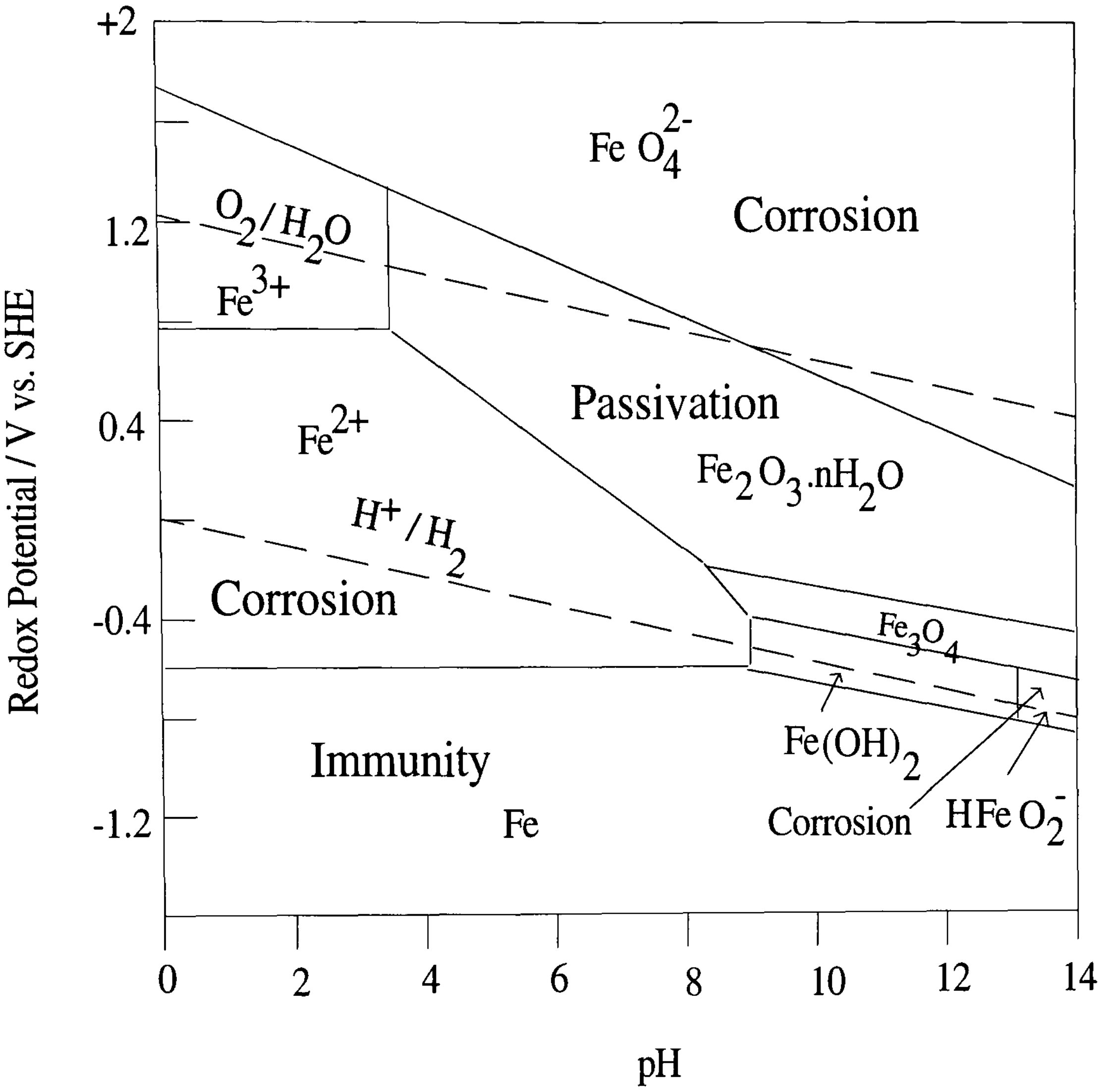

Figure 1.0 : Potential - pH diagram for iron at an iron concentration of 10^{-6} M, temperature 25°C.

Characteristics of the aluminium Pourbaix diagram

The aluminium Pourbaix shows that aluminium will corrode in both acid and alkaline aqueous solutions, but at potentials between about 4 and 8.5 a passive oxide film is formed of böhmite (γ Al_2O_3 . H_2O) which forms, with time, hydragillite (Al_2O_3). [9] This film has the effect of inhibiting the corrosion of aluminium.

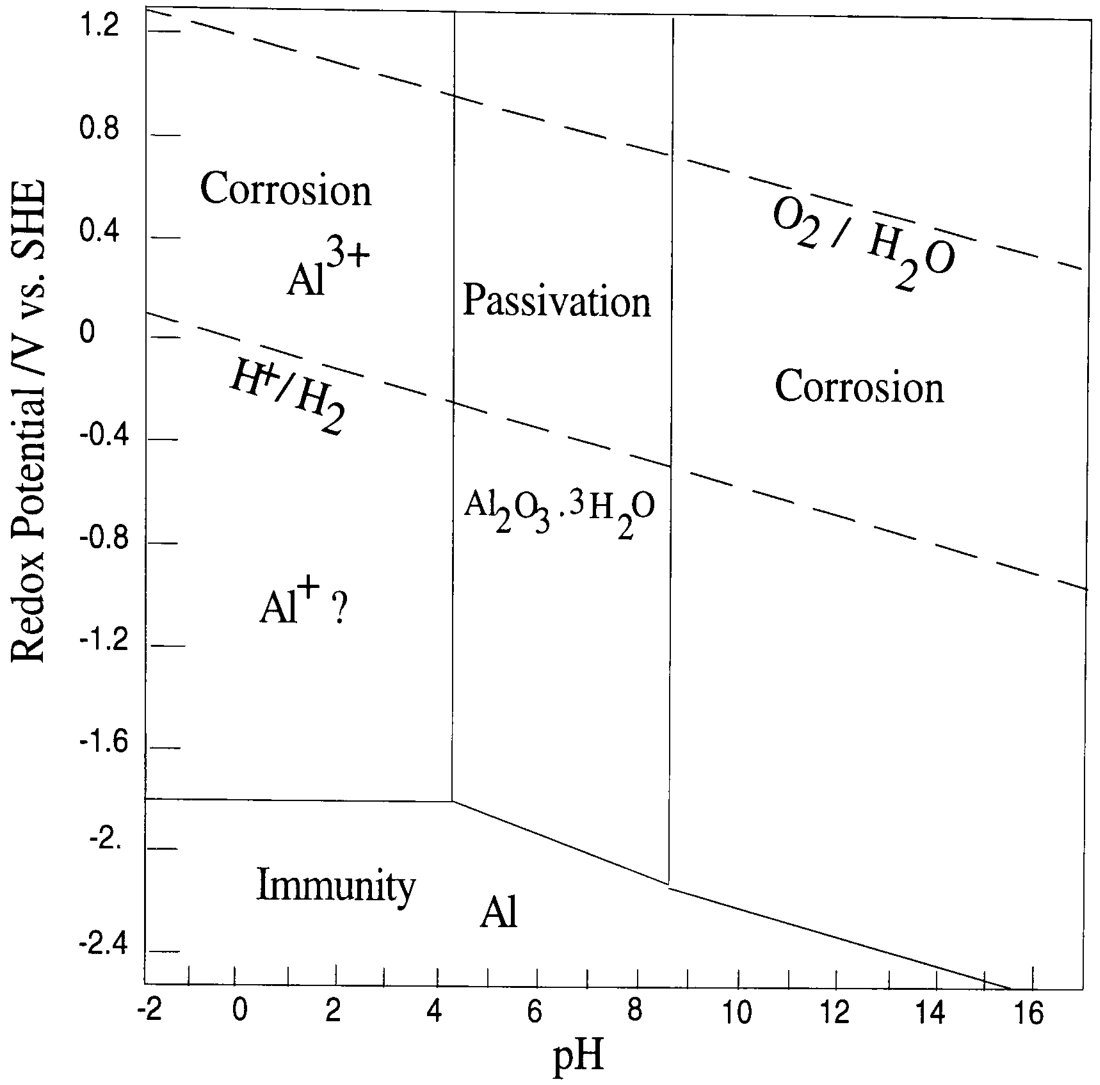

Figure 1.1: Potential-pH Diagram of Aluminium (when passivated by hydragillite $Al_2O_3 . 3H_20$). [9]

Corrosion protection by change in potential of metal

From these diagrams it is possible to see that changing the potential of a metal can affect electrochemical reaction that the metal undergoes, or even prevent it altogether. This is the basis of cathodic and anodic protection.

Cathodic protection is where the potential of a metal is lowered in order to take it into an immunity region *i.e.* in the case of steel, by polarising to potentials more negative than -0.6 V *vs.* SHE at pH 7. This technique is employed extensively on pipelines. A possible problem with this form of corrosion prevention is that it will greatly increase the rate of hydrogen evolution on the metal, which in some cases on steel has led to hydrogen embrittlement.

An alternative is to raise the potential of the metal to a region where it will passivate. On steel this is between approximately +0.4 V and +1.2V. This is known as anodic protection. However if the potential of steel is raised too far, then the metal will corrode at an enhanced rate.

Limitations of the Pourbaix diagram

Pourbaix diagrams are summaries of thermodynamic data but have certain limitations:

- An equilibrium situation is assumed to exist between the corrosion products of the metal and its ions in solution and between the metal and its ions. In practical corrosion situations, however, this is unlikely to be the case.
- The existence of sparingly soluble metal salts on the metal surface (passivation) may have little or no role in lowering the corrosion rate of the metal.
- The pH value in the diagram refers to the pH at the surface of the metal. However pH varies with changes between anodic and cathodic sites across the metal surface, and is usually different from the pH of the bulk solution.
- No information on corrosion *rate* is given since the diagrams are constructed solely from thermodynamic data.

1.5 Corrosion Kinetics

1.5.1. Introduction

A corroding metal consists of many separate cathodic and anodic sites. The size and separation of these sites varies, so for example in filiform corrosion - a form of localised corrosion, the anodic and cathodic sites are almost visible under a microscope [66], whilst on a reasonably homogenous piece of steel the separation and size of sites is much smaller. The anodic and cathodic reactions on the metal can be measured separately, by polarising the metal to potentials where only one reaction is significant. From this a polarisation diagram can be constructed as shown in figure 1.2. The current / applied potential relationship observed in polarisation curves is described by an equation analogous to the Butler - Volmer equation (4):

$$i = i_c\left[\exp\left\{\left(\frac{\alpha_a n_a F}{RT}\right)(E - E_c)\right\} - \exp\left\{-\left(\frac{\alpha_c n_c F}{RT}\right)(E - E_c)\right\}\right] \qquad \text{.............}(4)$$

where:
i = current
i_c= corrosion current
α_c and α_a = cathodic and anodic transfer coefficients.
n_a and n_c = number of electrons transferred in the anodic and cathodic reactions respectively.
E_c = corrosion potential
E-E_c = applied potential

At high negative and positive applied potentials, the Butler-Volmer equation simplifies:

At high positive applied potentials only metal dissolution is expected.

$$\log i = \log i_c + \left(\frac{\alpha_a n_a F}{2.3RT}\right)(E - E_c)$$

At high negative applied potentials only H_2 evolution or O_2 reduction is predicted.

$$\log i = \log i_c - \left(\frac{\alpha_c n_c F}{2.3RT}\right)(E - E_c)$$

Therefore, plotting log i vs. E-E_c will give a straight line, with a gradient of +/- $\alpha nF/2.3RT$ depending whether the slope is anodic or cathodic. The intercept on the current axis will give the corrosion current i_c. This is shown in figure 1.3.

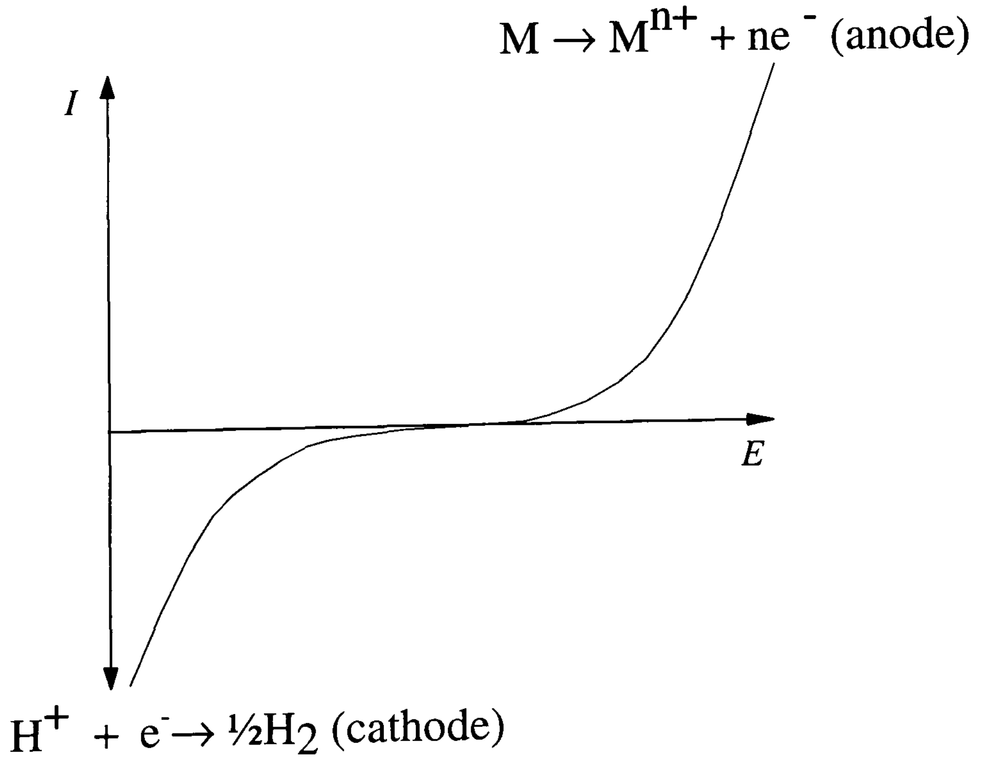

Figure 1.2 Current / Potential diagram of a corroding system

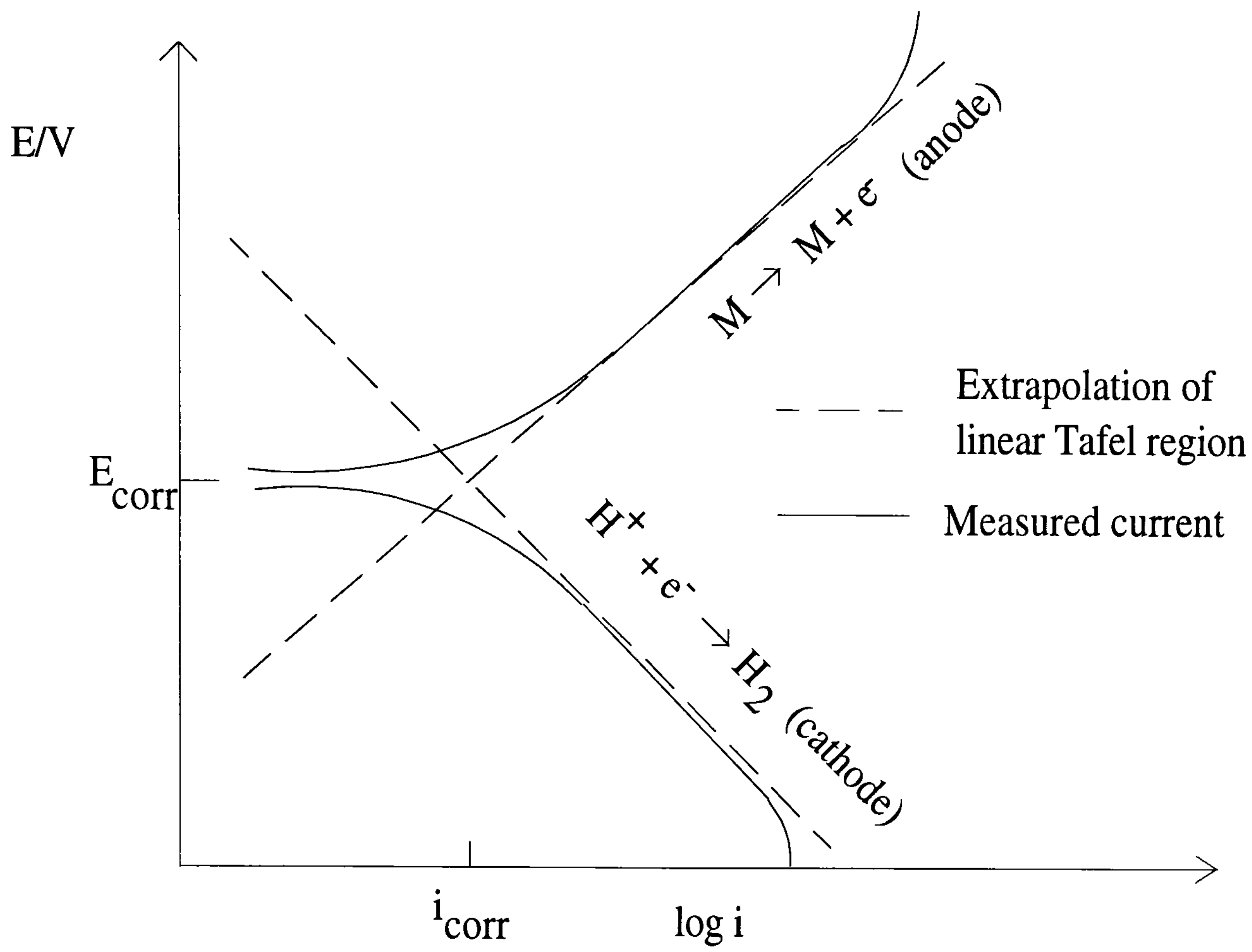

Figure 1.3 Experimental determination of the corrosion current i_C using the Tafel equations

At small perturbations from the corrosion potential, a linear relationship between applied potential and current exists. The ratio of potential and current in this region is known as the polarisation resistance of the metal. It was derived by Stern and Geary [10] and Stern [11], who showed that there is a relationship between the corrosion current, Tafel gradients and the polarisation resistance (5).

$$\frac{\Delta E}{\Delta i} = \frac{\beta_a \beta_c}{2.3 I_{corr}(\beta_a + \beta_c)} \quad \text{.......................................(5)}$$

β_a and β_c are the anodic and cathodic Tafel gradients respectively. ΔE / Δi is defined as the polarisation resistance.

1.5.2 Rate Controlling Steps

In corrosion reactions the extent (gradient) of the anodic and cathodic reaction is not always equal. If the Tafel gradient of either the anodic or cathodic line is greater than the other, then the reaction rate is controlled more by that reaction. The gradient of the anodic and cathodic Tafel lines are often unequal, due to differences in the charge transfer kinetics at the electrode of the two reactions. An example is the iron corrosion in deaerated acid, where the hydrogen evolution Tafel gradient is reported at about 140 mV decade^{-1} [65] and the iron dissolution Tafel gradient at 40 mV decade^{-1}. This is an example of cathodic control and is illustrated in figure 1.4 (c).

Figures 1.4 (a - c) demonstrate the effect of changing from mixed control to anodic and cathodic control in a corrosion reaction.

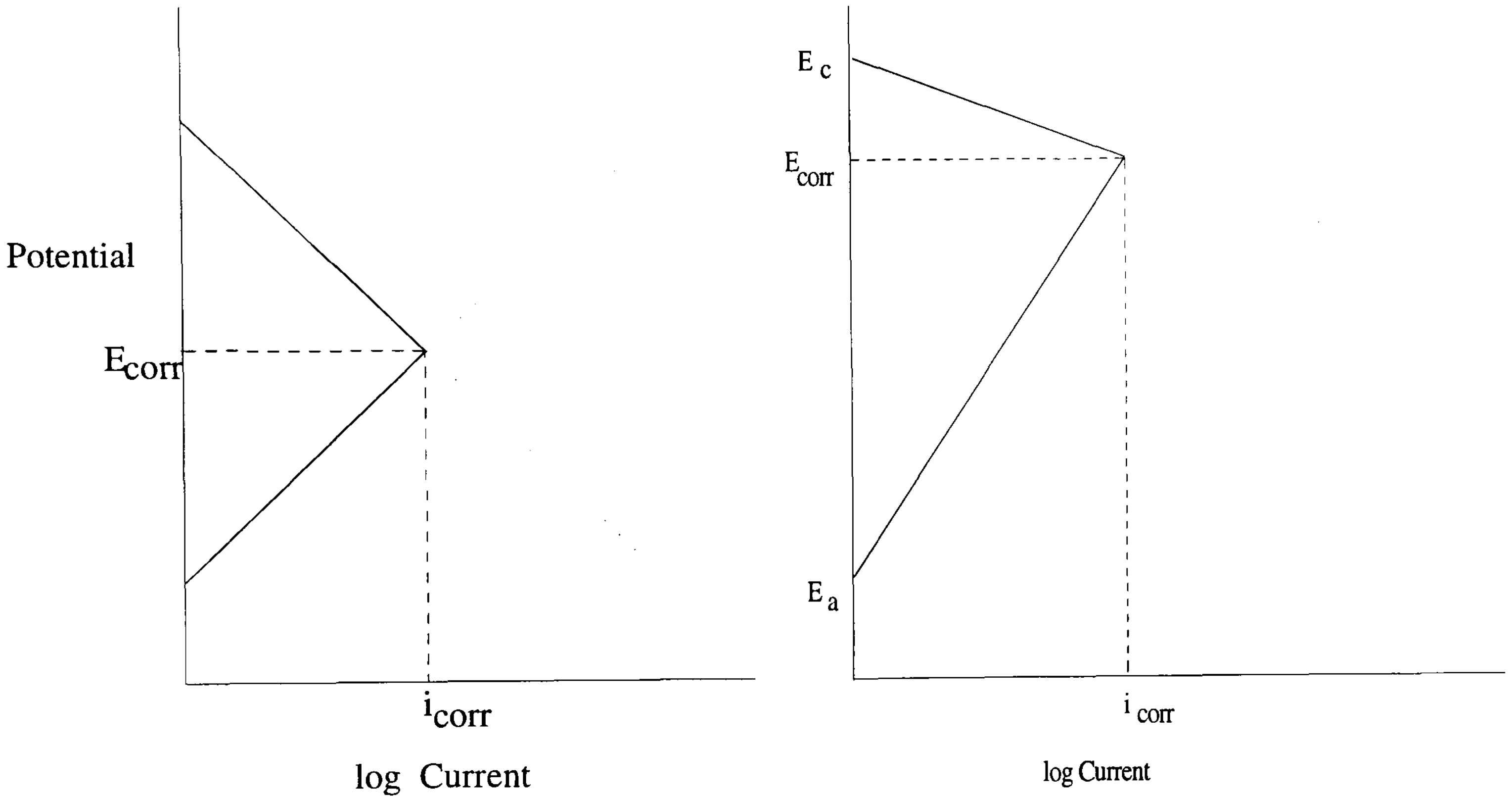

(a) Mixed Control

(b) Anodic Control

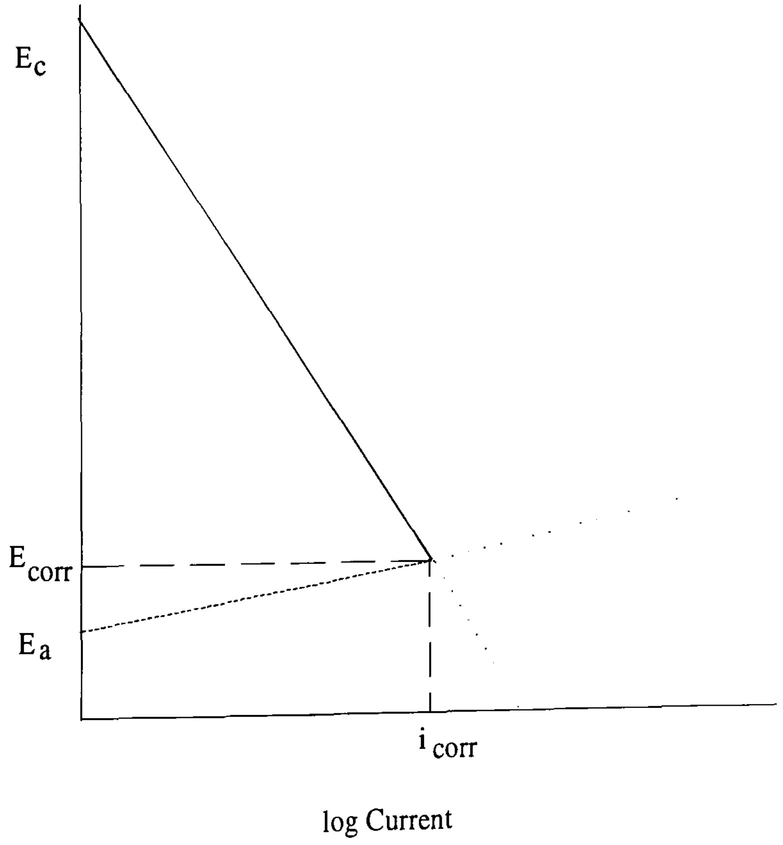

(c) Cathodic Control

Figure 1.4 (a - c)

Evans type diagrams demonstrating anodic, cathodic and mixed control of corrosion reactions.

In diagram (a), with mixed control, changing either the anodic or cathodic reaction would have an equal effect on the overall rate of corrosion. In (b), the corroding system is under anodic control. Changing the potential of the cathodic reaction will have a relatively small effect on the corrosion current, whilst changing the potential of the anodic reaction, even by a fairly small amount will have a large influence on the magnitude of i_{corr} and hence corrosion rate. System (c), under cathodic control is the opposite of (b), where a small change in the potential of the cathodic reaction - for example by varying the pH will have a proportionally large effect on corrosion rate.

1.5.3 Cathodic Reaction Kinetics

It has already been shown in section 1.4.2. that the concentration of oxygen in a system and pH both affect the thermodynamics of a reaction, in each case a one unit change in pH or pOH moves the potential of the related cathodic reaction by 59 mV. In this section, the effect of the oxygen reduction and hydrogen evolution reactions on the corrosion kinetics will be looked at.

1.5.3.1 Hydrogen Evolution

The cathodic reduction reaction on metals such as iron and aluminium in acidic solution, in the absence of oxygen is hydrogen evolution. The Pourbaix diagrams of iron and aluminium show that both metals will corrode in acidic solution. However, Pourbaix diagrams and the Nernst equation give no indication of how fast the metals will corrode at a given pH. At low pH, the concentration of H^+ ions is high, so the corrosion reaction proceeds quickly. At higher pH, the H^+ concentration is lower, so the reaction proceeds more slowly, as shown in figure 1.5.

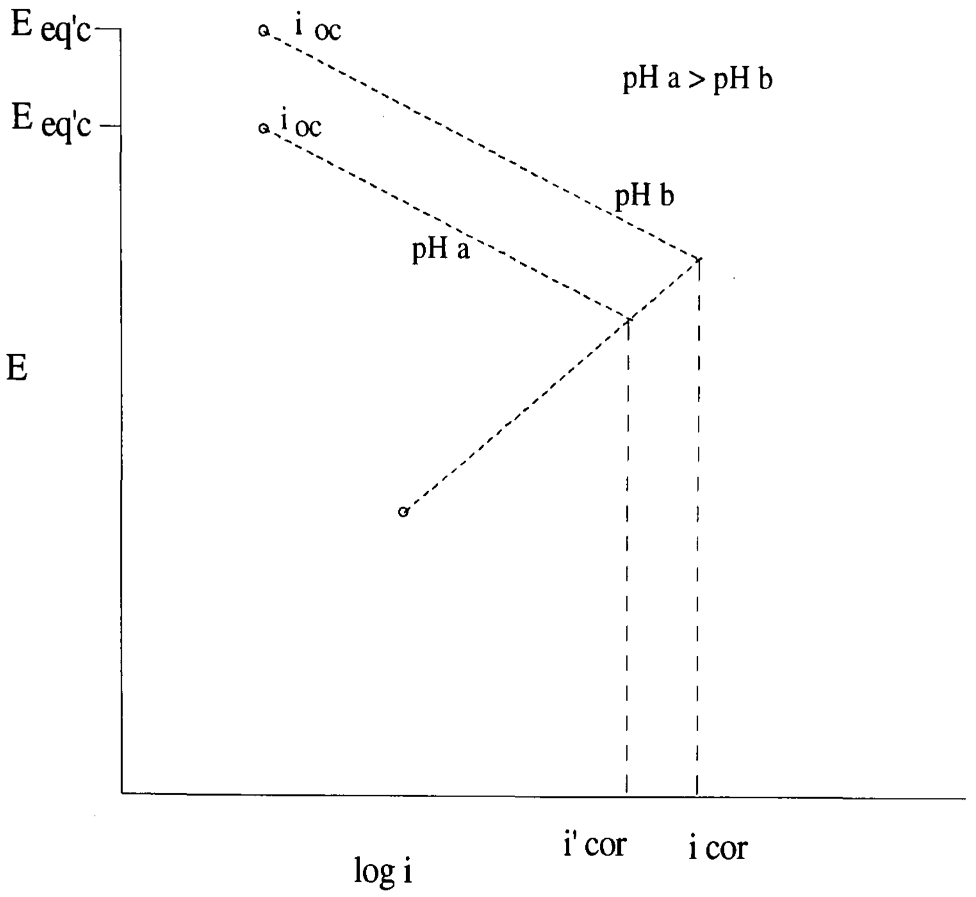

Figure 1.5. The effect of pH on corrosion rate.

Figure 1.5 shows that with increase in pH, so the E_{eq} of the cathodic reaction falls. This then changes the point of interception with the anodic reaction line, so the corrosion current falls from i_{corr} to i'_{corr}.

If the pH of a solution rises, then at about pH 7 another cathodic reaction becomes feasible - the reduction of water. This is thermodynamically feasible at lower pH values, provided sufficient water is available. However the activation energy of the H^+ reduction reaction is low compared with that for water, so water reduction is of importance in solutions of neutral pHs and higher.

1.5.3.2 Oxygen Reduction

In most 'real' corrosion environments oxygen will be present. The solubility of oxygen in pure water at 1 atm. and 25°C is 10^{-3} mol dm^{-3} [67]. This decreases significantly with temperature and slightly with concentration of dissolved salts. Oxygen is, in principle, a more powerful electron acceptor than H^+, with the electrode reduction potentials of oxygen ranging from +1.23V at pH 0 to +0.40V at pH 14. This can be compared with the reduction of H^+, where the electrode reduction potential ranges from 0.00V at pH 0 to -0.828V at pH 14. Therefore in neutral or near neutral solutions oxygen reduction is a more significant cathodic reaction than hydrogen evolution. In such solutions the kinetically limiting step will tend to be transport of oxygen to the metal, especially if insoluble corrosion products build up and passivate the electrode surface, which will increase the diffusion rate dependence of the oxygen reduction reaction.

Since the limiting step in the cathodic reduction of oxygen on a metal is often the transport of oxygen to the surface it therefore follows that a metal immersed in a solution with a higher concentration of dissolved oxygen will generally have a higher corrosion rate. This is clearly shown in figure 1.6 where C3 > C2 > C1:

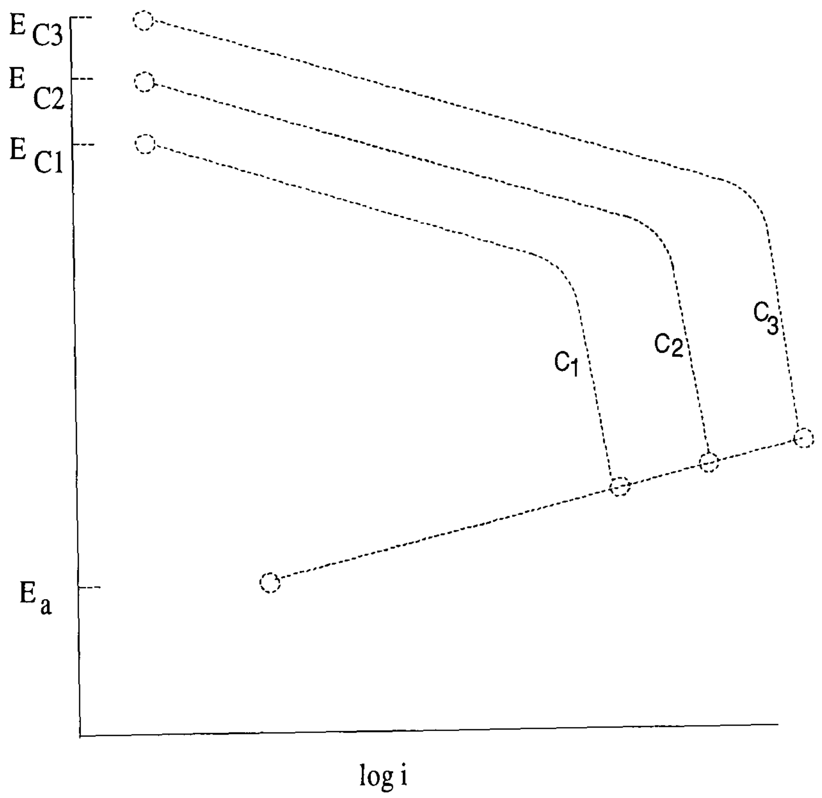

Figure 1.6 - The effect of oxygen concentration on corrosion current.

The corrosion rate of a metal with oxygen reduction as the cathodic reaction is also dependent on the degree of agitation of the solution, as oxygen concentration is lower at the surface of the metal than in the bulk. Stirring/agitation of the solution reduces the thickness of the diffusion layer so causing the limiting current i_L, which in the case of oxygen reduction is equal to the corrosion current to increase by:

$$i_L = \frac{nFADC_o^{\infty}}{\delta} \qquad (6)$$

Here, δ is the diffusion layer thickness, and C_o^{∞} the bulk concentration of oxygen.

1.6 Kinetics *vs.* Thermodynamics

Thermodynamics are important when calculating *if* a metal will corrode under specific conditions. However, thermodynamic measurements do not give any indication of rate. To illustrate this, situations can be envisaged where a system with a higher thermodynamic tendency (E_1 - E_2) has a lower corrosion rate than a system with a lower thermodynamic tendency (figure 1.7a) and where two system have the same corrosion potential, but different corrosion rates. (figure 1.7b)

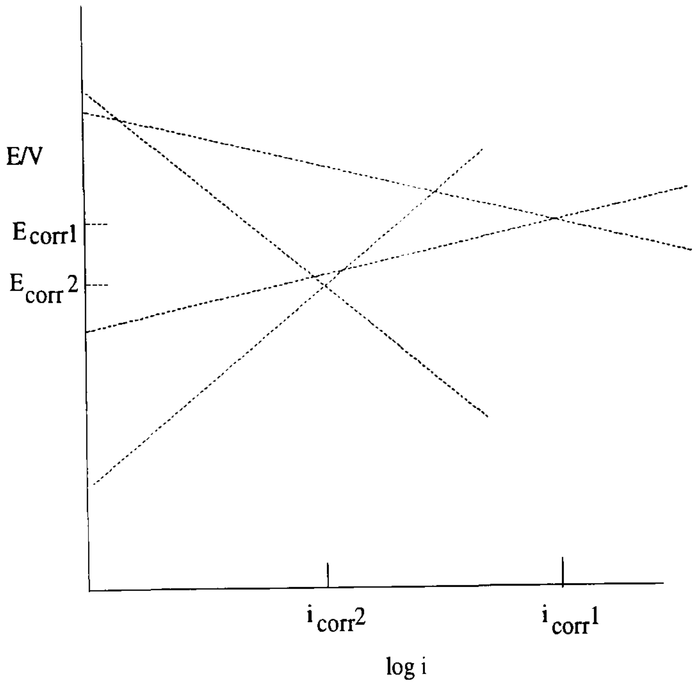

Figure 1.7 *(a)*

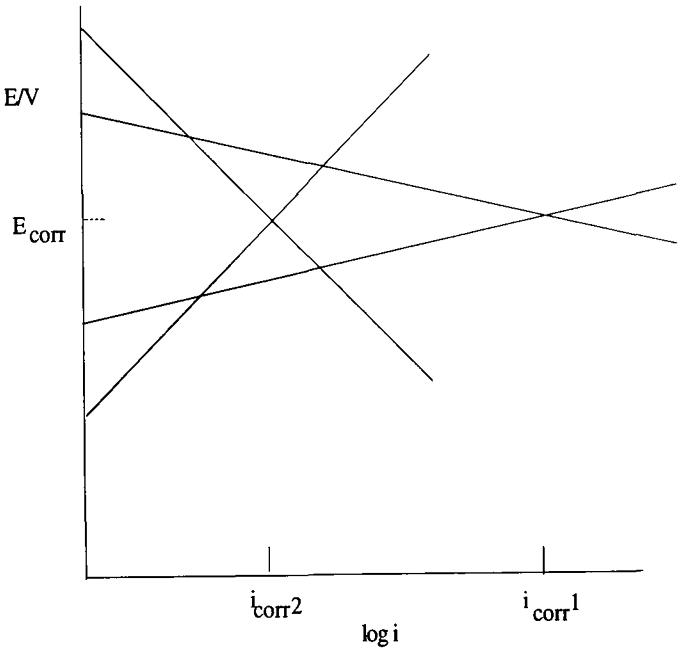

Figure 1.7 *(b)*

This lack of information on rate of corrosion from thermodynamic sources such as Pourbaix diagrams may lead to some questions on the overall usefulness of such diagrams. However, Pourbaix diagrams do give information on the conditions where corrosion will not take place, and information on how much a system would need to be changed - *i.e.* by anodic or cathodic protection to prevent corrosion.

1.7 Methods of Measuring Corrosion Rate

There are many different methods for determining corrosion rates of various systems. The method used will often depend on physical situation of corroding system *i.e.* in-situ in the field or modelling a system in a laboratory and the degree of accuracy required and cost.

1.7.1 Polarisation Resistance

The theoretical basis to this method has already been mentioned in section 1.5.1. It allows the corrosion current to be estimated from the slope of the polarisation curve at potentials close to the corrosion potential (± 10mV) using the Stern-Geary equation. The polarisation resistance can also, in many cases be found from AC Impedance spectroscopy, which will be discussed later. The advantage of using polarisation resistance to measure corrosion rate is the small polarisation potential required, thus preventing increased dissolution of the metal and/or increased hydrogen evolution / oxygen reduction.

1.7.2 Tafel Plots

Once again the theoretical basis of this method has been discussed in section 1.5.1. The corrosion current can be estimated by extrapolation of the linear cathodic and anodic lines of the log current vs. potential plot to their point of intersection. Typically the potential needs to be swept between 200 mV each side of the corrosion potential, although this varies depending on the exact system being studied.

1.7.3 Weight Change

This is a very common and fairly straightforward method for measurement of corrosion rate. However, corrosion products need to be removed prior to weighing. In the cases of a strongly adhering passive film, the weight gain can be measured.

1.7.4 Rate of Hydrogen Evolution

In this case the volume of evolved hydrogen from the cathodic reaction is measured and used to calculate the overall corrosion rate. This method is commonly used in acidic, deaerated solutions. In neutral water or aqueous solutions, in a closed system, the decrease in oxygen concentration can be measured.

1.7.5 Optical Examination

This technique is of most use with localised corrosion such as pitting or filiform corrosion. It can be semi-quantitative, especially if used on a statistically significant number of samples. From this the total corrosion area can be estimated.

1.7.6 Analytical Techniques

This involves analysis of the solution that the metal is immersed in, during and after a corrosion experiment for determination of dissolved metal ions, for example Fe^{2+}. This can be done using techniques such as atomic adsorption spectroscopy or polarography.

1.8 Accelerated Laboratory Tests

These are tests designed to speed up a corrosion process, by intensifying one of the corrosion factors. They allow the effects of long term exposure to different environments to be modelled and the effect on corrosion of the metal measured using some of the methods discussed in the previous section. Examples of such tests are salt spray chambers, humidity/temperature chambers, sulphur dioxide fog and UV light exposure. Use of UV light chambers and humidity/temperature chambers will be discussed in more detail later. Falling slightly outside the criteria of laboratory tests are site tests where materials are exposed to different environments, for example desert or marine. A number of sites exist around the world, notably in Florida, Arizona and Hook van Holland. These three sites offer different exposure regimes: humid sub-tropical, arid tropical and temperate marine respectively.

1.9 Reduction of Corrosion Rates

Corrosion of materials can be reduced in a number of different ways, these are outlined as follows:

1.9.1 Change of Metal

This is often an expensive option, so cannot always be used, for example changing from iron/steel to stainless steel. The mechanical properties of the new material may also be undesirable.

1.9.2 Metallic Coatings

These take two main forms. One is the addition of a layer of a sacrificial metal onto the metal to be protected i.e. galvanising of steel by zinc. Second is where a metal may be protected by the addition of a thin layer of a more noble metal, such as silver on steel - used on cutlery. In the former case the metal acts as a sacrificial anode towards the underlying metal. In the latter case of using a more noble metal, the coating needs to be dense and impervious, as areas of uncoated underlying metal will corrode more quickly due to the galvanic effects of being surrounded effectively by a large cathodic area. Both cases are designed to prevent the metal coming into contact with a corrosive environment.

1.9.3 Inorganic Coatings

These have a similar role to the metallic coatings previously mentioned in preventing the metal contacting a corrosive environment. Examples are glasses and vitreous enamels.

1.9.4 Anodic Protection

The principal of anodic protection is to connect the metal to be protected as an anode in a galvanic or electrolytic cell and thus raise the potential of the metal into passivity. The galvanic protection method is achieved by alloying noble metals with the metal to be protected to form local cathodes on the metal, or as a surface coating. The electrolytic method requires a direct current source from outside the system and an auxiliary cathode.

1.9.5 Cathodic Protection

In this case the potential of the metal is lowered into immunity at a potential below its steady state corrosion potential for a given solution. The metal thus becomes a cathode and reduces oxygen and H^+. Two methods are employed, illustrated in figure 1.8. The first method shown utilises a baser metal as a sacrificial anode, which corrodes preferentially to the metal being protected, and in so doing lowers the potential of that metal (a). The second method utilises an external electrical current, with the metal to be protected made negative relative to an inert anode (b).

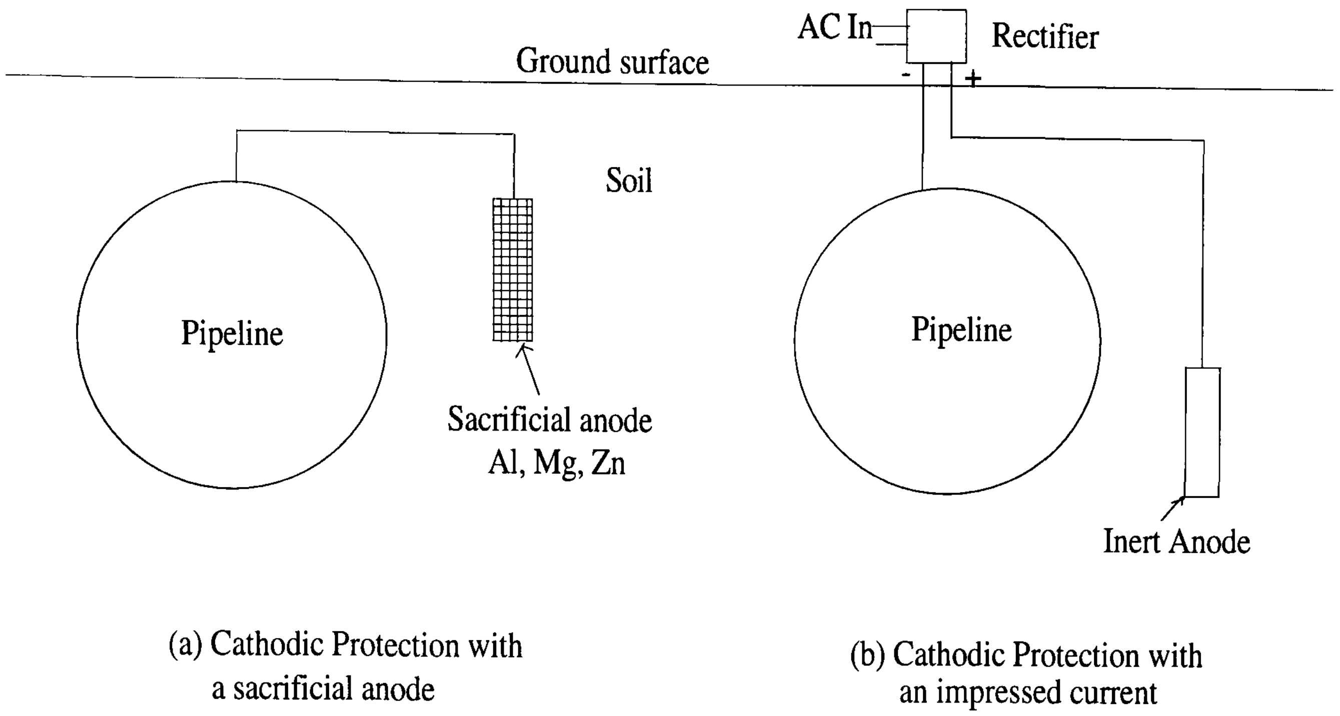

Figure 1.8 - Principle of cathodic protection in protecting underground metal structures [from reference 2]

1.9.6 Anodising

Metals that have a passive oxide film, such as aluminium can be given increased corrosion resistance by strengthening the oxide film. This is done by attaching the metal to an anode in a suitable electrolyte such as aqueous sulphuric acid or chromic acid and passing a DC current. The thickness of the oxide film can increase by up to one third.

1.9.7 Organic Coatings

Organic coatings find extensive use in preventing corrosion by two principle methods. Firstly by providing a barrier to water and ion penetration to the underlying metal and, in some paint systems by containing corrosion inhibitors that passivate the metal, should the coating be breached. In this thesis the issue of corrosion inhibitors in paints has not been examined, the role of organic coatings as barriers against water and ion penetration to the surface of the metal will be considered.

1.9.7.1 Composition of Paint Systems

There are many different types of polymers used in organic coatings. Examples are polyurethanes, acrylics, polyesters, chlorinated rubber and PVC. Such polymers can be used as single layer or in multilayer coatings, be cross linked with different materials and be applied in a number of different ways. In addition pigment may be added. A typical paint system consists of two and sometimes three principle parts, the binder, pigment and solvent.

The binder is the base polymer used and holds the paint film together as well as adhering to the surface of the substrate. The physical properties of binders can be changed, in some cases, by the addition of plasticisers. The binder is the most important component of the paint system.

The pigment is added to give the paint film colour and in some cases to alter the mechanical properties of the film. It can have anticorrosive properties, as in motor-car electrocoat and zinc rich primers or change the ease of diffusion of ions and liquids through the film.

A solvent is used where the binder is a solid at the temperature of application of the paint, and the paint is applied as a liquid. Thus systems such as oil based paints have no solvent, as the binder is a liquid at room temperature and powder coatings where the paint is applied as a solid.

1.10 Polyester Powder Coatings

This thesis is concerned with the breakdown and subsequent corrosion under polyester powder coatings. It is therefore necessary to consider the composition and properties of such coatings.

1.10.1 Background [12 - 13]

Powder coatings are a relatively modern class of coating that are used for protective and decorative applications on a range of substrates such as on architectural coatings on buildings, car brake pipes and some bicycles. Thus they need to be capable of protecting the underlying metal in a number of different exposure conditions such as extremes of temperature, chemical contamination and from UV light. Powder coatings are electrostatically applied to a metal as a dry powder with mean particle size ~ 50 μm. The coated metal is then cured by stoving in an oven, where the powder melts into a film.

1.10.2 Manufacture [12 - 13]

The precise details of the powder coating system considered in this thesis will be considered in Chapter 2. The general method for production of powder coatings is to mix raw materials (polymer and cross linker plus additives) as dry powder then electrostatically apply to the substrate metal, where the powder coat is cured by stoving to cross-link and melted onto the substrate.

1.10.3 Categorisation of Powder Coatings [12 - 13]

Powder coatings can be classified into two classes, thermoplastic and thermosetting powder coatings. Thermoplastic powders undergo no chemical change during formation, with the stoving of the coated metal used solely to change the powder to a solid film. Examples of such powders are polyethylene, PVC, polypropylene and nylon-11. Thermosetting powders comprise of a polymer component known as the prepolymer or resin and a cross-linker or curing agent. On stoving the cross-linker and prepolymer react to form a crosslinked network. As a result the thermosetting polymers show superior thermal and chemical resistance. an example of a thermosetting polymer is the polyester cross-linked with PRIMID® system considered in this thesis.

1.10.4 Polyester Powder Coatings

In this thesis a polyester cross-linked with a multifunctional amide, PRIMID® XL-552 has been studied. During stoving the PRIMID® reacts with acid groups on the polyester, cross linking the polyester chains and evolving water. This gives the coatings good chemical and mechanical properties. The precise composition of the of the polyester system cannot be given as it is commercially sensitive.

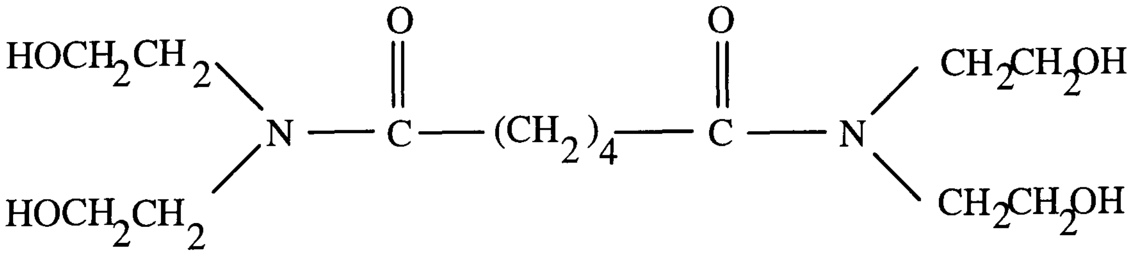

PRIMID® XL-552

(N,N,N',N'-*tetrakis*(2-hydroxyethyl)adipamide

PRIMID has been developed to replace a previously widely used cross-linker, Triglycidyl Isocyanurate (TGIC). This cross linker accounted for 19% of the European powder coating market in 1989 [14], but has problems associated with its toxicity. PRIMID has an LD_{50} (Dose required to kill 50 % of a test group of rats) level of > 5000 mg Kg^{-1} [15], while TGIC has an LD_{50} level of 300 mg Kg^{-1} [16]. The melt and flow (rheological changes) characteristics of the powder when heated during the curing process, after application to the substrate, lies outside the scope of this thesis, however they are discussed further in reference [17].

1.11 Application of Electrochemical Impedance Spectroscopy to Study the Breakdown of Organic Coatings and the Associated Degree of Underfilm Corrosion

1.11.1 Introduction

The principle electrochemical 'tool' employed in this thesis is Electrochemical Impedance Spectroscopy (EIS). In this section EIS is considered in detail. The analysis considered in this section, and used subsequently for analysis of experimental data is based on the work of Armstrong and Wright [19]. Different interpretations of EIS data in the literature are reviewed in section 1.12.

1.11.2. Experimentally Determinable Impedance Parameters

EIS is an extremely useful technique for studying corrosion under organic coatings and changes in coating properties. The EIS response of a perfect coating will just give the capacitance of the coating. In a defective coating, in principle, four pieces of information on the substrate/coating system can be obtained [19]:

1. Coating (Geometric) Capacitance, C_g. This gives information on the dielectric constant of the coating and has been used to calculate water uptake [20].

2. Bulk Resistance, R_b, of the coating. In a defective coating thin channels of electrolyte run through the coating, giving the coating a finite resistance. In a system where these pores have a near uniform cross section and are orthogonal to the surface

of the coating, then the number and area of pores in a system can be related to the bulk resistance by:

$$R_b = \frac{d}{aN\kappa} \quad \text{...}(6)$$

where d is the coating thickness, N the number of pores, a the average cross sectional area of a single pore and κ is the conductivity of the electrolyte. This can then be related to the porosity of the coating, by defining porosity as the ratio of the bulk resistance of a system containing 100% pores with the bulk resistance of the coating, R_{bt}.

$$R_{bt} = \frac{d}{\kappa A}$$

Here A is the area of the electrode.

So porosity, P is the ratio of pore areas of a 100% porous system with a defective system:

$$P = \frac{Na}{A} = \frac{R_{bt}}{R_b} \quad \text{...}(7)$$

3. Metal Interfacial (Double Layer) Capacitance, C_{dl}. This is the capacitance formed by electrolyte contact with the substrate metal. The double layer capacitance comes from the coulombic attraction of hydrated ions by the charge on the metal. The double layer capacitance can be used to used to estimate the reactive area on the surface of the metal, beneath the coating by:

$$C_{dl} = \frac{\varepsilon_o \varepsilon_r A}{d} \quad \text{.................................}(8)$$

4. Charge Transfer Resistance, R_{ct}. This is the charge transfer resistance of the Faradaic processes taking place on the metal surface. If R_{ct} is measured at the corrosion potential of the system then it is equivalent to the polarisation resistance of the metal. Hence the corrosion current can be estimated by using the Stern-Geary equation [10,11]. R_{ct} is, in principle, related to the reactive area of the metal in a similar way to the double layer capacitance. However inhomogeneity of the metal surface can make this correlation poor.

Note: The analysis of EIS data is a subject of some controversy in the literature. The analysis described in this thesis is based on the work by Armstrong and Wright [19]. Alternatives to this analysis are discussed later.

1.11.3 Theoretical Basis of Electrochemical Impedance Spectroscopy [21-24]

Electrochemical Impedance Spectroscopy involves the application of a sinusoidal potential to an electrochemical cell.

The instantaneous applied AC potential is given by:

$$E = \Delta E \sin \omega t \quad \ldots\ldots\ldots\ldots\ldots\ldots\ldots (9)$$

where ω = 2πf (the angular frequency), ΔE is the maximum potential, This is illustrated in Figure 1.10a. The result of applying a sinusoidal potential to a cell will be a sinusoidal current at the same frequency, but it may have different amplitude and phase to the potential (Figure 1.10b):

$$i = \Delta i \sin (\omega t + \phi) \quad \ldots\ldots\ldots\ldots\ldots\ldots\ldots (10)$$

ϕ is the phase difference between the applied potential and current.

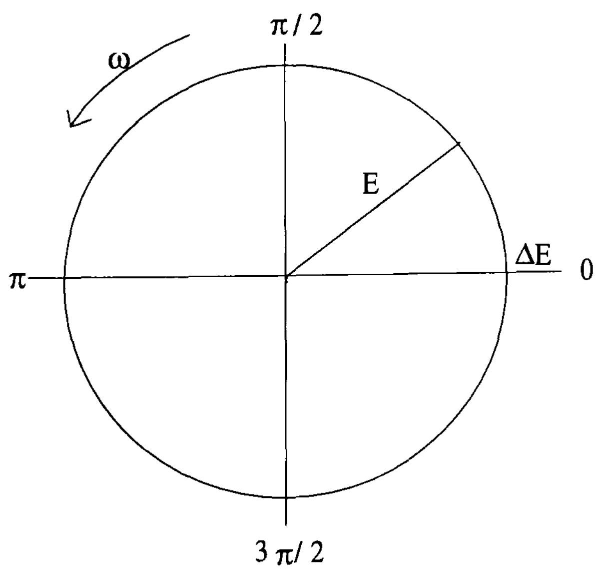

Figure 1.10a: Phasor Diagram showing an alternating potential

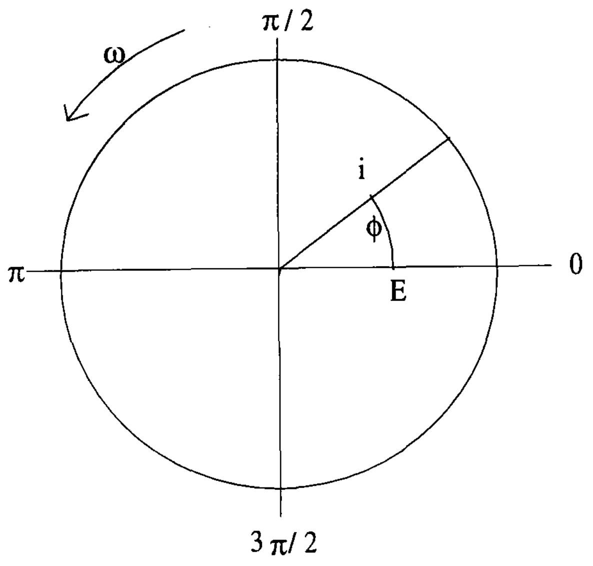

Figure 1.10b: Phasor Diagram showing phase difference between current and potential ϕ

Impedance is a form of generalised resistance taking into account the resistance (the ratio of potential and current) of a system and any phase change between current and potential:

$$Z = \frac{\Delta E}{\Delta i} \qquad \text{and a phase change } \phi$$

Impedance is a vector, as it possesses both magnitude and direction and can thus be conveniently expressed in complex plane notation with a real element, Z' in phase, and an imaginary element Z" out of phase:

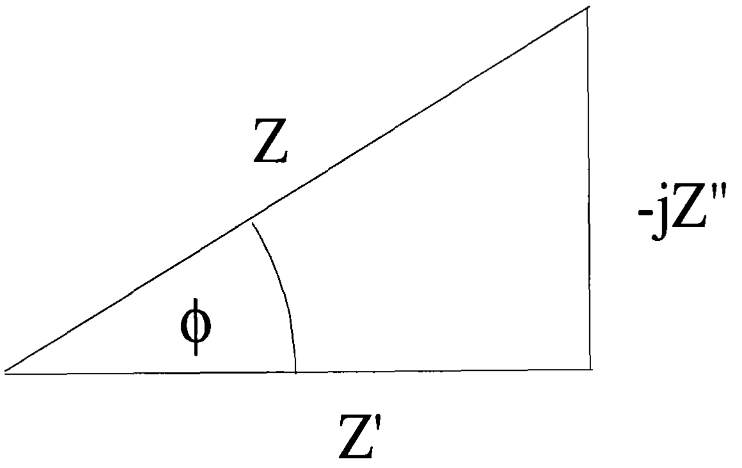

Therefore the total Impedance Z, can be broken down into two separate components, Z' on the real axis and Z" on the imaginary axis:

$$Z = Z' - jZ'' \qquad \text{where } j = \sqrt{-1}$$

where $Z' = Z\cos\phi$ and $Z'' = Z\sin\phi$

From here the impedance response of individual and coupled electronic elements can be predicted.

Impedance Response of a Pure Resistor

A pure resistor simply obeys Ohms law, and will be represented as a point on the real axis of the Argand diagram (Z') with no phase difference between current and potential. This can clearly seen:

$$i = \frac{E}{R} \qquad E = \Delta E\, sin\omega t \qquad i = \left(\frac{\Delta E}{R}\right)\sin\omega t \text{.........} (11)$$

The resultant impedance spectrum of such a system can be seen in figure 1.11a.

Impedance Response of a Pure Capacitance

For a capacitor the situation is slightly more complex as the relationship between the charge on the capacitor and the potential needs to be considered:

$$q = CE$$

As current is the rate of change of charge per unit time then current and potential are related by:

$$i = \frac{dq}{dt} = C\frac{dE}{dt} \quad \text{.................................(12)}$$

Substituting in the equation for an alternating potential, $E = \Delta E \sin\omega t$, gives:

$$i = \omega C \Delta E \cos\omega t$$

so:

$$i = \omega C \Delta E \sin(\omega t + \pi/2) \quad \text{...........................(13)}$$

Therefore the maximum value of the sinusoidal current is equal to $\omega C \Delta E$. This shows that the current is frequency dependent and $\pi/2$ out of phase with the potential.

The impedance of a pure capacitance is frequency dependent as:

$$Z = \frac{\Delta E}{\Delta i} \qquad \text{substituting for } \Delta i \text{ gives:}$$

$$Z = \frac{\Delta E}{\omega C \Delta E} \quad \text{...(14)}$$

Hence the impedance response of a pure capacitance is given by:

$$Z = \frac{1}{\omega C} \quad \text{and since} \quad Z = Z' - jZ'', \text{ then:}$$

$$Z'' = -j\frac{1}{\omega C}$$

As the phase difference between current and potential is $\pi/2$ then the impedance response is solely on the imaginary axis - there is no real component. This is illustrated in Figure 1.11b.

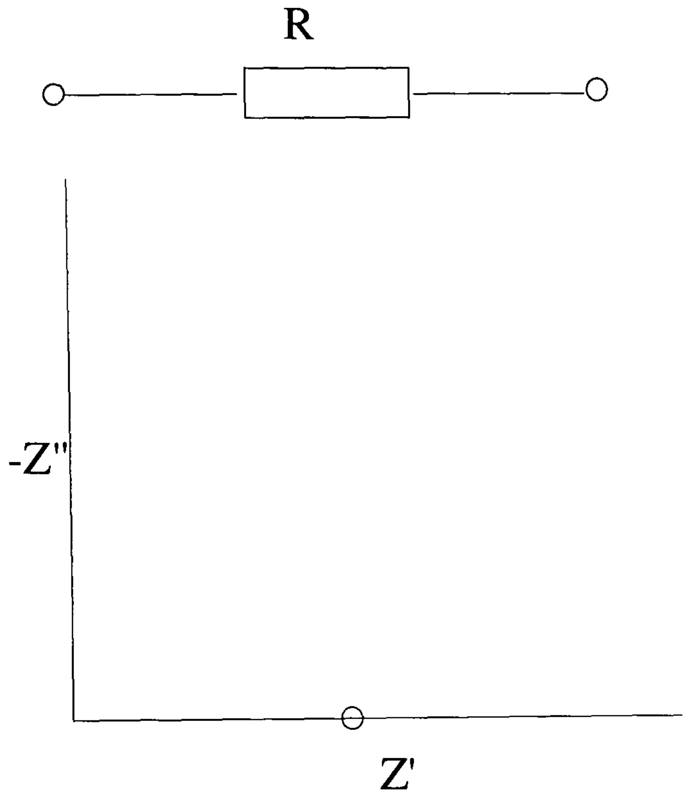

Figure 1.11a - Impedance Response of a Pure Resistance

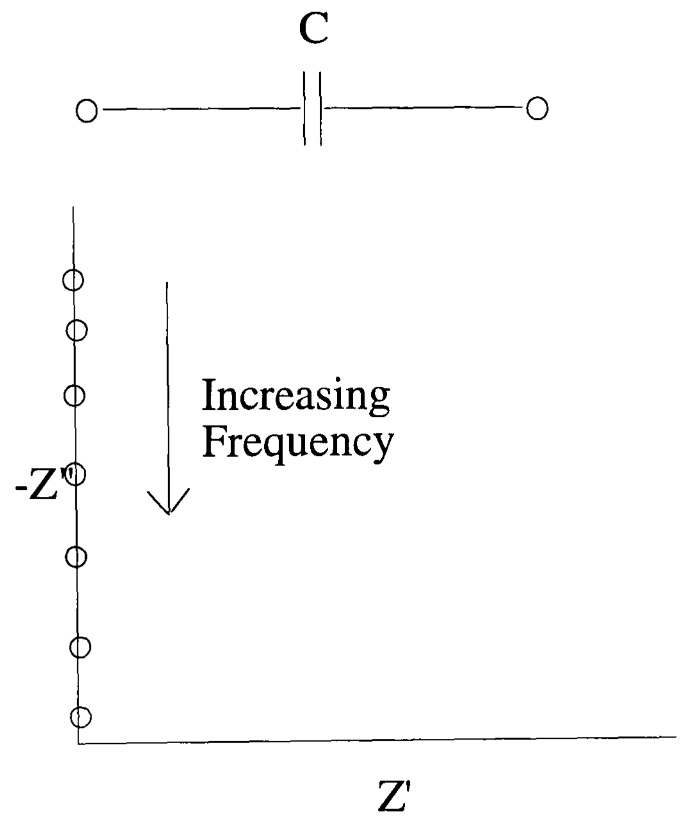

Figure 1.11b - Impedance Response of a Pure Capacitance

Impedance Response of a Resistor and Capacitor in Series

A resistor and capacitor in series give an impedance response equal to the sum of the individual impedances of the resistor and capacitor. Therefore the impedance spectra will show a vertical line as for a single capacitance displaced along the real axis by the value of the resistance (figure 1.13a). This can be written mathematically as:

$$Z = R - j\frac{1}{\omega C} \quad \ldots\ldots\ldots\ldots\ldots\ldots\ldots\ldots(15)$$

Impedance Response of a Resistor and Capacitor in Parallel

This situation is considerably more complex than the previous case of a resistor and capacitor in series. Here the impedance is the reciprocal sum of the resistance and capacitance of the system (16), calculated in a similar way to DC parallel resistance.

$$\frac{1}{Z}=\frac{1}{R}+j\omega C \qquad (16)$$

The impedance spectrum of this system gives a semi-circle shown in figure 1.12. This can be understood as the change in impedance response of the circuit components as the frequency is swept from high to low frequency. Each point on the semicircle has a different phase angle. The length of the vector from the origin to the point is the total impedance at that frequency containing the relative impedance of both the resistance and capacitance.

At high frequencies virtually no current can be thought of as flowing through the resistance pathway as the capacitance is an effective high frequency AC 'conductor'. Therefore the impedance of the system comes almost purely from the capacitance. The phase angle of this point is going to be around 90°. As the frequency begins to fall, the capacitance becomes a less effective 'conductor', with current starting to flow through the resistance. The resistance starts giving a measurable impedance, although the impedance response is still greater from the capacitance. Therefore the phase angle of the impedance points starts to decrease.

The top of the semicircle represents a point where the impedance response from the resistance and capacitance is equal, roughly half the total charge in the circuit flows through each component. This point therefore has a phase angle of 45°. As the frequency continues to decrease, the impedance response from the resistance becomes more dominant, since low frequency AC currents can not easily flow through a capacitance. The limiting case here is where a DC current is totally blocked from flowing through a capacitance. At low frequencies therefore the phase angles is close to that of a pure resistance - at 0°. This effect is illustrated in figure 1.12.

In summary:

	Component giving principle impedance response	Phase angle
High frequency	Capacitor	90°
Mid frequency	Resistor + Capacitor	45°
Low frequency	Resistor	0°

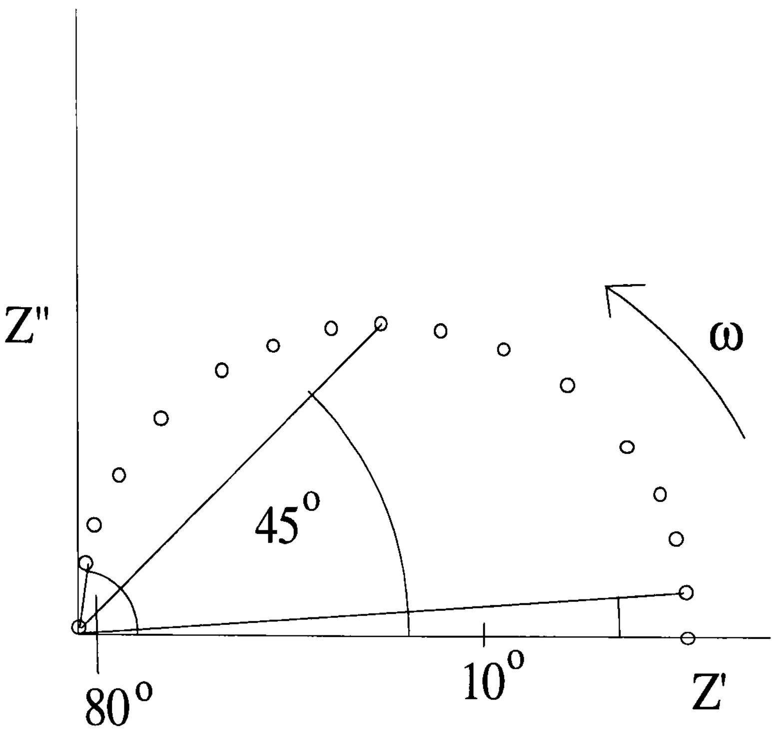

Figure 1.12 - Diagram Showing the Change in Phase Angle of the Points on the Impedance Spectrum as the Frequency is Increased and the System changes from a Purely Resistive Response to a Mixed Response to a Purely Capacitive Response.

Figure 1.13b illustrates the effect of adding a resistance in series with a resistor and capacitor in parallel. The effect is to offset the RC impedance semicircle by the value of the series resistance along the real axis.

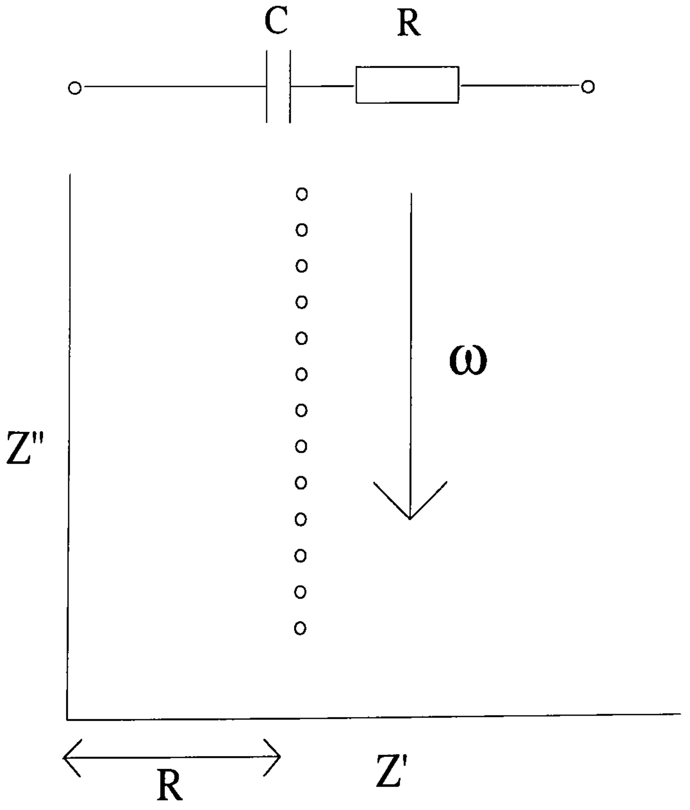

Figure 1.13a - Impedance Response of a Resistor and Capacitor in Series.

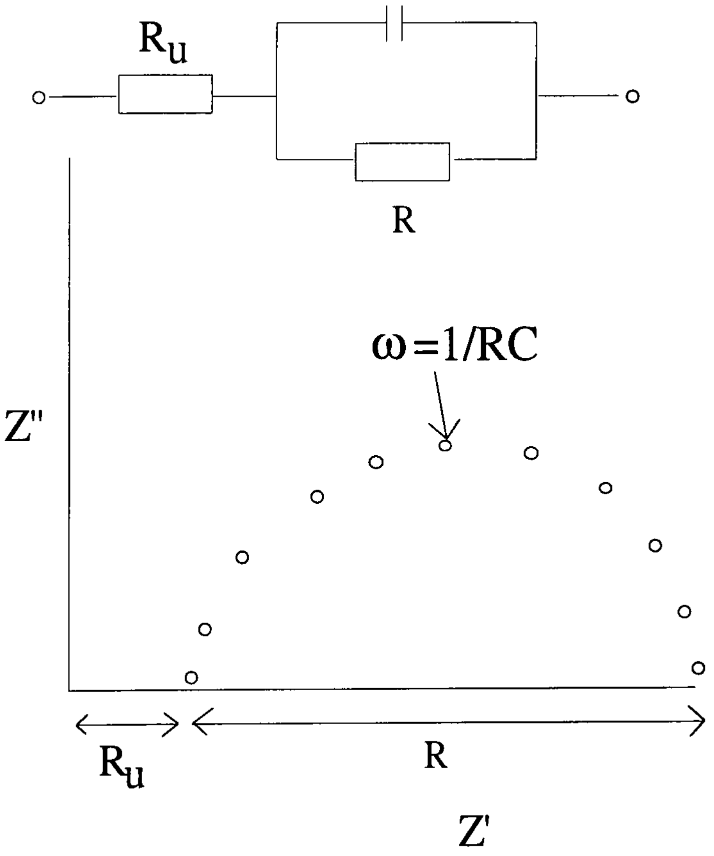

Figure 1.13b - Impedance Response of a Resistor in series with a Resistor and Capacitor in Parallel.

1.11.4 Modelling of Electrode Interfaces Using Equivalent Circuits

The previous two subsections have demonstrated which basic parameters E.I.S. is capable of measuring and how these measurements produce the observed Impedance Spectra. The most straightforward way of interpreting experimental E.I.S. spectra is to fit the data to an equivalent circuit - a model of an interface comprising of resistors and capacitors.

As previously stated a perfect protective coating will give a purely capacitive impedance response, therefore the model for this situation is simply a capacitor. The resultant E.I.S. spectra will be a straight line vertically up the imaginary axis of the Complex plane (Nyquist) plot. (Figure 1.11b)

A simple electrode interface to model is that of a metal, such as steel undergoing corrosion. This situation can be modelled as the charge transfer resistance (R_{ct}) and double layer capacitance (C_{dl}) of the metal in a parallel combination and any electrolyte resistance (R_u) in series with this. This is shown in Figure 1.13b.

A more complex situation is to consider a defective polymer coating on a reactive metal, for example a polyester on steel, in contact with an aggressive electrolyte. In this situation the capacitance of the coating is in parallel with the resistance of channels / pores running through the coating. The resistance of these pores is itself in series with the interfacial impedance of the bare metal at the pore base. The interfacial impedance of the bare metal is given by the parallel combination of the charge transfer resistance and double layer capacitance. This will in principle, experimentally give the four impedance parameters described in section 1.11.2.1. The equivalent circuit for this situation is then a combination of these parameters, as shown in figure 1.14. The resultant impedance spectra will comprise of two semicircles. At high frequencies the impedance of the coating system - bulk resistance and geometric capacitance will be measured, at low frequencies the metal interfacial impedance - charge transfer resistance and double layer capacitance.

The polymer coating impedance is generally found at high frequencies because the coating impedance time constant, R_b x C_g is smaller than the metal interfacial impedance time constant R_{ct} x C_{dl}. This comes about because of the difference in 'plate' separation (d) in the two dielectrics which make up the two capacitances (d in equation (8)). The bulk coating has a separation (d) of around 50 μm, while the metal interfacial impedance has a separation (d) around the magnitude of the radius of a hydrated ion (~ 1-2 nm). It is therefore clear that the interfacial capacitance will generally be 3-4 orders of magnitude greater than the bulk coating capacitance. As the metal interfacial area on a polymer coated metal is generally many times smaller than area of polymer coating, the measured bulk resistance, R_b can be close to the charge transfer resistance R_{ct} for the total electrode area.

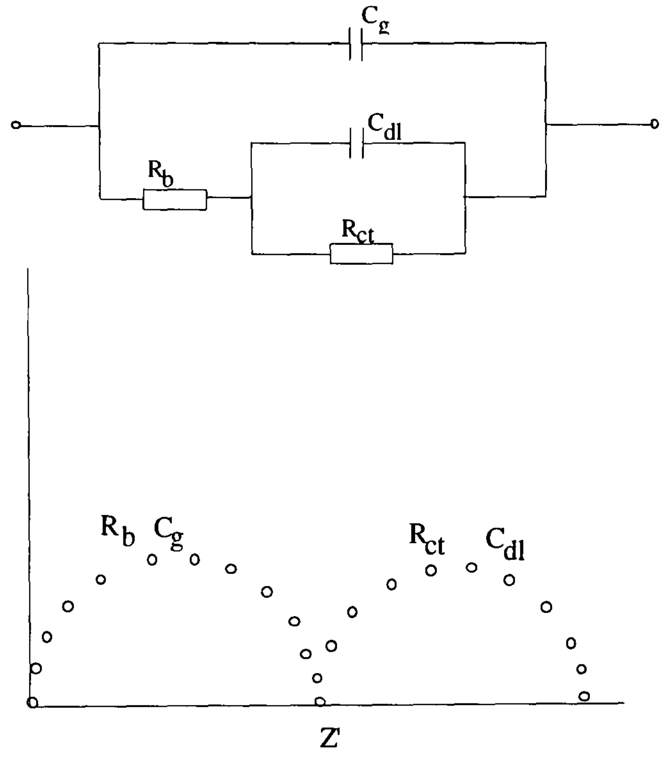

Figure 1.14 - The Impedance Response of a Defective Polymer Coating on a Corroding Substrate in a Corrosive Solution.

1.12 Applications of Electrochemical Techniques for Measuring Corrosion of Painted Metals.

1.12.1 Introduction

Measurement of corrosion rates under paint films is generally less straightforward than measuring corrosion rates of bare metal due to a variety of difficulties not present with bare metal measurements such as the propensity for paint films to be destroyed when subjected to high potentials. In this section some of the literature considering the measurement of corrosion under paint films is reviewed.

1.12.2 DC Measurements

1.12.2.1 Introduction

There are four principal DC electrochemical techniques used for measuring corrosion: Potential / Time Measurements, DC Resistance, Polarisation Curve Measurement and Polarisation Resistance Measurement. Of these, the latter method using Polarisation Resistance has been discussed earlier in section 1.5.1 and 1.7.1. Two principal reviews exist on the subject of DC measurements, by Wolstenholme [25] and Walter [26]. DC measurements on coated metals do have certain disadvantages compared with AC measurements, which will be described.

1.12.2.2 Potential / Time Method

This is the simplest of the electrochemical techniques used to evaluate corrosion. It involves measuring the open circuit potential of the coated metal as a function of time. The evaluation of such data has to be done with care, as the open circuit potential of a metal in itself is not a reliable indication of rate of corrosion, as has been indicated by Evans and in Pourbaix diagrams (section 1.4.3). However, within the potential limits of an active corrosion region as shown on the Pourbaix diagrams changes in the potential of the metal have been taken as indicative of changes in corrosion rate. In general, a positive change in the open circuit potential of the metal has been taken to indicate an increase in the corrosion rate [25]. A review by Wormwell and Brasher [27] produced some results on totally immersed painted steel intended for marine applications. This showed a sharp decline in the potential of the system, followed by a gradual rise to a peak which was at the onset of rusting of the underlying metal. Therefore the time to reach this peak was given as the useful life of the paint. However, a study by Walter [26] on 25 μm thick silicone modified polyester painted galvanised steel, immersed in 5% NaCl has shown the potential to fall prematurely, and then to recover, making interpretation difficult. In addition it is not always possible to measure a stable potential early on in immersion if the coating is very insulating. Kendig and Leidheiser [28] have observed a cathodic shift in the corrosion potential as the coating thickness is decreased suggesting that the cathodic reaction is rate determining. In some recent work done by Burstein and Liu [29], the open circuit potential of freshly cut aluminium was measured as it passivated in phosphate and chromate electrolytes. This showed a rise in the open circuit potential of the system as the aluminium passivated. Measurement of the open circuit potential of steel coated by a zinc rich primer [30] has clearly shown the galvanic protection afforded by the zinc powder within the paint, and the deterioration in this protection with time, shown by a positive increase of the open circuit potential with time.

1.12.2.3 DC Resistance

DC resistance is measured by sandwiching the coating to be measured between either two planar electrodes or the substrate and a planar electrode. This can be done either on a paint film attached to a substrate or a free detached film, although it has been reported that the detached films DC resistance does not always give a good indication of the performance of the paint film [26]. Bacon, Smith and Rugg [32] have used this method and claim that good corrosion protection is given by a paint film with a resistance of greater than 10^{10} Ω. One problem of using this method to determine coating performance is that it can damage or destroy the paint film being measured.

Doubts over whether the DC resistance is actually the true paint film resistance have been raised by Sussex and Scantlebury [31]. They have cast doubt on the interpretation of DC resistance data, as they failed to detect certain types of defects in coal tar epoxy films with more accurate AC techniques and have attributed the DC resistance to a diffusion effect. Wolstenholme [25] has pointed out that that the measured DC resistance includes not just the paint film resistance (if actually measured) but in addition the polarisation resistance of the metal, although this is often small in comparison with the resistance of the paint film.

1.12.2.4 Polarisation Resistance

This is a method has been discussed earlier in section 1.5.1. It is a technique developed by Stern and Geary [10,11] which involves measuring the gradient of the polarisation curve at small perturbations from the open circuit potential. The polarisation resistance method is only really applicable to activation controlled anodic metal dissolution or in some cases by cathodic diffusion control and where there is no ohmic drop, which occurs in high resistance paint films [26]. A problem noted by Popova *et.al* [33] is that the polarisation resistance measured on a coated film includes the ohmic drop and resistance of pores running through the paint film. As a result of these extra resistances they found that corrosion rates were underestimated by a factor of two on measurements made on lacquered tin plate. Therefore polarisation resistance measurements need to be compensated for the effect of the ohmic resistance and pore resistance. Other difficulties using this method come from the time taken for the system to stabilise and give a stable open circuit potential, which has been reported to be up to 30 days [34]. Some of the constraints of this method have been reviewed by González *et.al.*[35] looking at low corrosion rate systems.

1.12.2.5 Polarisation Curves

Polarisation curves have long been used to analyse corroding systems. The background to measurements on bare metal is discussed in section 1.5.1. On a coated metal measurements are complicated by various factors: notably the fact that the ohmic drop from the paint film and electrolyte will be added to the potential of the metal so giving an important source of error [25]. Other problems come from the need to polarise the metal to high positive and negative potentials which can destroy the system under study. To overcome this the anodic polarisation of the system can be minimised and the corrosion current estimated from the intercept of the cathodic line and the corrosion potential, although this can cause problems such as cathodic delamination. Work has been done by Oyabu *et.al* [36] on classifying corrosion under paint films by looking at the position of peaks on the cathodic polarisation curves. They claim that the shape of the cathodic polarisation curve is related to the reduction reactions taking place on the surface of the metal. They, in addition claim to be able to calculate the permeability of the paint film to oxygen. Popova *et.al* [33] have used polarisation curves to calculate the corrosion rate on lacquered tin plate using Tafel analysis.

1.12.2.6 Summary of DC Methods

The use of DC electrochemical methods for studying corrosion under coated metals are more complex than on bare metal. They are not always ideally suited for this type of corrosion testing as they can be destructive and results hard to interpret.

The measurement of Polarisation curves for example, requires that the metal is polarised to high potentials where the film coating system can be damaged. In addition the ohmic drop must be taken into account as this can be a serious source of error when making measurements on coated metals.

Polarisation resistance measurements have the advantage of only applying a small potential to the system, and so are none destructive, but can be difficult to measure accurately as the rest potential on coated metals tends to be unstable.

Potential - Time measurements can be relatively simply and easily performed, but the results can be ambiguous and so does not perform as a reliable corrosion test method on its own

1.12.3 AC Measurements

1.12.3.1 Introduction

The use of Electrochemical Impedance Spectroscopy to make corrosion rate measurements and coating breakdown measurements on painted metals has been discussed previously in section 1.11. The theoretical basis of the analysis of EIS data used in this thesis was proposed by Armstrong and Wright [19]. However there is some controversy in the literature regarding the interpretation of EIS data. In this section some of literature referring to EIS measurements on coated metals is reviewed.

1.12.3.2 Overview

It is generally accepted in the literature that the high frequency response from an EIS analysis of a polymer coated electrode contains information about the nature of the coating [37]. Most of the recent literature states that the low frequency response of the impedance spectrum gives information on the metal-electrolyte interface [38]. This has been virtually proved by the impedance analysis of free and attached coatings made by Feliu *et.al* [39] who found that the low frequency part of the Nyquist impedance plot was not present on detached coatings when comparing directly with coatings attached to metal substrates. Similarly, Walter [40] found the high frequency capacitance values for free and attached coatings to be similar, whilst the value of the metals double layer capacitance was several orders of magnitude higher. This however is where the low frequency part of the impedance spectrum does not give a Warburg type diffusion limited impedance.

1.12.3.3 High Frequency Impedance Response: Coating Impedance

The high frequency part of the impedance spectrum gives information on the coating properties. It can be used to calculate the capacitance of the coating, and from this information can be obtained on the dielectric constant of the coating. Work has been done using the change in dielectric constant of the coating to measure water uptake, and comparing with gravimetric analysis of water uptake [20, 41-43]. The measured dielectric constant of the coating is sensitive to water uptake because the dielectric constant of the water phase in a coating is about twenty greater than the dielectric constant of the pure coating [44].

A perfect coating will give a purely capacitive impedance response. As the coating degrades, ionically conducting pores or cracks in the coating may develop. This situation can be represented as the geometric (coating) capacitance in parallel with the resistance of pores in the coating (bulk resistance). This is discussed more fully in section 1.11.2. This model of the coating is now well established and derives from work by Brasher and Nurse [20], Kendig and Leidheiser [43] and Kendig, Mansfeld and Tsai [45]. Kendig, Mansfeld and Tsai [46] have compared the change in the bulk resistance of the coating with a visual examination of the extent of corrosion of steel coated with polybutadiene. They found a reasonable correlation between the decrease in bulk resistance with immersion time and an increase in the extent of corrosion. However attempts to correlate the delaminated area of the coating with the bulk resistance of the coating proved more difficult.

Skerry and Eden [47] have used the ratio of the theoretical coating resistance of a bare electrode covered with a 60 μm layer of 0.5M NaCl with the bulk resistance of the electrode covered with a 60 μm coating to calculate the 'apparent pore area'. This analysis has been used by Armstrong and Wright [19] to calculate the total porosity of the coating. Skerry and Eden [47] use the pore area values obtained to quantify the performance of coatings: An intact coating having a pore area of in the order of 0.012 $(\mu m)^2$ per cm^2 whilst a degraded coating would have pore areas in the order of 6700 $(\mu m)^2$ per cm^2 or more. More recently many researchers have utilised the break point frequency technique proposed by Haruyama [49] to calculate defect areas in coatings. This is discussed more fully in the next subsection.

Popova *et.al* [33] have suggested that a high value of the bulk resistance indicates a good adhesion of the coating to the substrate. This conclusion seems unlikely, as the bulk resistance only gives information on the properties of the coating and gives no about delamination or adhesion.

1.12.3.4 Low Frequency Impedance Response: Interfacial Impedance

The low frequency part of the impedance spectrum contains information on the reactions occurring at the metal-electrolyte interface. The precise modelling of the charge transfer reactions and double layer capacitance which make up the low frequency impedance is open to some controversy. Mansfeld, Kendig and Tsai [45] propose that the equivalent circuit for the interfacial impedance can be one of two types: Type I has the double layer capacitance and charge transfer resistance in parallel in series with the bulk resistance of the coating, as shown in section 1.11.2. Type II replaces the parallel charge transfer resistance and double layer capacitance with a charge transfer resistance in series with a Warburg impedance. Armstrong and Wright [19] and Schueller and Taylor [48] have considered a transmission line in order to model the resistance of an electrolyte when a coating is delaminated around a defect site. This takes into account the increase in resistance as electrolyte spreads out under a coating.

It is agreed by some researchers [19, 49, 50, 54, 55] that the double layer capacitance and charge transfer resistance of the metal are proportional to the active corrosion area at the bottom of pores and defects in the coating. The measurement of the active corrosion area - the metal-electrolyte interface has been the subject of some discussion in the literature. Some researchers measure it as the total pore area, thus effectively ruling out delamination around the bottom of pores [59]. Haruyama [49] has proposed a model where the double layer capacitance of the metal and the charge transfer resistance of the metal are proportional to what they claim to be the delaminated area.

$$A = \frac{C_{dl}}{C_{dlo}} \qquad A = \frac{R_{cto}}{R_{ct}}$$

Where A is the delaminated area. This is in agreement with Armstrong and Wright [19]. Haruyama goes on to state that the delaminated area is inversely proportional to the bulk resistance:

$$A = \frac{R_{bo}}{R_b}$$

Now this would only be true if the total pore area was equal to the total delaminated area or, in effect, the coating is not delaminated at all. If the coating is delaminated from the substrate metal *i.e.* there is electrolyte spread along the metal-coating interface, then data from the high frequency part of the impedance spectrum will give no information on this [60]. This analysis was found by analysis of the high frequency break point on Bode plots [49]. This is the point where the impedance response changes from either being purely resistive or purely capacitive to contain both elements. This is the same point as the top of the semi-circle on Nyquist plots. The analysis of the high frequency breakpoint has been used by a number of researchers to determine the area of coating defects [49, 52 - 54, 56]. Whilst this breakpoint will give the bulk resistance of the coating and coating capacitance it gives no information on the metal interfacial impedance, as this is found from high frequency impedance data.

McCluney *et.al* [57] have compared Haruyama's breakpoint method [49] for measuring delamination with using ratios of bulk resistance, double layer capacitance and charge transfer resistance to calculate delamination - four separate calculation methods. These were then compared with visual observation of delamination of the coating. They draw no firm conclusion on which is the optimum method to use, despite large deviations in calculated delaminated area after long immersion times.

Van der Weijde *et.al* [58] cast doubt on the equivalent circuit proposed by Haruyama as it separates the impedance response from defects in the film from impedance response from delamination. This, they propose is a rather unlikely situation, since delamination will take place, in most cases, where defects are present on the coating. They go on to say that Haruyama's breakpoint frequency model can not measure delamination as it is based on an inappropriate equivalent circuit.

Deflorian *et.al* [54] compare the breakpoint method proposed by Haruyama with using simple ratios of charge transfer resistance [19] to calculate the delaminated area. It was found that the active area (delaminated area) was found to increase when using the charge transfer resistance ratios to calculate the area, but the active area stayed almost constant when measured by the break point method. They state that the use of charge transfer resistance ratios allows the real active area under the coating to be obtained.

1.12.3.5 Summary of AC methods

Electrochemical Impedance Spectroscopy is possibly the most useful electrochemical tool for studying polymer coated metals. It gives information on, in many cases, the substrate corrosion reactions and the change in properties of the coating. In addition

EIS is none destructive, as it can be performed at the rest potential of the substrate with only small perturbations in the potential required for measurement.

1.13 Aim of this work: Breakdown Mechanisms of Barrier Properties of Organic Coatings

1.13.1 Introduction

Organic coatings can fail, or decrease in effectiveness as a result of various factors. In this thesis three factors that decrease the effectiveness of the polyester-PRIMID system are examined in detail, with the degree of breakdown of the coating and underfilm corrosion rate being measured by various electrochemical and surface techniques. The three causes of coating breakdown examined in this thesis are Mechanical Damage, Artificial UV Weathering and Filiform Corrosion. They are described briefly here, a more complete analysis is presented in later chapters.

1.13.2 Mechanical Damage

Mechanical damage is the impact and perforation of a paint coating by an external object. Damage to paint coatings in this manner is a serious problem, especially in situations where a painted component is in use in a high wear situation, for example in the hold of a bulk carrier or in aircraft. In order to attempt to decrease the effect of mechanical damage, paint coatings are being developed to be more durable or to contain anticorrosive agents which decrease the rate of corrosion on a metal after the overlying paint film has been damaged. An example of this is the use of a zinc rich primer where the zinc cathodically protects steel once in contact damage has occurred. Work in this thesis has concentrated on damage to a durable paint coating, without any anti corrosive agent. The effect of different substrates and different size defects on the delamination of coatings around defects has been studied. The theoretical basis to the instrumentation used has been largely considered already in section 1.11.4 and 1.12.3.4.

1.13.3 Ultra-Violet light weathering

Polyester powder coatings of the type considered in this thesis are commonly used as architectural coatings on, for example, window frames. Thus one of the most significant ways that these coatings degrade is by the action of ultra-violet (UV) light from the sun. Work has been carried out to artificially weather polyester coatings on steel using a QUV_b weathering test chamber and to quantitatively measure the breakdown in the coating barrier properties using Impedance spectroscopy [61].

Ultra violet light degrades polymers because it causes photochemical reactions to occur within the polymer chain. Often the pure polymer may be photochemically stable in itself, but be photosensitised by impurities within the coating. These may absorb light and transfer the energy to the polymer causing oxidative degredation of the free radical chain ends [64]. This causes a general breakup of the polymer binder, which is eventually reduced down to constituent small molecules. This causes the bulk properties of the coating to change: becoming embrittled and cracked. The background to UV degradation of polymer coatings is considered in detail in Chapter 3.

1.13.4 Filiform Corrosion

Filiform corrosion is a type of localised corrosion where thin corrosion filaments grow under polymer coatings. Filiform corrosion was first identified by Sharman in 1944 on lacquer coated steel [62]. It is, perhaps, the least understood of the degradation mechanisms considered, with considerable controversy in the literature on the precise mechanism of initiation and growth. In this thesis, filiform corrosion has been induced on aluminium in accordance with the DIN standard [63] and measured. Substrate and coatings have been varied to see the effect on the rate of filiform corrosion advance and damage to coating. Impedance spectroscopy has been used to measure any breakdown in the coating overlying filiform corrosion filaments. Scanning Electron Microscopy (SEM) has been used to look at the bare substrate and coating. A number of other techniques have been used to look at the mechanical properties of some of the coatings. This has given a better understanding of the mechanism of filiform corrosion.

References

[1] L.L. Shrier, R.A. Jarman, G.T. Burstein (eds.), Corrosion (vol. 1 & 2), 3rd edition, Butterworth-Heinmann (1994).

[2] G. Wranglén, An Introduction to Corrosion and Protection of Metals, Institut for Metallskydd, Stockhom (1972).

[3] M.G. Fontana, Corrosion Engineering, 3rd Edition, McGraw Hill (1987).

[4] J.C. Scully, The Fundamentals of Corrosion, 2nd Edition, Permagon Press (1975).

[5] U.R. Evans, An introduction to Metallic Corrosion, 3rd Edition, Edward Arnold (1981).

[6] S.J. Gregg, W.B. Jepson, *J. Inst. Met.*, **87**, 187, (1958-59).

[7] Corrosion Education Manual, prepared by the Working Party on Corrosion Education of the European Federation of Corrosion, 2nd international edition, Swedish Corrosion Institute, Stockholm (1974).

[8] Defense Research Agency summary on corrosion and protection of aerospace materials. D.R.A. 1993, DRATL 9350.

[9] M. Pourbaix, Atlas of Electrochemical Equalibria in Aqueous Solutions, 2nd Edition, NACE 1974.

[10] M. Stern, A.L. Geary, *J. Electrochem. Soc.*, **104**, 1, 56, (1957).

[11] M. Stern, *Corrosion,* **44**, 60, (Sept. 1958).

[12] G.D. Crapper, University of Manchester, Ph.D thesis 1993.

[13] "Powder Coatings, II, A Multiple-Client Study", Skeist Incorporated, Whippany, NJ 07981 (September 1990).

[14] J.M. Loutz, *Chimia*, **44**, 10, 326 (1990).

[15] "Materials Safety Data Sheet, PRIMID® XL-552", Rohm and Haas Company, Philadelphia, PA 19105 (1991).

[16] "Product Safety Information, Araldite PT 810", Ciba Geigy Plastics, Duxford, Cambridge (1987).

[17] P.G. de Lange, *J. Coat. Tech.,* **56**, 717, 23 (1984).

[18] H. Leidheiser Jr., *Prog. Org. Coat.* **7**, 79 (1979).

[19] R.D. Armstrong, J.D. Wright, *Electrochim. Acta,* **38**, 14, 1799 (1993).

[20] D.M. Brasher, T.J. Nurse, *J. Appl. Chem.,* **9**, 96 (1959).

[21] Southampton Electrochemistry Group, *Instrumental Methods in Electrochemistry,* Ellis Horwood.

[22] A.J. Bard, L.R. Faulkner, *Electrochemical Methods - Fundamentals and Applications,* Wiley.

[23] J.D. Wright, Ph.D Thesis, University of Newcastle upon Tyne, (1992).

[24] B.W. Johnson, Ph.D Thesis, University of Newcastle upon Tyne, (1990).

[25] J. Wolstenholme, *Corrosion Science,* **13**, 521 (1973).

[26] G.W. Walter, *Corrosion Science* **26**, 39 (1986).

[27] H.E. Haring, R.B. Gibney, *Trans. Electrochem. Soc.* **76**, 287 (1939).

[28] M.W.Kendig, H. Leidheiser, *J. Electrochem. Soc.* **123**, 982 (1976).

[29] G.T. Burstein, C. Liu, *Electrochim. Acta* **39**, 873 (1994).

[30] C.A. Gervasi, A.R. Di Sarli, E. Cavalcanti, O. Ferraz, E.C. Bucharsky, S.G. Real, J.R. Vilche, *Corrosion Science* **36**, 1963 (1994).

[31] G.A.M. Sussex, J.D. Scantlebury, *JOCCA*, **66**, 142, (1983).

[32] R.C. Bacon, J.J. Smith, F.M. Rugg, *Ind. Engng. Chem.* **40**, 161 (1948).

[33] S.N. Popova, B.N. Popov, R.E. White, D. Drazic, *Corrosion*, **46**, 1007 (1990).

[34] A. Kliniewski, *Br. Corr. J.* **10**, 91 (1975).

[35] J.A. González, A Molina, M.L. Escudero, C. Andrade, *Corrosion Science*, **25**, 917 (1985).

[36] Y. Oyabu, M. Oda, T. Yamamoto, *Corr. Ctrl. Org. Coat.* 277 (1981).

[37] G.W. Walter, *Corrosion Science*, **26**, 681 (1986).

[38] B.J. Hepburn, K.R. Gowers, J.D. Scantlebury, *Br. Corr. J.* **21**, 105 (1986).

[39] S. Feliu, J.C. Galván, M. Morcillo, *Corrosion Science* **30**, 989 (1990).

[40] G.W. Walter, *Corrosion Science* **32**, 1041 (1991).

[41] G.W. Walter, *Corrosion Science* **32**, 1059 (1991).

[42] D.M. Brasher, A.H. Kingsbury, *J. Appl. Chem.* **4**, 62 (1954).

[43] H. Leidheiser, Jr. , M.W. Kendig, *Corrosion* **32**, 69 (1976).

[44] M.W. Kendig, J. Scully, *Corrosion* **46**, 22 (1990).

[45] M.W. Kendig, F. Mansfeld, S. Tsai, *Corrosion* **38**, 478 (1982).

[46] M.W. Kendig, F. Mansfeld, S. Tsai, *Corrosion Science* **23**, 317 (1983).

[47] B.S. Skerry, D.A. Eden, *Prog. Org. Coat.* **15**, 269 (1987).

[48] G.R.T. Schueller, S.R. Taylor, *J. Electrochem. Soc.***139**, 3120 (1992).

[49] S. Haruyama, M. Asari, T. Tsuru, in "*Corrosion protection by Organic Coatings", The Electrochem. Soc. Proc.* 87-2, 197 (1987).

[50] J. Titz, G.H. Wagner, H. Spähn, M. Ebert, K. Jüttner, W.J. Lorenz *Corrosion* **46**, 221 (1990).

[51] J.R. Scully *J. Electrochem. Soc.* **136**, 979 (1989).

[52] H.P. Hack, J.R. Scully, *J. Electrochem. Soc.* **138** 33 (1991).

[53] I. Thompson, D. Campbell, *Corrosion Science* **36**, 187 (1994).

[54] F. Deflorian, L. Fedrizzi, A. Locaspi, P.L. Bonora, *Electrochim. Acta* **38**, 1945 (1993).

[55] F. Mansfeld, C.H. Tsai, *Corrosion* **47**, 958 (1991).

[56] C. Compère, É. Fréchette, E. Ghali, *Corrosion Science* **34** 1259 (1993).

[57] S.A. McCluney, S.N. Popova, B.N. Popova, R.E. White, *J. Electrochem. Soc* **139**, 1556 (1992).

[58] D.H. Van der Weijde, E.P.M. van Westing, J.H. de Wit, *Corrosion Science* **36**, 643, (1994).

[59] F. Mansfeld, *J. Appl. Electrochem.* **25**, 187, (1995).

[60] R.D. Armstrong, A.T.A. Jenkins, *J. Appl. Electrochem.* Accepted for publication, May 1995.

[61] R.D. Armstrong, A.T.A. Jenkins, B.W. Johnson, *Corrosion Science*, **37** 1615, (1995).

[62] C.F. Sharman, *Nature* **153**, 621 (1944).

[63] Deutsches Institut für Normung e. V. , Number 65 472. Filiform Corrosion Test of Coatings on Aluminium Alloys. 1989. (draft).

[64] B. Rånby, A. Hult, *Org. Coat. Sci & Tech.*, Vol. 7, Eds. G.D. Porfitt and A.V. Patsis.

[65] J. O'M Bockris, J. McBreen, L. Nanis, *J. Electrochem. Soc,* **110**, 102, (1965).

[66] K. Nisancioglu, H. Leth-Olsen and O. Lunder, *Proc. Corr. Prev. Org. Coat.* Cambridge, (1994).

[67] P.W. Atkins, *Physical Chemistry*, 4th Edition 1990, Oxford.

PAGE

NUMBERING

AS ORIGINAL

Chapter 2

Experimental

2.1 Introduction

This chapter details the experimental procedures used in the work carried out for this thesis. Electrochemical Impedance Spectroscopy (EIS) has been described in detail in Chapter 1. so will be dealt with here only with relevance to the specific experimental equipment used. This chapter is divide into roughly five sections. The first section will deal with general techniques common to all of the work, the next three sections will concentrate on the areas of mechanical damage to paint films, UV weathering and filiform corrosion respectively. Finally the use of a different impedance analysis program is considered, the Boukamp NLLS fit program [6] is compared with the Gary Evans fitting program [5].

2.2 Production of Coated Substrates [1,2]

2.2.1 Coating Preparation

The precise details of the formulation of the coatings used cannot be given owing to their commercial sensitivity.

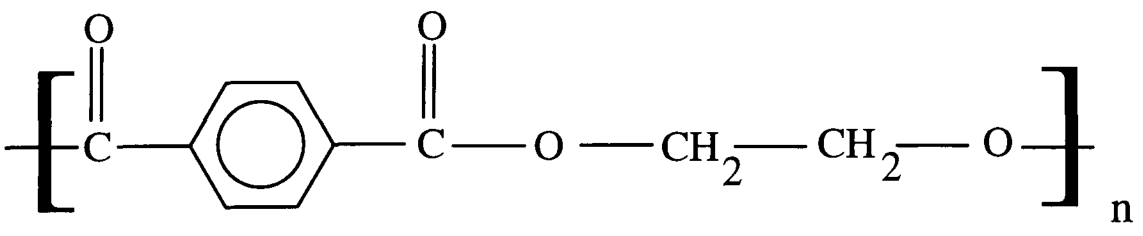

Figure 2.1 General structure of polyester resin.

Polyester resin of a nature similar to that shown in figure 2.1, PRIMID® (A multifunctional amide cross linker), pigment (if used) plus additives were weighed out and mixed together as a powder. This powder was extruded twice through a twin screw extruder where the powder was heated and mixed to above its melt temperature, but below its cure temperature, so cross linking reactions are negligible. The resultant extrudate was broken into coarse chips and ground in a rotary grinder to a fine powder. This powder was sieved to give particle diameters in the range 8 μm to 106 μm.

Oversize particles were re-ground. Different pigmentation was used in the various experiments, and slightly different formulations used, although all coatings consisted of the PRIMID® cross linked polyester system.

2.2.2 Substrate Preparation

An important aspect in the production of coated metal is the preparation of the substrate to ensure good adhesion of the paint coating. All the steel panels used were purchased commercially as 6" x 4" 'Q panels'. These panels were degreased by rinsing in xylene and then acetone. This removed the oil film covering the panels, as supplied. The aluminium panels were immersed in 1M sodium hydroxide for approximately 4 minutes to remove the air formed oxide film, then rinsed in ultra pure water.

2.2.3 Coating Application to Substrate

This was done using an electrostatic spray system shown in figure 2.2. In an electrostatic spray system, the powder is blown by compressed air through a spray gun where it is electrically charged by a high voltage corona electrode (30 - 100 KV). The substrate metal being coated is earthed. Thus a combination of electrostatic attraction and mechanical carrying by compressed air carries the powder particles onto the metal. Oversprayed powder can, in principle, be reapplied by a continuous feed back system.

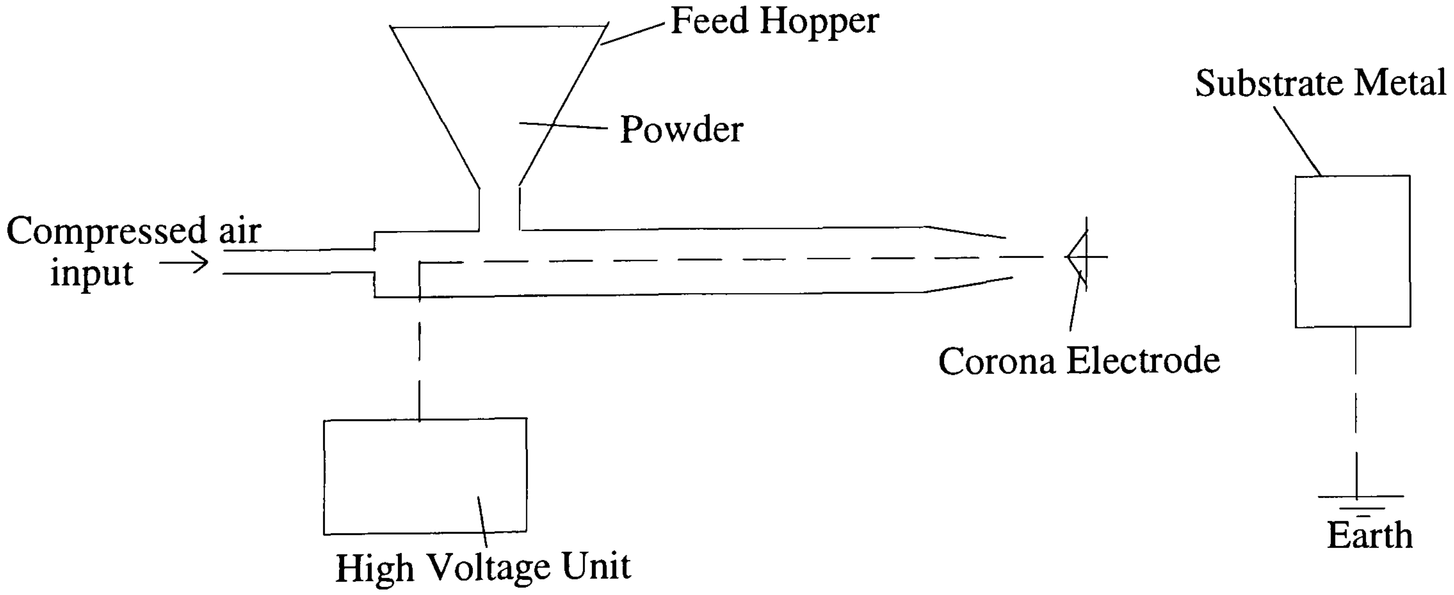

Figure 2.2 Simplified diagram of electrostatic spray appuraters.

Following application of the powder to the substrate, the powder layer has to be turned into a durable film. This was achieved by heating the powder coated substrate to 200° Celsius for fifteen minutes. This allows the PRIMID® to cross link the polyester and for the powder to melt and flow over the substrate surface. The thickness of the coating was measured using an Elcometer™ ultrasound film thickness tester. This was done at nine points on each coating and averaged.

2.3 Study of Substrate Metal

The substrate metal has been analysed principally by electrochemical measurements, using DC and AC electrochemical methods. This has allowed the corrosion rate of the metal under different electrolytes to be measured.

Non-electrochemical analysis of the substrate was performed on the aluminium used in the filiform corrosion experiment, where knowledge of the nature of the substrate was critical. Scanning Electron Microscopy (SEM), EDX and Laser profilemetry were employed,. This will be decribed in more detail in the relevant chapters.

2.4 Electrochemical Methods

All electrochemical measurements were made in deaerated electrolyte by bubbling with nitrogen unless explicitly stated otherwise.

2.4.1 Electrolyte

In this thesis, three different electrolytes have been used for the electrochemical experiments:

Mechanical Damage Analysis:

Steel: Acetate buffer initially, 0.1M Hydrochloric acid later
Aluminium: 0.1M Sulphuric acid.

Acetate Buffer electrolyte comprised 0.1M sodium acetate, 0.1M sodium chloride and 0.1M acetic acid.

UV Weathering:

0.1 M Hydrochloric acid throughout.

Filiform Corrosion:

0.1 M Sulphuric acid throughout.

All electrolytes were made from AnalaR® grade chemicals and Purite® Ultra pure water.

2.4.2 Reference Electrodes [3]

Silver / Silver Chloride

The Silver / Silver Chloride electrode was used for all the mechanical damage experiments on steel and all the experiments on UV weathering.

The Ag/AgCl electrode was made from 2mm diameter silver rods (Goodfellow Ltd.). These rods were cleaned with emery cloth and dipping in conc. HNO_3 and rinsing with ultra pure water. The silver was then anodised in 0.1M KCl at a current of 0.5 mA for ten minutes. The electrodes were then tested against each other, a potential difference of less than 2 mV was considered satisfactory.

Saturated Calomel

The Saturated Calomel Electrode (SCE) was used in all the filiform corrosion experiments and the mechanical damage experiments involving aluminium. The electode was constructed by taking an electrode holder and creating a frit with glass wool. On top of this was put twice distilled mercury. A mercury / mercurous oxide paste was then added and this was covered with a mercurous chloride top layer. The electrode was topped up with saturated potassium chloride solution and the outside of the glass frit kept immersed in saturated potassium chloride. Measurements were made via a salt bridge.

The salt bridge was constructed by heating 100 ml of saturated potassium nitrate and adding 3g of agar. The mixture was simmered and stirred for ten minutes and then sucked through clean plastic or glass tubing and cooled until a gel formed [4]. One end was kept in the saturated KCl attached to the SCE, the other in the cell electrolyte.

2.4.3 Electrochemical Cell

The electrochemical cell was based on a design used by J.D. Wright [3]. It is shown in figure 2.3. The cell was clamped to the substrate by means of Araldite™ expoxy adhesive. Two different flange diameters at the base of the cell were used. For all the experiments carried out on mechanical damage and UV weathering a 2.5 cm diameter flange was used, giving a working electrode area of 4.9 cm^2. For the filiform corrosion experiments a smaller flange was used, in order to more effectively discriminate between different areas of coating. The diameter here was 1 cm, giving an area of 0.785 cm^2.

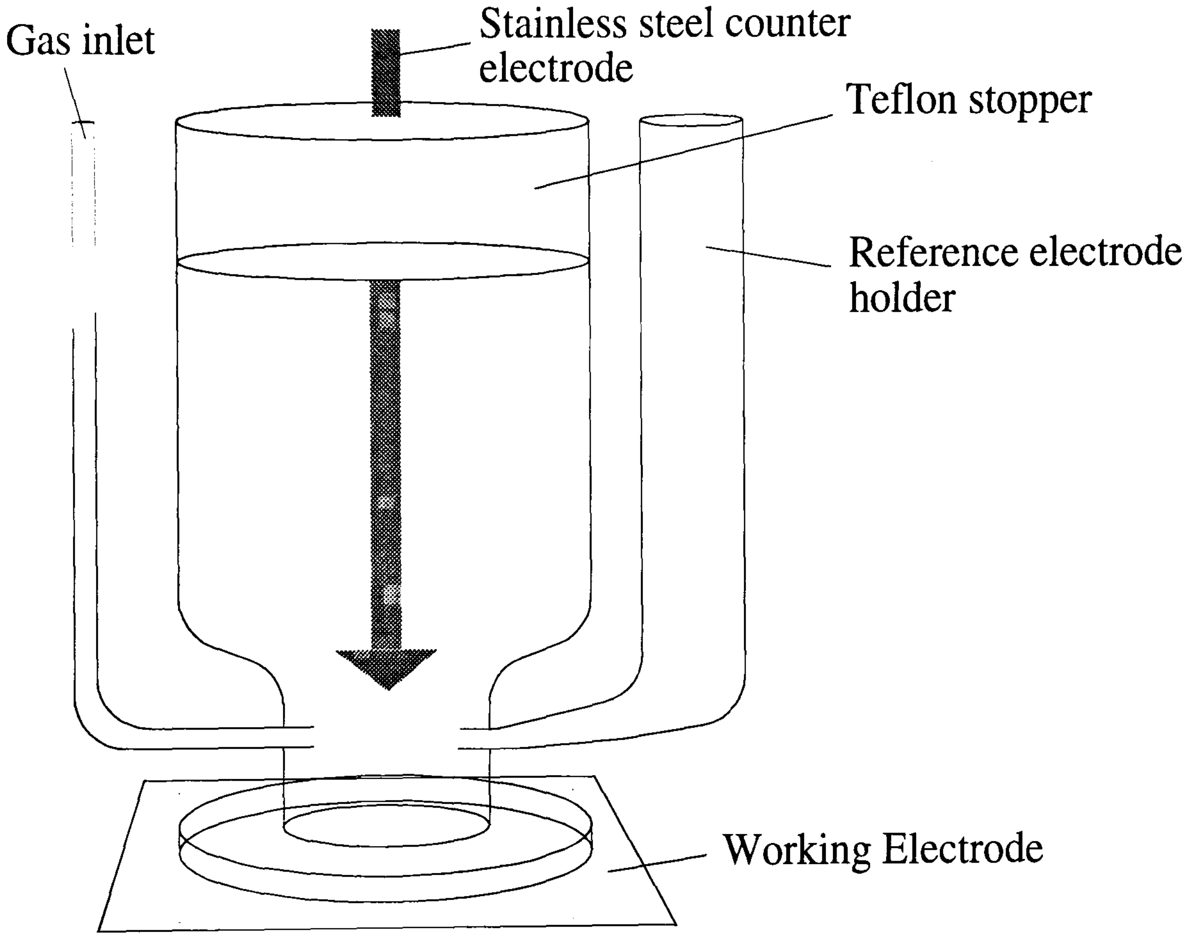

Figure 2.3

Between experiments the araldite was removed by soaking in dichloromethane and then washing in conc. HNO_3 followed by rinsing in ultra pure water.

2.4.4 DC Measurements

DC measurements were made on the bare metal substrate using an EG&G Versastat™ potentiostat, connected to a 80386 Personal Computer via an IEEE 488/GP-IB interface, which allowed two way communication between computer and potentiostat. The resultant data were either analysed using the software suplied by EG&G or exported to a spread sheet such as Microsoft Excel. Linear Sweep Voltammetry (LSV) was the principle DC technique. Tafel slopes of the data were found by taking the log of the current and extrapolation of the linear region used to calculate corrosion current and potential.

2.4.5 AC Measurements

AC measurements were made using a Solatron 1255 Frequency Response Analyser (FRA) connected to a potentiostat constructed 'in house'. The FRA is an AC signal generator with a lock in amplifier. The FRA was connected via a IEEE 488/GP-IB interface to a Viglen 80286 Personal Computer.

AC measurents on steel were made at the rest potential of the bare steel at -470 mV vs. Ag/AgCl. This was to prevent increased rate of anodic or cathodic reaction. AC measurements on aluminium were all made at -500 mV vs. SCE unless explicitly stated otherwise. This was because aluminium does not have a well defined rest potential, like steel. Therefore a potential that would allow effective comparison of spectra was chosen that would be near the rest potential. The AC signal was 10 mV RMS / 30 mV Peak - Peak. This was high enough to give a reasonably noise free signal (in most cases) but low enough to prevent irreversible changes to the metal-polymer interface. The frequency was swept down from 10 kHz to around 100 mHz, although a lower frequency limit was sometimes used if necessary.

The resultant AC Impedance spectrum was displayed as a Nyquist (complex plane) plot, with 'best fit' semi circles being fitted to the data. The principle software fitting program used to fit a semicircle to the impedance data was developed by G.P. Evans [5]. This program fitted all selected points to a simple semi-circle using an iterative best fit routine.

A more complex semi circle fitting program was looked at, the Boukamp Analysis Program [6]. This program initially fits a three point semi circle to the impedance. This three point fit was then modified by considering all the required points on the semicicle and using an iterative best fit routine and fitting an equivalent circuit to the data. However, this program is more sophisticated in that it allows a none standard semicircle - a flattened semicircle, down to a quarter circle to be fitted, and measures the degree of depression on the semi circle. This was only investigated latterly due to the acquisition of the software towards the end of this Ph.D work. It is considered in more detail in section 2.9.

2.4.6 Processing of EIS Data to provide Porosity and Wetted Metal Area Parameters.

In chapter 1 the means by which the four essential parameters from a metal / defective coating system could be obtained from a Nyquist impedance plot were examined. These parameters are:

Coating (geometric) capacitance,	C_g
Bulk (pore) resistance,	R_b
Double layer capacitance,	C_{dl}
Charge transfer resistance,	R_{ct}

Once these parameters have been obtained for a system, the method of calculation of wetted metal area and porosity developed by Armstrong and Wright [9] was utilised in the way shown:

Porosity was determined as the ratio of the theoretical bulk resistance of the film at 'infinite' porosity (R_{bt}) to the measured coating bulk resistance (R_b) :

$$Porosity(P) = \frac{R_{bt}}{R_b} \qquad \text{Where:} \qquad R_{bt} = \frac{d}{A\kappa}$$

d = Film Thickness
A = Electrode area
κ = conductivity of electrolyte

The wetted metal area was taken to be the ratio of the double layer capacitance of the bare metal of the same area (C_{dlo}) to the double layer capacitance at the bottom of pores on the film covered metal (C_{dl}).

$$\text{Wetted metal area, } W = \frac{C_{dl}}{C_{dlo}}$$

This has been considered in detail in Chapter 1, section 1.11.

2.5 Scanning Electron Microscopy

Scanning Electron Microscopy (SEM) was used to look at localised area of the surface on many of the films. SEM images were obtained using a JEOL JSM-T20 scanning electron microscope. The coatings were sputtered with a few nanometers of gold prior to analysis - to form a conducting surface. Potential problems of damage to the surface of the polymer were avoided by generally not scanning at very high magnifications, which concentrates the electron beam and not spending too long examing a single piece of the polymer. Where damage was caused, the results were not used.

In a Scanning Electron Microscope, a probe of electrons is scanned across the surface of the sample [10]. Electrons that are excited or reflected by the surface are detected and displayed to form an image of the surface.

2.6 Mechanical Damage Experiments

In these experiments coated steel or aluminium was perforated with drill or mill end cutter to a fairly precise geometry. Holes were made at 1.5 mm in diameter on coated steel, 1.5mm and 0.6 mm diameter on coated aluminium. Care was taken to ensure that the all the coating in the drilled area was removed. The change in double layer capacitance and charge transfer resistance were measured with respect to immersion time in electrolyte. The degree of delamination under the film was correlated with delamination that could be measured visually. On the coated aluminium, two different size holes were made, on separate samples, with the relative rate of delamination with respect to defect size measured.

2.6.1 Modelling of Mechanical Damage using Equivalent Circuits

This work was done in order to model the type of delamination taking place with resistors and capacitors in parallel and series. Basic RC elements corresponding to the interfacial impedance were connected together as a transmission line with resistors modelling change in resistance under the delaminated coating.

The resultant equivalent circuit was connected to the FRA and run in the same way as a real cell, apart from a 0.00V DC offset and in two electrode mode on the potentiostat. Comparison of the resultant impedance spectra with the known impedance values of the circuit elements gave an indication of the degree of accuracy of the impedance measuring system, for different equivalent circuits. This information could then be used to determine whether impedance measurements on real systems can, in certain circumstances either over-estimate or under-estimate the impedance of the system.

2.7 Artificial UV Light Weathering of Polymer Coatings

For this work two polyester powder coatings were prepared. They were identical apart from the fact that one was clear and the other pigmented with photo-deactivated titanium dioxide (white). The powders were applied to steel in the way previously described.

The coated panels were weathered in a QUV weathering chamber [7] for up to 450 hours which provide four hours on a light irradiation cycle and four hours on a humidity cycle. The panels were then attached to a cell, and the EIS response measured with respect to different immersion times in 0.1M hydrochloric acid. Each panel had a none weathered section measured as a control. The EIS response gave information on the change in porosity of the coating and, in most cases, the degree of wetted metal area (delamination of the coating) on the substrate.

A sample of the panels were subjected to thermal cycling between 20°C and 50°C in order to measure the effect of the heating experienced by the QUV weathered panels but without the UV exposure.

The light reflectance (gloss loss) of the pigmented films were measured after different weathering times. Gloss is a measure of the refection of a beam of visible light off the surface at two angles, 20° and 60° to the normal. Gloss loss gives a picture of the break-up of the surface of the coating, with the degree of light reflection (gloss) decreasing as the coating degrades.

Scanning Electron Microscopy was used to look at the weathered and non-weathered coatings. The results were compared with the results obtained from impedance spectroscopy of identical films. The highest magnification achieved was x 20,000. The effects of different weathering times in the QUV test chamber were examined.

Finally the results from the EIS analysis, Light reflection and SEM were compared in order to see if the three methods gave compareable information on the degree of coating degredation after QUV weathering.

2.8 Filiform Corrosion

The experimental work on filiform corrosion has looked at the influences of substrate and coating on filiform corrosion. EIS was used to measure if coatings overlying filiform corrosion filaments broke down, and if so, to what extent.

2.8.1 Substrates and Coatings

Two aluminium substrates were studied. Q panel aluminium, a commercial available sheet aluminium and Alcan aluminium, an extruded aluminium. The two substrates were coded Q and A aluminium, respectively. Physically, the Q aluminium had a fairly uniform surface with a milled finish whilst the A aluminium had extrusion lines running vertically down its length. A range of tests were done on the two substrates prior to coating:

2.8.1.1 Electrochemical Testing

This was done to look at the linear sweep voltammograms of the aluminium and the AC response, under 0.1M sulphuric acid, under oxygen and nitrogen. The AC experiments were performed at different DC offset potentials, in order to determine a sutiable potential at which to polarise the coated aluminium. The electrochemical setup is as described previously. Specific details relating to the individual experiments will be given in the relevant chapter.

2.8.1.2 Non-Electrochemical Substrate Analysis

Three principle experiments were performed on the aluminium:

1. Scanning Electron Microscopy

This gave an impression of the surface morphology of the surface and the distribution of intermetallics on the surface and has been considered already.

2. EDX

EDX stands for Energy Dispersive X-ray spectroscopy. EDX was used to determine the degree of non-aluminium metallic impurities in the aluminium substrates by measuring the energy of X-rays emitted from the surface of the aluminium and impurity metals as the electron beam passed over different elements. The energy of these X-rays is characteristic of the elements present. The intensity of the resultant X-ray beam is proportional to how much of an element is present in the top surface of the metal [10].

3. Laser Profilemetry

This involves scanning a laser stylus over an area of substrate. The instrument used was a UBM Optical Surface Measurement System. More information on this technique is given in Chapter 5.

2.8.2 Initiation of Filiform Corrosion

Two separate experiments were done on filiform corrosion, the first largely looked at the effect of substrate, the second experiment largely at the effect of the glass transition temperature of the coating on filiform corrosion advance.

The coatings on the substrate were scored through to the substrate with a tungsten carbide blade and then exposed to a hydrochloric acid vapour for one hour. This was done by putting 1 litre of concentrated hydrochloric acid in a covered Nalgene® tank and leaving for one hour. The scored coated aluminium was then put into the tank, but held 10 cm above the hydrochloric acid liquid. They were kept in this vapour for one hour. After one hour the coated aluminium was put in a humidity cabinet for up to 55 days at 40° Celsius, 82% relative humidity. This was done to in accordance with the standard [8].

2.8.2.1 Experiment 1

The aim of this work was to determine the effect of substrate on filiform corrosion, and to compare the porosity measurements of the two coatings on the substrates. In this experiment the A and Q aluminium were pretreated by immersion in 1M sodium hydroxide for five minutes, to remove the air formed oxide film. The aluminium substrates were coated with two polyester coatings, a grey coloured pigmented coating (G1) and a clear, none pigmented coating (W1). In all there were six samples of each substrate-coating combination, twenty four in all. In addition the substrates were coated on both sides.

Six A aluminium + G1 coating
Six A aluminium + W1 coating
Six Q aluminium + G1 coating
Six Q aluminium + W1 coating

The resultant filiform corroded substrate / coating systems were subjected to study described in 2.8.2.3.

2.8.2.2 Experiment 2

This experiment was done to see if using two coatings, with different glass transition temperatures (T_g) on identical substrates would give different levels of filiform corrosion growth.

Two blue coloured pigmented polyester powder coatings (D200 and D42) were prepared and applied to pretreated Q aluminium. They were treated as previously described in order to initiate filiform corrosion. In addition samples of the coatings were removed and analysed by Differential Scanning Calorimetry (DSC) in order to measure the T_g's of the coatings. The resultant filiform corroded substrate / coating systems were subjected to study described in 2.8.2.3.

2.8.2.3 Analysis of Filiform Corrosion

Filiform Growth Rate Measurement

After approximately four days filiform corrosion filaments started to grow. These were measured roughly every six days for a fifty five day period. One or two filiform corrosion filaments were selected on each substrate-coating combination. These were selected on the basis of how representative they are of the all the filiform corrosion filaments growing on the coated substrate. The filaments were measured to an accuracy of about ± 0.5 mm, with a ruler.

Measurement of Barrier Properties of Coating overlying Filiform Corrosion

The coating overlying the filiform corrosion filaments was measure by placing a small impedance cell of 10 mm diameter over the coating, with the filiform corrosion filament running under the coating and running an EIS experiment. This enabled the porosity of the coating above the filiform corrosion to be measured. The coating unaffected by filiform corrosion was also measured in a similar way as a comparison. This method gave an area of coating overlying the filiform corrosion of about 0.04 cm^2 in a total electrode area of 0.786 cm^2 or about 5 %.

Scanning Electron Microscopy

SEM images of the coating overlying the filiform corrosion filaments were obtained by tilting the coating in the microscope up to 45° to the incident beam of electrons. This allowed the degree of deformation of the coating be better observed.

2.9 Comparison of the Gary Evans Software for Impedance Data Analysis with The Boukamp NLLS Program

A study of the Boukamp Impedance analysis program [6] was been carried out. This has involve comparing impedance data from various experiments and fitting circles to them using three techniques:

1. Gary Evans software [5], utilising a multi point true semicircle fit, but no figure for n, the depression of the semicircle.

2. Boukamp's 3 point circle fit.
3. Boukamp's simplified None Linear Least Squares (NLLS) fit.

Boukamp's NLLS fit is the most accurate fitting program, so a cross section of experimental results, which were previously analysed using the Gary Evans software were re-analysed using Boukamp's NLLS fitting program. This was to determine if there were significant differences in results using Boukamp's software. The Boukamp NLLS program fits a circle between a semi and quarter circle to the experimental data, and gives an indication of the degree of semi-circularity by the number, n. When n = 1 a perfect semicircle is fitted.

These systems were re-examined:

1. Bare Steel. Hydrochloric acid electrolyte. N_2
2. Bare aluminium. Acetate buffer electrolyte. N_2
3. Bare aluminium. Sulphuric acid. O_2
4. Mechanically damaged polyester on aluminium. Sulphuric acid electrolyte. N_2
5. Filiform corrosion damaged polyester on aluminium, sulphuric acid, N_2.
6. Mechanically damaged polyester on steel. Hydrochloric acid electrolyte. N_2

Results

1. Bare Steel under Hydrochloric acid, N_2

Gary Evans software:	$R = 75.3\ \Omega$; $C = 211\mu F$
Boukamp 3 Point fit:	$R = 74.9\ \Omega$; $C = 282\mu F$; $n = 0.926$
Boukamp Partial NLLS Fit:	$R = 75.5\ \Omega$; $C = 297\mu F$; $n = 0.914$

2. Bare Aluminium under acetate buffer electrolyte, N_2

Gary Evans software:	$R = 3.16\ K\Omega$; $C = 65.6\ \mu F$
Boukamp 3 Point fit:	$R = 3.15\ K\Omega$; $C = 69.0\mu F$
Boukamp Partial NLLS Fit:	$R = 3.18\ K\Omega$; $C = 69.6\mu F$; $n = 0.958$

3. Bare Aluminium under sulphuric acid, O_2

Gary Evans software: R = 362 Ω ; C = 34.9 μF
Boukamp 3 Point fit: R = 359 Ω ; C = 30.9 μF
Boukamp Partial NLLS Fit: R = 376 Ω ; C = 37.0 μF ; n = 0.978.

4. Mechanically Damaged Polyester on Aluminium, sulphuric acid, N_2.

Gary Evans Software: R = 237 KΩ ; C = 0.08 μF
Boukamp 3 Point fit: R = 200 KΩ ; C = 0.12 μF ; n = 0.9806
Boukamp Partial NLLS Fit: R = 257 KΩ ; C = 0.15 μF ; n = 0.941

5. Filiform Corrosion Damaged Polyester on Aluminium, sulphuric acid, N_2.

(a) High Frequency (Coating Impedance)

Gary Evans Software: R = 2 MΩ ; C = 200 pF
Boukamp 3 Point fit: R = 1.62 MΩ ; C = 593 pF ; n = 0.850
Boukamp Partial NLLS Fit: R = 1.50 MΩ ; C = 279 pF ; n = 0.945

(b) Low Frequency (Interfacial Impedance)

Gary Evans Software: R = 7.0 MΩ ; C = 0.3 μF
Boukamp 3 Point fit: R = 6.33 MΩ ; C = 0.49 μF ; n = 0.797
Boukamp Partial NLLS Fit: R = 5.86 MΩ ; C = 0.44 μF ; n = 0.823

6. Mechanically Damaged Polyester Coating on Steel, hydrochloric acid, N_2.

Gary Evans Software: R = 6.17 KΩ ; C = 7.11 μF
Boukamp 3 Point fit: R = 6.22 KΩ ; C = 9.21 μF ; n = 0.901
Boukamp Partal NLLS Fit: R = 6.77 KΩ ; C = 11.4 μF ; n = 0.808

Conclusion

From the re-analysis of results it can be seen that the results from using the Boukamp analysis program are not substantially different from the results calculated from the

Gary Evans Software program where n, the degree of semicircularity - the depression of the semicircle is close to 1. This is to be expected as the Gary Evans Software program only fits a perfect semicircle. As the data moves away from being a perfect semicircle so the Gary Evans program becomes less accurate. It can generally be seen that when the value n deviates along way from unity, the Gary Evans Software underestimates the measured capacitance by up to 40%. However this degree of error is not too impprtant as most comparrisons of impedance results are based on order of magnitude differences between quantities.

References

[1] G.D. Crapper, University of Manchester, Ph.D thesis 1993.

[2] "Powder Coatings, II, A Multiple-Client Study", Skeist Incorporated, Whippany, NJ 07981 (September 1990).

[3] J.D. Wright, Ph.D. Thesis, University of Newcastle upon Tyne. (1992).

[4] H.V. Newton, Ph.D. Thesis, University of Newcastle upon Tyne. (1994).

[5] G.P. Evans, Ph.D. Thesis, University of Newcastle upon Tyne. (1985).

[6] B.A. Boukamp, *Solid State Ionics*, **18 & 19,** 136 (1986).

[7] ASTM Standard G53, Designation D 4587 - 86.

[8] Deutsches Institut für Normung e. V. , Number 65 472.

[9] R.D. Armstrong, J.D. Wright, *Electrochim. Acta,* **38**, 14, 1799 (1993).

[10] I.P. Jones, *Chemical Microanalysis using Electron Beams,* (1992), Institute of Materials.

PAGE

NUMBERING

AS ORIGINAL

Chapter 3

A Study of the Electrochemical Response of Uncoated Steel and Aluminium and the effect of Mechanical Damage to Polyester Coatings

3.1 Aim

The initial aim of this work was to gain information on the electrochemical response of the bare metal substrates used in the various experimental work described in this thesis. Subsequently the EIS response of polyester coated steel and aluminium was studied, before and after damage to the coating. EIS measurements made on the mechanically damaged polyester coated substrate were used to estimate the degree of delamination of the coating around the defect site. This was used to determine differences in delamination on different substrates and the effect of defect size on delamination rates on damaged, coated aluminium.

3.2 Electrochemical Response of Bare Steel and Aluminium

The electrochemistry of bare steel and aluminium corrosion is well documented in the literature [1, 3-6, 11]. However, for the subsequent analysis of the EIS data described in this thesis, a precise knowledge of the impedance characteristics of the substrates used under the respective electrolytes was required. In addition, a knowledge of the DC response of the substrates was required in order that the overall electrochemical response of the substrate could be visualised and the Tafel gradients obtained to allow the Stern - Geary approximation to be used (in the case of steel). The discussion and results of the corrosion and DC response of aluminium are given in Chapter 5. Knowledge of the bare metal resistance and capacitance values was required to subsequently calculated wetted metal areas of coated, damaged polymer coated steel and aluminium.

3.3 Bare Steel

3.3.1 DC Response (Linear Sweep Voltammetry)

The general electrochemical behaviour of bare steel has been well documented in the literature [1]. The linear sweep polarisation curve of steel under deaerated 0.1M HCl was found. The gradients of the anodic and cathodic Tafel slopes were determined and the corrosion current and potential found from Tafel slope extrapolation. The plot is shown in figure 3.1. The Tafel region and region of current limited by the iR drop between the reference electrode and working electrode are shown.

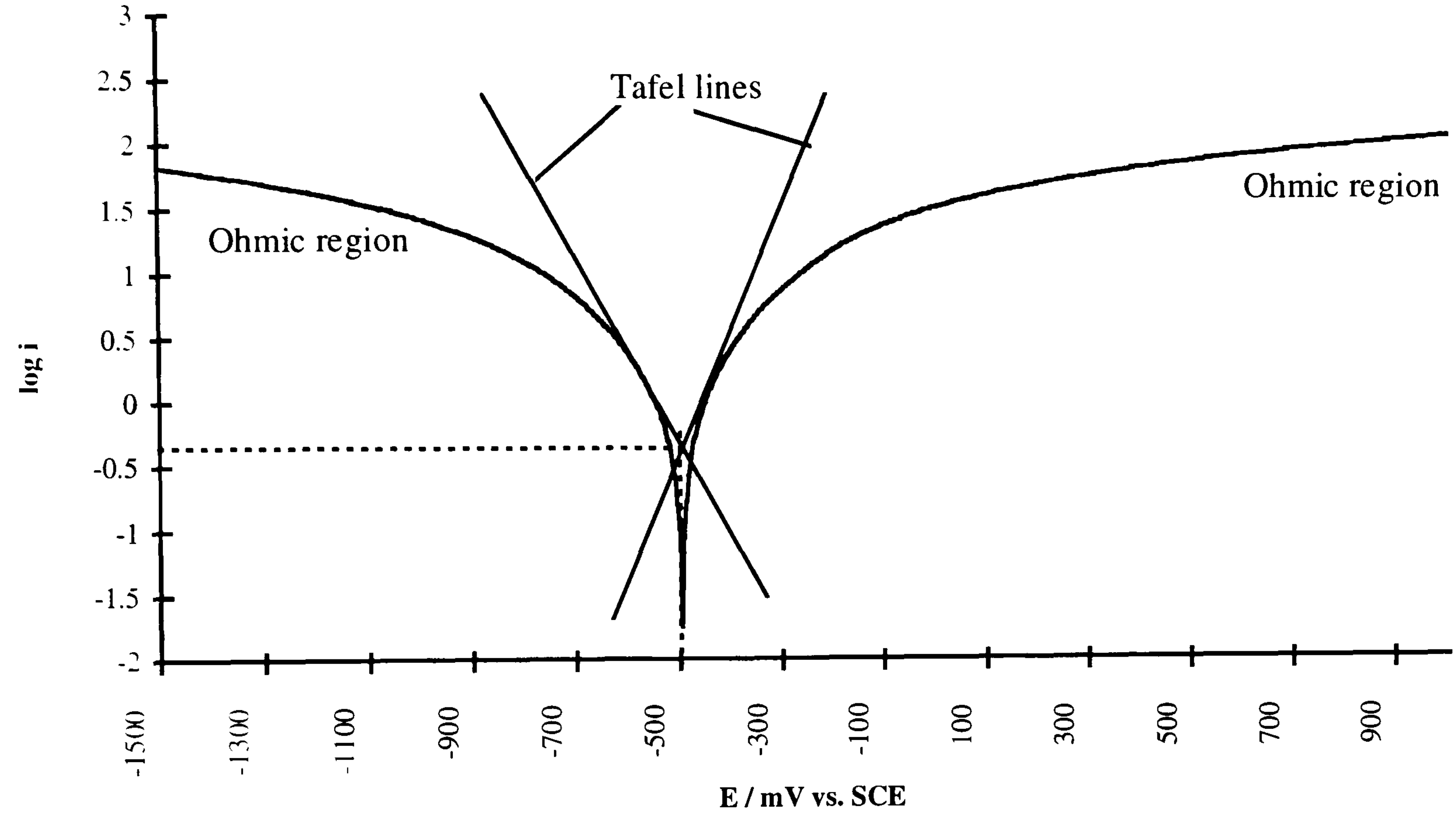

Figure 3.1- Tafel Plot of Steel under deaerated 0.1M HCl

In figure 3.1 the anodic (iron dissolution) gradient is approximately 60 mV decade^{-1} and the cathodic (hydrogen evolution) gradient is 150 mV decade^{-1}. This is reasonably close to the literature [11] values of 40 mV decade^{-1} (anodic) and 140 mV decade^{-1} (cathodic). From the extrapolation of the Tafel lines it can be seen that :

The corrosion current is 0.40 mA cm^{-2}.
The corrosion potential is ~ -490 mV *vs.* SCE.

3.3.2 AC Response (EIS)

The EIS response of the bare steel in 0.1M HCl is shown in figure 3.2. The EIS results of steel in acetate buffer electrolyte are also given. The appearance of the EIS data (displayed as a Nyquist plot) is similar for both electrolytes, as a single semi-circle. EIS measurements on steel were made at the open circuit potential of the steel.

Fitting of a best-fit multi point semicircle to both plots gave the double layer capacitance and charge transfer resistance of the steel under the different electrolytes. Note: Working electrode area = 4.9 cm^2

Acetate Buffer

Double layer capacitance, $C_{dl} = 400\ \mu F$
$C_{dl} = 81.6\ \mu F\ cm^{-2}$

Charge transfer resistance, $R_{ct} = 80\ \Omega$
$R_{ct} = 392\ \Omega\ cm^{-2}$

0.1 M Hydrochloric acid

Double layer capacitance, $C_{dl} = 210\ \mu F$
$C_{dl} = 42.9\ \mu F\ cm^{-2}$

Charge transfer resistance, $R_{ct} = 75\ \Omega$
$R_{ct} = 367.5\ \Omega\ cm^{-2}$

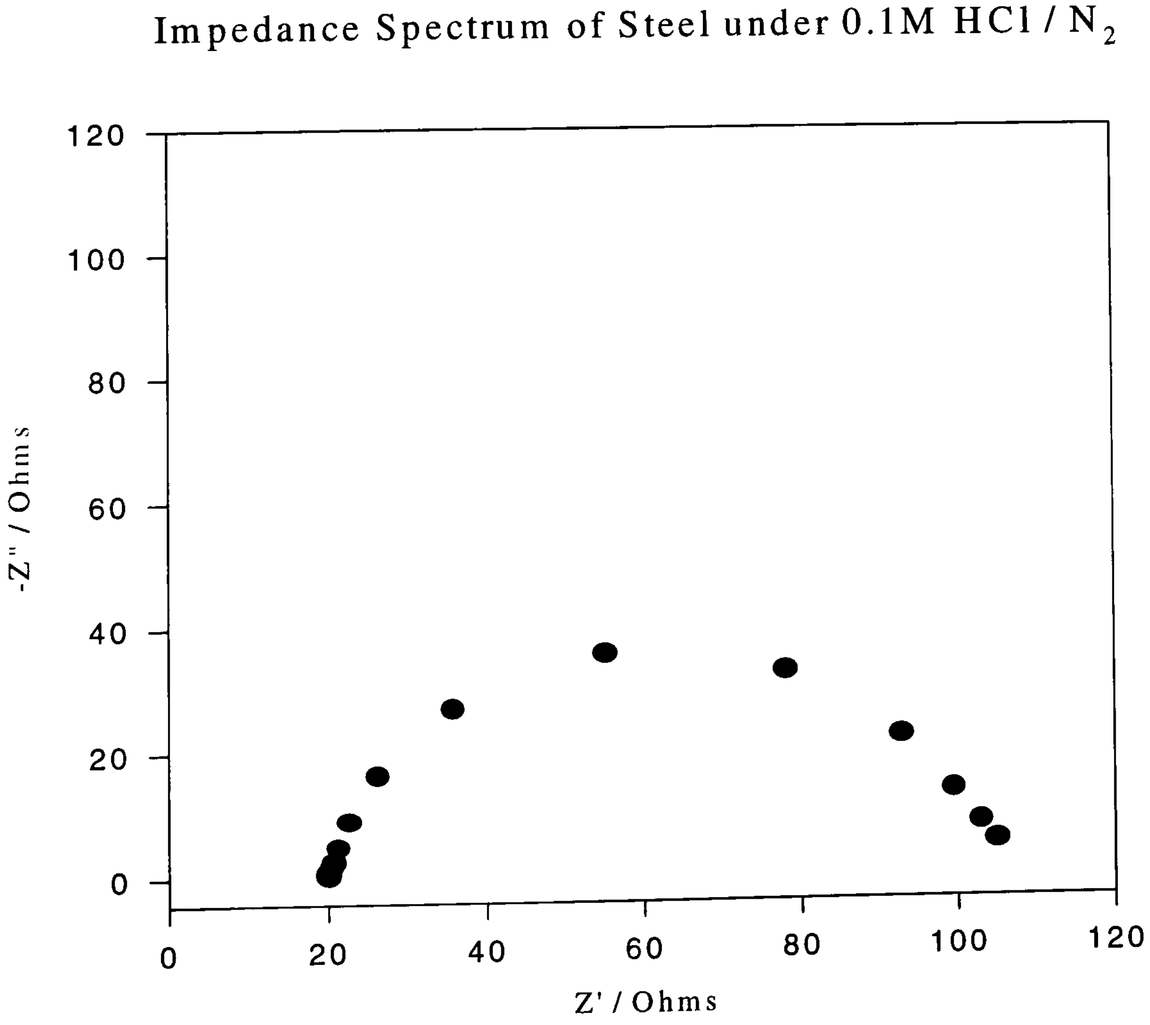

Figure 3.2 - Impedance Spectrum (Nyquist Plot) of Bare Steel in 0.1M HCl / Nitrogen

3.3.3 Determination of Corrosion Current of Steel using The Stern-Geary Equation

The use of The Stern - Geary equation to calculate corrosion current has been previously discussed in section 1.5.1. The equation is used here in order to illustrate an alternative method of deriving the corrosion current of steel under 0.1M hydrochloric acid. The method utilises the fact that the AC impedance perturbing potential is of a low amplitude. Therefore the potential / current response is in the linear region. The potential / current response is measured as the charge transfer resistance found from the EIS response of the metal. This is equal to the polarisation resistance at low amplitudes of applied AC potential.

$$I_{corr} = \frac{\beta_a \beta_c}{2.3(\beta_a + \beta_c)R_p}$$

Steel under 0.1M HCl:

$\beta_a = 60$ mV decade^{-1}
$\beta_c = -150$ mV decade^{-1}
$R_p = 367.5\ \Omega$ cm^{-2}

Therefore, $I_{corr} = 0.118$ mA cm^{-2}

This value is approximately three times smaller than the value of the corrosion current calculated from the Tafel extrapolation. This is likely to be due to differences in the mechanism of iron dissolution / hydrogen evolution at the small overpotentials used in the Stern-Geary approximation compared with the large overpotentials used in Tafel analysis.

3.4 Electrochemical Measurements of Aluminium

The Electrochemical measurements made on aluminium involved both DC Linear Sweep Voltammetry and AC Electrochemical Impedance Spectroscopy. The background to aluminium corrosion and the DC linear sweep measurements made on bare aluminium are all presented in Chapter 5.

The Tafel Plot results for Q aluminium given in Chapter 5 are summarised here:

	Q Aluminium
E_{corr} / Nitrogen	-510 mV
E_{corr} / Oxygen	-270 mV
Cathodic Tafel gradient / Nitrogen	200 mV decade^{-1}
Cathodic Tafel Gradient / Oxygen	560 mV decade^{-1}
Corrosion Current / O_2	0.13 mA cm^{-2}
Corrosion Current / N_2	0.013 mA cm^{-2}

3.4.1 AC Response (EIS)

3.4.1.1 Characteristics of the Aluminium Impedance Spectrum (Nyquist Plot)

EIS studies of aluminium have been reported in the literature, and the cause of the observed features discussed [4,5]. Three essential features have been noted for the corrosion of aluminium in acid. At high frequencies the semi-circle is attributed to the oxide layer on the aluminium [5] or the reactions involved in its formation [6]. At mid range frequencies an inductive loop is observed. This has been attributed to adsorbed intermediates such as in the reduction of H^+ [5]. The low frequency feature, has been associated with the dissolution of the oxide layer [5]. This is illustrated below:

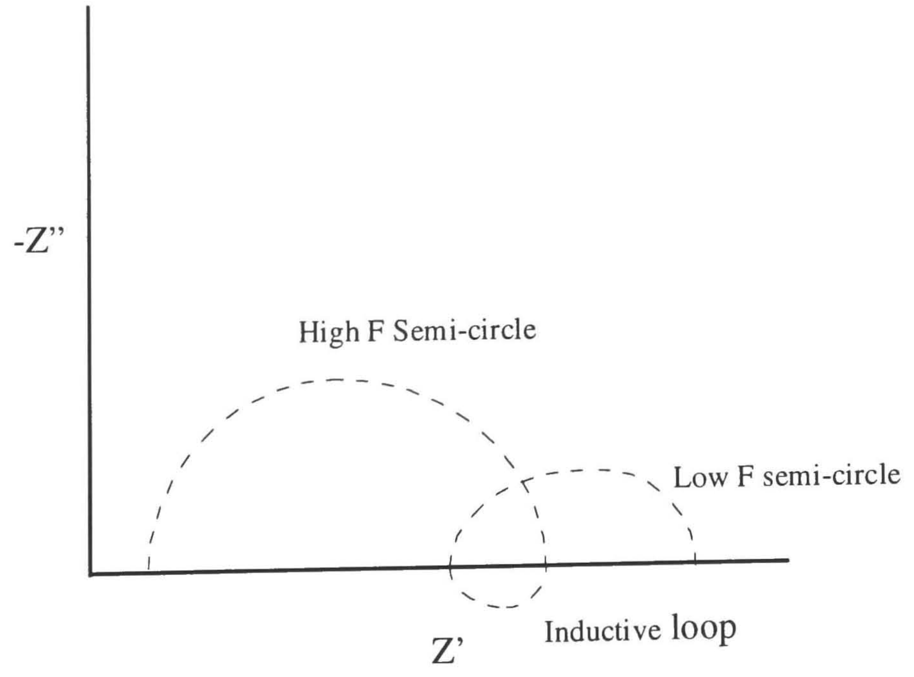

Figure 3.3a Diagramatic Representation of High Frequency, Mid Frequency and Low Frequency Elements of the Aluminium Impedance Response.

In the experiments performed on aluminium described in this thesis, where the aluminium impedance is clearly measured, the high frequency and mid frequency features are generally distinguishable. However the low frequency feature has not been observed as it is lower in frequency than the experimentally utilised low frequency limit. Both the high frequency and the mid frequency impedance features can be clearly seen in figure 3.3b.

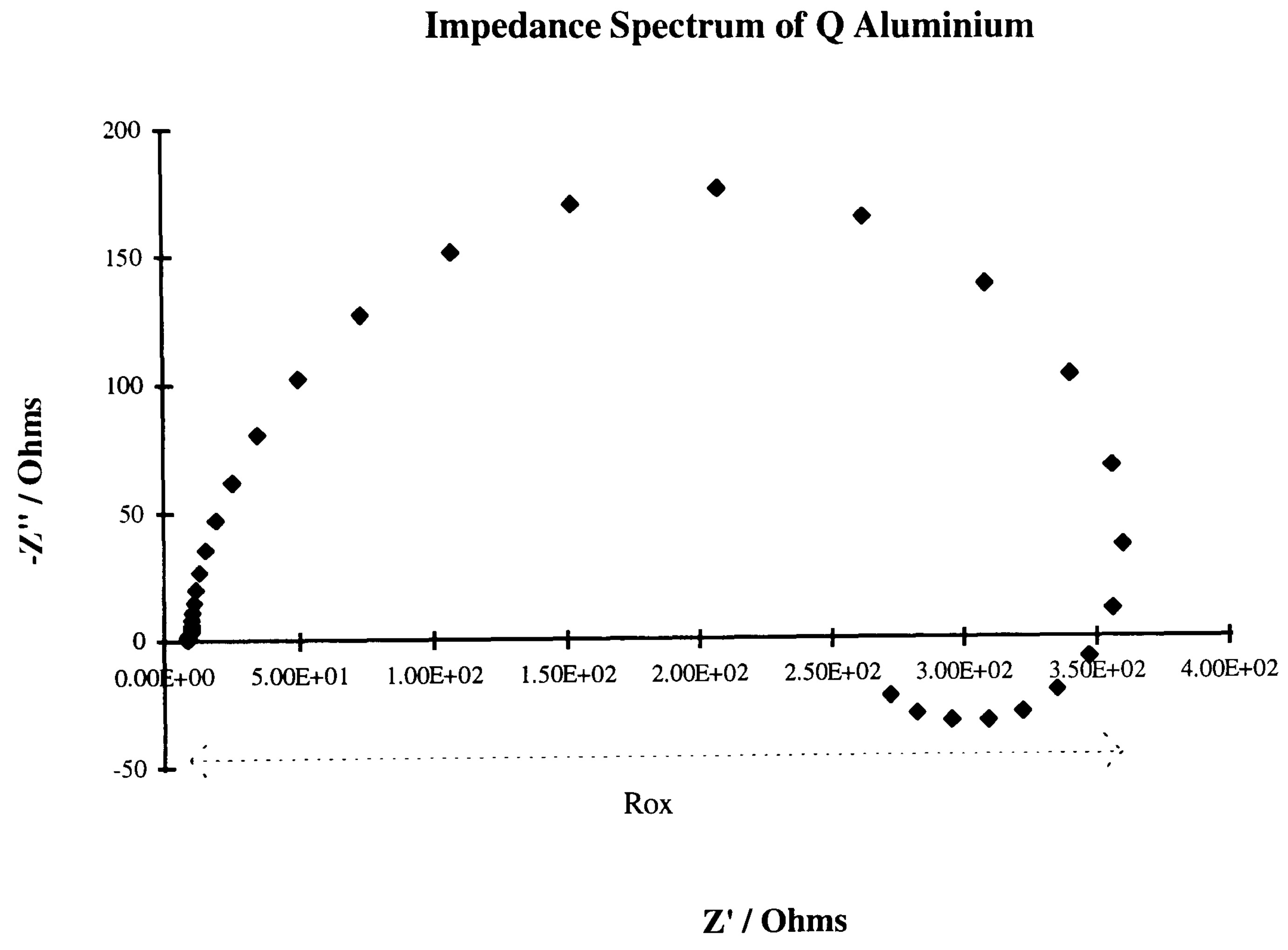

Figure 3.3b Impedance spectrum of Q Aluminium at -500mV vs. SCE under Nitrogen in 0.1M H_2SO_4 after 1/2 hour immersion.

Figure 3.3b shows the impedance response of bare aluminium, polarised at -500 mV *vs*. SCE after less than 1/2 hour immersion in electrolyte

The surface resistance and capacitance parameters, R_{ox} and C_{ox} are generally considered to be the resistance and capacitance of the oxide film on the aluminium [9]. They can be regarded as analagous to the charge transfer resistance / double layer capacitance of bare steel.

$$R_{ox} \approx R_{ct} \qquad C_{ox} \approx C_{dl}$$

However, this is a simplified assumption, as defects in the oxide film, such as at pits (areas of localised corrosion) will have separate impedance values, giving an equivalent circuit analogous to that of steel coated in a defective polymer coating. In addition, each interface will have its own impedance. A double layer on the aluminium is said to be created [3], but *within* the oxide film, with the oxide film acting as a solid electrolyte.

The equivalent circuit that most accurately describes the nature of the aluminium / oxide / electrolyte interface is shown in figure 3.4a.

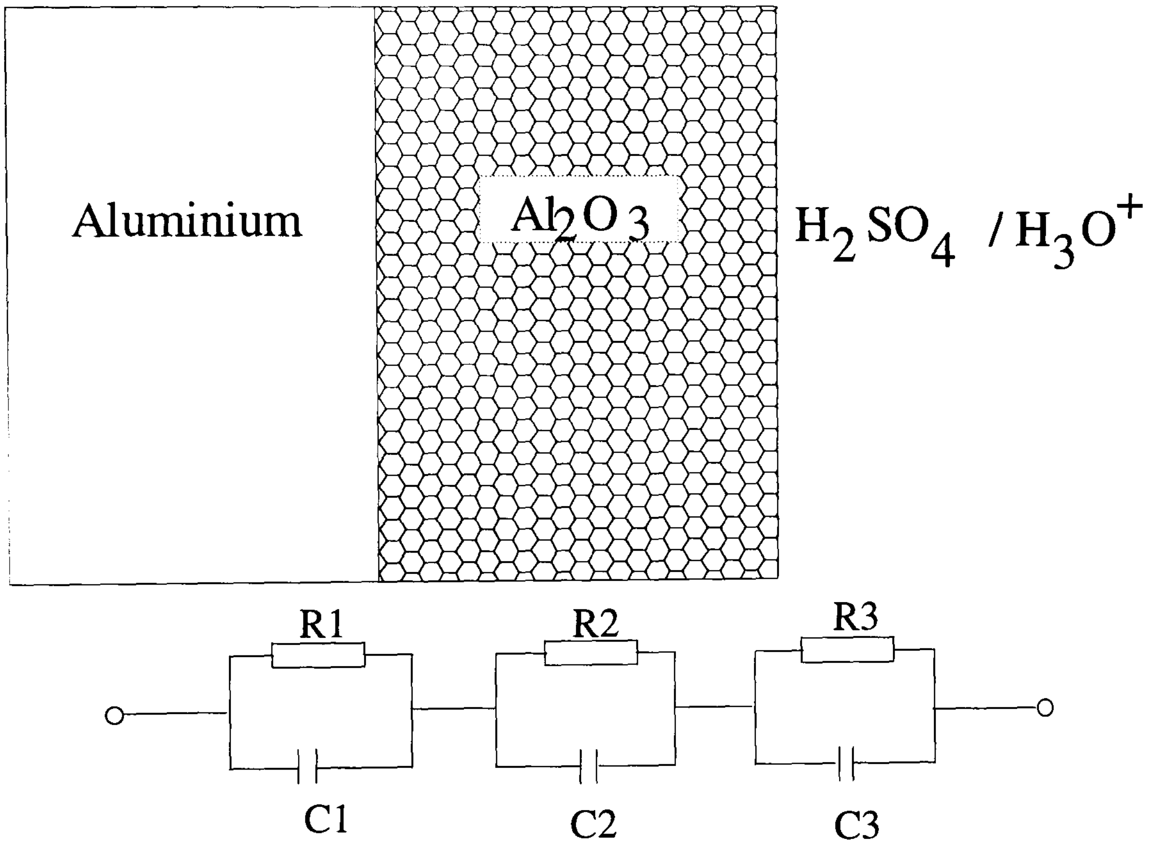

Figure 3.4a. Model and Equivalent Circuit of Aluminium / Oxide / Electrolyte Interface

Three parallel RC elements are used to modify each of the three interfaces:

R1, C1 is the double layer capacitance / charge transfer resistance formed by a build up of charge against the metal *within* the oxide layer.
R2, C2 is the oxide capacitance and resistance.
R3, C3 is the double layer / charge transfer resistance formed at the oxide / electrolyte interface by the lining up of solvated anions or cations in the electrolyte against the oxide.

This fairly complex circuit can be simplified by taking into account that the impedance of the oxide will be likely to be larger than the impedance of the metal / oxide interface and the oxide / electrolyte interface. Therefore, $R_{ox} >> R_{ct}$ (metal) & R_{ct} (oxide). Bessone *et.al* [4] have proposed that in aggressive electrolyte (such as NaCl), the total capacitance of the system is the reciprocal sum of the oxide and double layer capacitance:

$$\frac{1}{C}=\frac{1}{C_1}+\frac{1}{C_2}$$

Where C_1 is the double layer capacitance of the metal and C_2 the capacitance of the oxide. For the purposes of this thesis, the measured capacitance of the aluminium / oxide / electrolyte interface will be termed C_{ox}.

By neglecting the aluminium metal impedance C_1 & R_1, (equivalent to the double layer capacitance and charge transfer resistance of the aluminium within the oxide), as this will generally be far smaller than the resistance of the oxide and low frequency inductive effects, the following equivalent circuit can be envisaged:

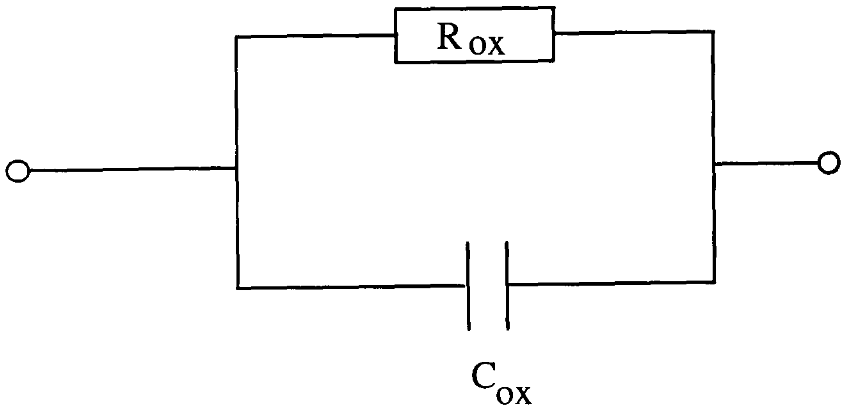

Figure 3.5b Simplified Equivalent Circuit for Aluminium / Oxide / Electrolyte System

This equivalent circuit models the high frequency response of aluminium, but disregards the inductive features and the low frequency semi-circle. This equivalent circuit is similar to the one proposed by Hitzig *et.al* in [10]

3.4.1.2 Impedance Measurements

The first model used to understand the corrosion of aluminium was based on the corrosion of steel, where the impedance parameters C_{dl} and R_{ct} do not change dramatically with immersion time.

Initially therefore, measurements were made on aluminium immediately the aluminium was immersed in electrolyte. The oxide film resistance of the aluminium R_{ox} and the oxide film capacitance, C_{ox} of the aluminium were calculated from the Nyquist plot almost immediately on immersion. The aluminium was polarised at -500 mV vs. SCE.

$R_{ox} = 793\ \Omega$:(for W.E. area of 4.9 cm^2)
$R_{ox} = 3886\ \Omega\ cm^{-2}$
$C_{ox} = 35.8\ \mu F$:(for W.E. area of 4.9 cm^2)
$C_{ox} = 7.30\ \mu F\ cm^{-2}$

In subsequent experiments the aluminium was polarised at different potentials between 0.00V *vs.* SCE and -1.00V *vs.* SCE. The results of this work are discussed in more detail in chapter five. From these experiments it was decided to polarise aluminium in subsequent experiments on the coated substrate at -500 mV *vs.* SCE as this was near the average measured rest potential of aluminium.

3.4.1.3 Effect of Immersion Time in 0.1M H_2SO_4 on Impedance Response of Bare Aluminium.

An experiment was performed to determine if the impedance characteristics of the aluminium changed greatly with immersion time in 0.1M sulphuric acid. figure 3.6 shows the change in the Nyquist Plot with immersion time after polarising the aluminium near its rest potential at -550mV *vs.* Ag/AgCl (-500 mV *vs.* SCE). The change in the values of R_{ox} and C_{ox} are significant and are summarised in table 1.

Time of Immersion / d	**R_{ox} / Ω**	**C_{ox} / μF**
0	1190	22.4
1	426	72.4
2	361	74.1
3	313	78.0
4	275	80.6
5	319	84.9
6	267	86.9

Table 1 - Change in the impedance response of bare aluminium with immersion time in 0.1M H_2SO_4

The decrease in R_{ox} indicates that the thickness of the oxide film has decreased on reaction with sulphuric acid. The corresponding increase in capacitance (C_{ox}) would also support this hypothesis. The air formed film, in place before immersion on the aluminium could be quite thick giving a relatively low capacitance on initial immersion in electrolyte. As the oxide film reacts with acid upon immersion, more aluminium is converted into aluminium oxide, by reaction with O^{2-} ions. Therefore reactions are taking place over the two phase boundaries. The eventual thickness of the oxide layer will be determined by the relative rate of the oxide dissolution reaction and the rate of aluminium oxidation. This is illustrated in the above table and in figure 3.6 where the values of R_{ox} and C_{ox} are tending towards a steady state, indicating a constant thickness coating. C_{ox} is proportional to the thickness of the oxide layer by:

$$C_{ox} = \frac{\varepsilon_o \varepsilon_r A}{d}$$

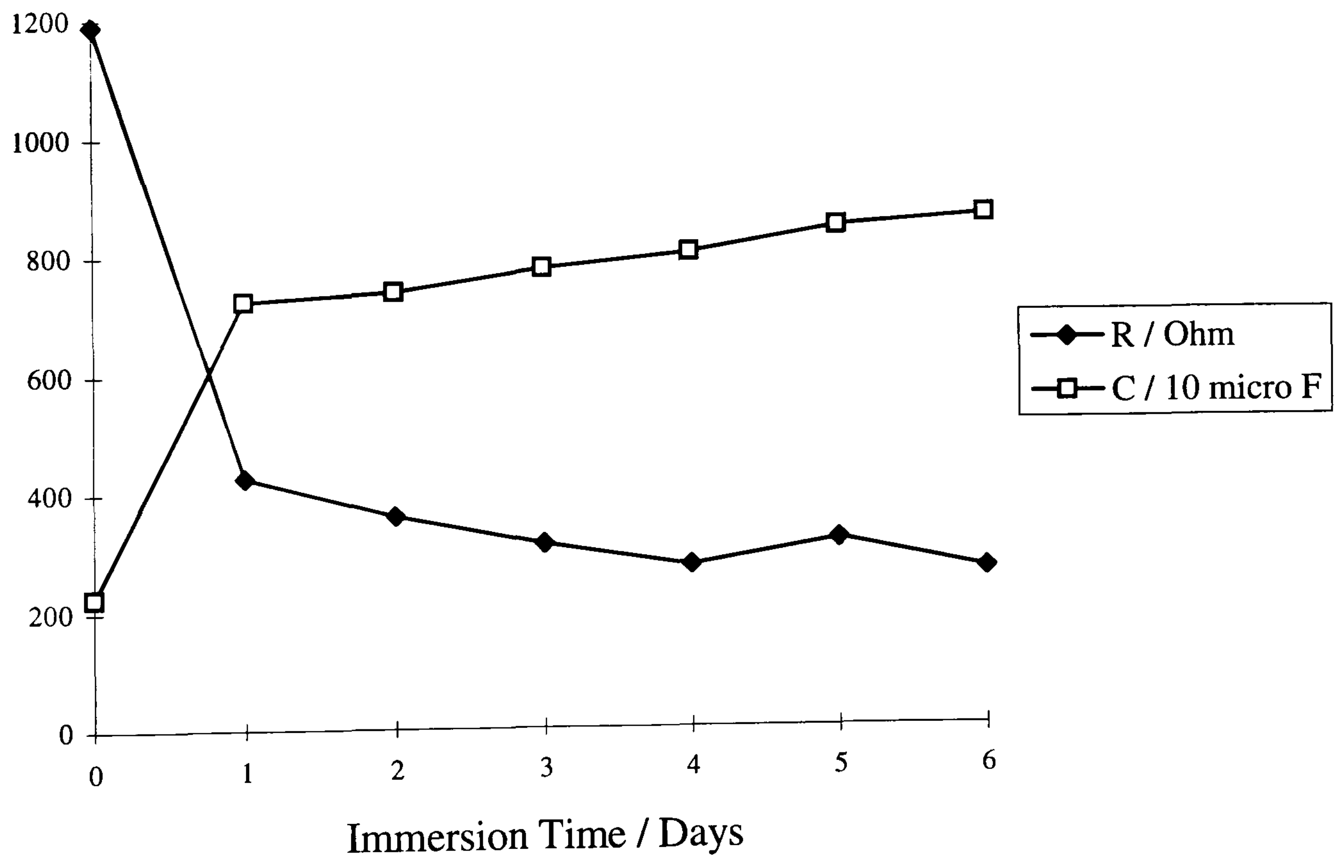

Figure 3.6 Change in impedance response of bare Q aluminium immersed in 0.1M H_2SO_4, polarised at -500 mV *vs.* SCE.

3.5 Summary of Electrochemical Analysis of Bare Steel and Aluminium

The electrochemical measurements have provided the values for the charge transfer resistance (R_{ct}) and double layer capacitance (C_{dl}) of the steel and oxide resistance (R_{ox}) and capacitance (C_{ox}) for the aluminium. These values are essential for calculating the porosity and wetted metal area of a defective coated metal. The bare metal resistance and capacitance values are, from this point, labelled as R_{cto}, C_{dlo}, R_{oxo}, C_{oxo} in order to distinguish them from the measured metal interfacial resistance and capacitance values from the polymer coated metal. The background to this is described in Chapter 1 (1.11.2.).

3.6 Mechanical Damage of Polymer Coated Metal

3.6.1 Introduction

Mechanical damage is a common mode of failure of paint coatings. Mechanical damage tends to be the first step in a general delamination of the coating, starting around the defect site. In the literature the EIS response of mechanically damaged polymer coatings has been widely reported, but with different interpretations of the EIS data. This has been discussed in detail in Chapter 1 (1.12.3.4). In general, it has been found that the impedance response of mechanically damaged coatings comes purely from the substrate / electrolyte interface, which effectively swamps the impedance response of the coating.

Studies on mechanical damage in the literature have generally used the break point frequency method suggested by Hirayama [7] to calculate delaminated area around a paint film defect. In the analysis of the experimental impedance data described in this thesis the analysis suggested by Armstrong and Wright [12] is used. This analysis gives a good fit to the experimental results obtained, especially where delamination was measured visually.

3.6.2 Transmission Line Model

In order to more accurately model the change in impedance on delamination around the base of a defect site a transmission line model has been developed by Armstrong and Wright [12]. Titz *et.al* [8] have proposed that the value of the $R_{\Omega,por}$, the pore resistance is proportional to the delaminated area, although this is contary to the ideas of Armstrong and Wright [12]. The transmission line model takes into account the electrolyte resistance in the thin film of electrolyte that exists under a delaminated coating. Schueller and Taylor [9] have modelled the effect of delamination on coated aluminium using a transmission line of impedance elements. They found that using an electrolyte of high resistivity could prevent the whole defect area being penetrated by the current.

3.6.2.1 Modelling of Delamination

In studies carried out for this thesis the delamination around the base of a circular defect site was modelled by connecting capacitors and resistors of appropriate values to form a transmission line (Fig. 3.10). This was connected to the FRA and the impedance response measured.

Two models of delamination were considered. The first model envisages a circular delamination away from the defect area, as shown in figure 3.7.

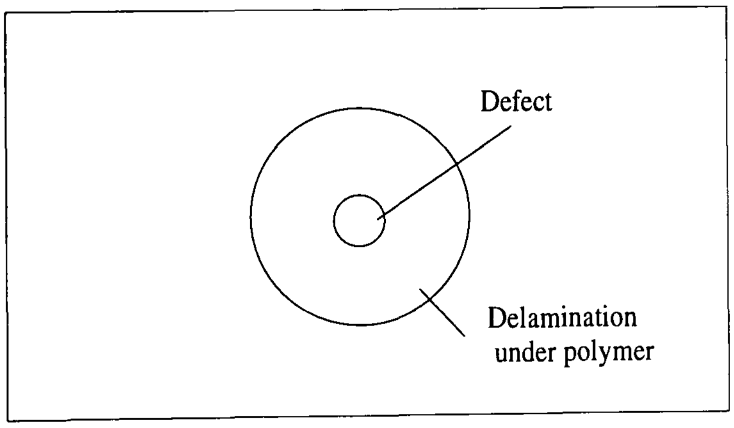

Figure 3.7. - Model of Circular Delamination around a Defect Site

The second model envisages discreet channels of electrolyte running out from the central defect, shown in figure 3.8. giving a star shape:

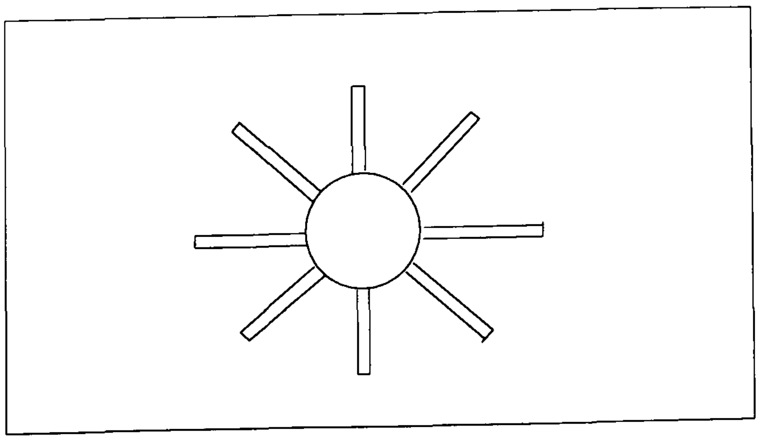

Figure 3.8. - Discrete Channels of Electrolyte Radiating from Defect Site.

3.6.2.2 Change in Resistance Under Coating

Model 1 - Circular Delamination

The way the resistance of the electrolyte under the coating changes with distance under the film, and with capacitance can be calculated theoretically.

The resistance of an area of electrolyte, with cross sectional area A and length l is given by:

$$R = \frac{\rho l}{A}$$

Where ρ is the resistivity of the electrolyte (inverse of conductivity κ).

The circular spread of electrolyte from a pore or defect in a polymer is represented in the model situation shown in figure 3.9. Here the current having travelled through the pore runs horizontally under the polymer, so the resistance of the electrolyte under the coating is:

$$R = \frac{\rho r}{2\pi r h}$$

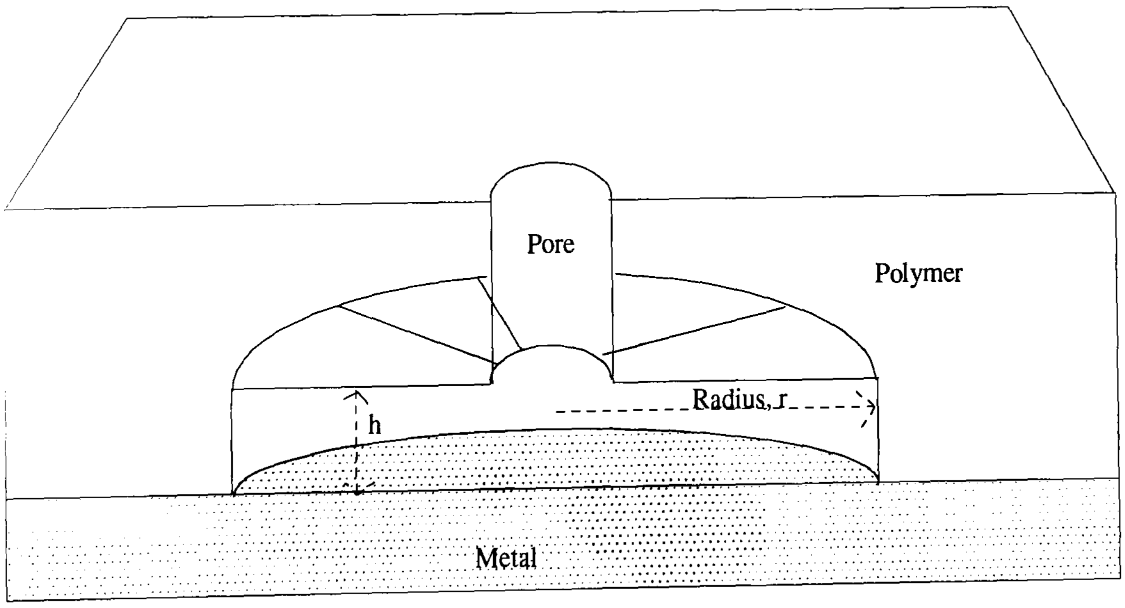

Figure 3.9 Model of Circular Delamination under a Coating

The change in resistance of the electrolyte, dR after a small increase in radius, dr is therefore:

$$dR = \frac{\rho dr}{2\pi r h}$$

The change in area, dA after a small increase in radius, dr is given by:

$$dA = dr.2\pi r$$

The change in double layer capacitance, dC after a small increase in area, dA is:

$$dC_{dl} = dAC_{dlo}$$

Therefore the change in resistance of electrolyte, with respect to the change in double layer capacitance as the current moves under the film is given by:

$$\frac{dR}{dC_{dl}} = \frac{\rho}{4\pi^2 hr^2 C_{dlo}}$$

Therefore if double layer capacitance is constant, resistance of the electrolyte changes by the inverse square of the radius:

$$dR \propto \frac{1}{r^2}$$

The electrical model (equivalent circuit) of the electrolyte under the coating is shown in figure 3.10. This model has the RC units of the metal interfacial impedance connected by resistors representing the electrolyte resistance:

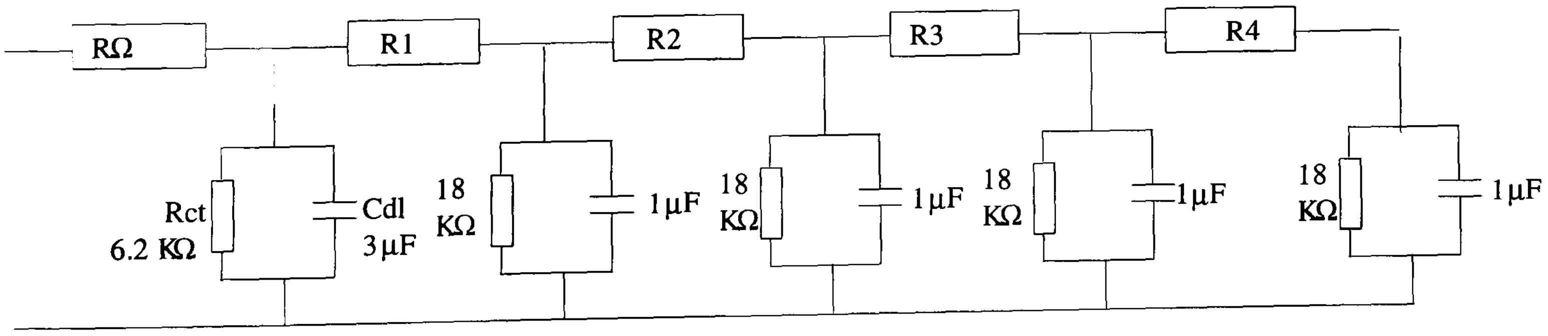

Figure 3.10. - Transmission line Equivalent Circuit of a Delaminated Paint Coating on a Metal Substrate.

In figure 3.10, RΩ represents the ohmic resistance of the electrolyte between the luggin of the reference electrode and the working electrode (substrate) at the base of a defect or pore in the coating. The first RC unit represents the equivalent circuit at the base of the defect, subsequent RC units represent the interfacial impedance under the coating. R1, R2 *etc.* represent the electrolyte resistance under the coating.

Using the mathematical analysis previously shown, the resistances R1, R2 *etc.* can be calculated:

If each resistor represents one unit increase in radius under the coating, and $R \propto 1/r^2$ then if R1=1kΩ:

R2 = 1/4 of R1 = 250Ω, R3 = 1/9 of R1 = 111Ω and R4 = 1/16 of R1 = 62Ω.

Model 2 - Discrete Channels of Electrolyte

The second proposed model of coating delamination, the 'star model' is far simpler. Here, because the area of electrolyte does not change per unit length along the radius, the resistance per unit length also does not change. Therefore R1 = R2 = R3 = R4 *etc.*

3.6.2.3. Impedance Results From Equivalent Circuit Modelling

1. Circular Delamination.

In the equivalent circuit shown in figure 3.10. the maximum value of capacitance that could be measured is 7 μF, from the addition of the individual capacitances. This would be found if the current flowed through the complete circuit. This would mean that in a real system, all the delaminated area would be measured. In visual measurements of delamination, shown later in this chapter, the delamination observed was circular in nature around a defect.

Table 2 shows the correlation between the value of R1, and the total measured capacitance (with R2 *etc.* all being related to R1 as shown).

R1 / Ω	Measured capacitance / μF
100	6.86
330	6.45
1000	5.33
2000	4.41
5600	3.38
9000	3.19
18000	3.05

Table 2

It is clear from table 2 that as the value of R1 (and therefore R2 *etc.*) increases then the measured capacitance decreases, until a point where little more than the first RC unit, representing the base of the pore, is carrying significant current.

2. Discrete Channels of Electrolyte

The result of keeping all the values of R1, R2 *etc.* equal is shown in table 3. Once again, the total capacitance of the system is 7 μF.

R1 / Ω	Measured capacitance / μF
100	5.22
1000	4.81
10000	3.2

Table 3

The situation is similar to the results from the first model. Table 3 shows that even at low values of R1, the total capacitance of the system is not measured. At high values of R1 only the first RC unit, corresponding to the base of the pore is measured.

The implications of this study are, that if either the electrolyte has a low conductivity, or the cross sectional area of electrolyte under the film is very small, then EIS analysis of corrosion under delaminated paint coatings will tend to under-estimate the total double layer capacitance of the corroding metal, and hence under-estimate the corroding area.

3.6.3 Mechanical Damage of Real Systems

Two systems have been examined, polyester coated steel and polyester coated aluminium. The experimental details are given in Chapter 2 (2.6).

3.6.3.1 Steel Substrate

Polyester powder coatings on steel were damaged with a 1.5 mm diameter drill. Two electrolytes were used (in different experiments), acetate buffer and 0.1M hydrochloric acid. Impedance measurements were made for up to fifteen days immersion in electrolyte. The double layer capacitance and charge transfer resistance were found from the EIS spectrum.

Wetted metal area was calculated by using the ratio of double layer capacitance of the bare steel to the double layer capacitance of the coated (damaged) steel. The ratio of charge transfer resistances could, in principal have been used ($W=R_{cto}/R_{ct}$), but this was considered less accurate than the double layer capacitance ratio because the metal was scored by the drill when the polymer was perforated. This will have two effects:

1. Higher surface area / unit of average electrode area due to the increased roughness of the surface.

2. Higher energy iron atoms at the surface : more adatoms, kinks and defects in the crystal lattice at the surface of the cut metal : hence will have a more active surface than non-drilled metal.

Experimental Results

The impedance data of the three systems is given as both the impedance parameters obtained and the calculated wetted area and porosity parameters. In addition the wetted area in cm^2 was calculated and subtracted from the pore area (defect area) to give the area of delaminated coating. The three systems which gave meaningful results were given the coding:

defilm3:	Acetate buffer electrolyte.
defilm6:	Acetate buffer electrolyte.
defilm9:	0.1M hydrochloric acid.

The EIS spectra were all single feature semicircle with a resistive displacement along the real axis due to the ohmic drop in the cell (figure 3.11).

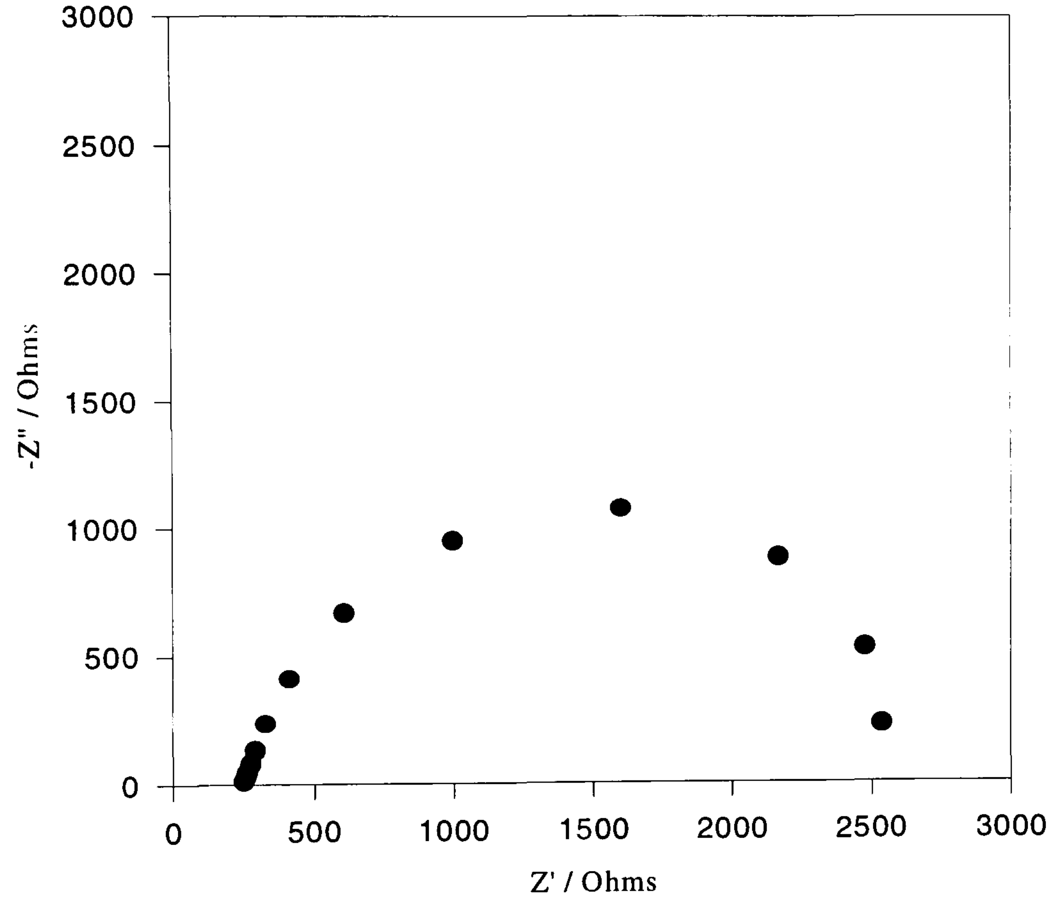

Figure 3.11 - EIS spectrum of mechanically damaged polyester on steel.

Tables four to six show the experimentally obtained impedance data and the calculated wetted area and porosity parameters.

Note: R_{ct} and C_{dl} values are all given for a cell with a working electrode area of 4.9 cm^2.

Time / Days	R_{ct} / kΩ	C_{dl} / µF	Wetted area (W)	W - P	W/P	W - P (in cm^2)
0	11.5	1.71	0.0043	0	1	0
1	2.94	2.46	0.0062	0.0019	1.44	0.0093
2	28.8	3.07	0.0077	0.0034	1.8	0.0166
3	9.14	8.61	0.021	0.0167	4.9	0.082
4	14.9	8.06	0.020	0.0157	4.7	0.077
5	19.9	8.33	0.021	0.0167	4.9	0.082
8	22.9	9	0.023	0.0187	5.3	0.092

Table 4: *Impedance results and calculated wetted area parameters for defilm3*

Time / Days	R_{ct} / kΩ	C_{dl} / µF	W	W - P	W/P	W - P (in cm^2)
1/8	2.38	3.91	0.0098	0.0062	2.72	0.0304
1	1.99	7.73	0.019	0.0154	5.27	0.0755
2	10.8	7.65	0.019	0.0154	5.27	0.0755
4	14.8	8.32	0.021	0.0174	5.83	0.0853
8	17.4	11.8	0.03	0.0264	8.33	0.1294
13	18	12.3	0.031	0.0274	8.61	0.1343
15	23.5	8.93	0.022	0.0184	6.11	0.0902

Table 5: *Impedance results and calculated wetted area parameters for defilm6*

Time / Days	R_{ct} / kΩ	C_{dl} / µF	Wetted area (W)	W - P	W/P	W - P (in cm^2)
1/8	1.88	2.0	0.0095	0.0059	2.64	0.029
3	6.19	1.4	0.0067	0.0031	1.86	0.015
6	7.00	1.58	0.0075	0.0039	2.10	0.019
8	4.23	1.82	0.0087	0.0051	2.42	0.025
13	3.51	5.46	0.026	0.0224	7.22	0.109
15	13.5	4.85	0.023	0.0194	6.39	0.095

Table 6: *Impedance results and calculated wetted area parameters for defilm9*

Wetted area is initially given as a dimensionless ratio, then converted into real area in cm^2. Porosity is calculated directly from dimensions of the drill used to create the defect.

Porosity was calculated as:

Diameter of artificial defect, $\phi = 1.5$ mm
Area of defect = 1.77×10^{-6} m^2 or 0.00177 cm^2

Proportion of electrode as pore, $P = 1.77 \times 10^{-6} / 4.9 \times 10^{-4}$
$= 0.0036$
= 1 part in 276.

This calculated value of porosity is close to the value of wetted metal area at the initial time of immersion of the coating in electrolyte, before electrolyte had spread far under the coating.

The calculation of wetted metal area (W) has been previously described in Chapter 2 (2.4.6). As an example, the calculation of the wetted metal area of defilm3 after two days immersion is given.

Defilm3 at two days:

$C_{dl} = 3.07$ µF
C_{dlo} (from 3.3.2) = 400 µF

Therefore, $3.07 \times 10^{-6} / 400 \times 10^{-6} = 0.0077$ (as a dimensionless ratio).
This means that 1 part in $(0.0077)^{-1}$ of the metal is in contact with electrolyte.

Evaluation of Results

The change in delaminated area with immersion time of the three systems is plotted as a graph in figure 3.12.

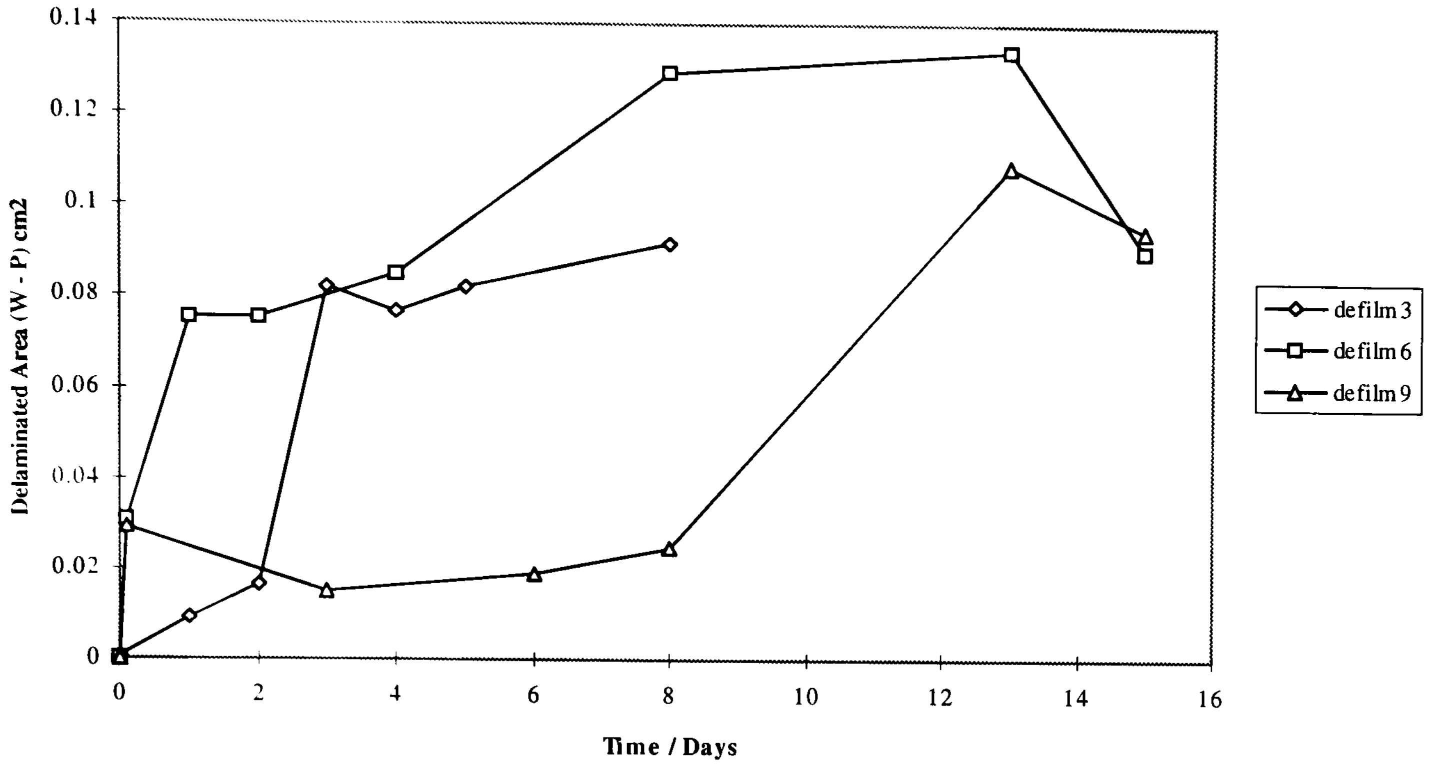

Figure 3.12. Variation of the delaminated area with immersion time for the three mechanically damaged systems.

Figure 3.12. shows that for all the systems there is a rapid rise in delaminated area over the first eight days of immersion in electrolyte. The two systems, defilm6 and defilm9 which were measured for fifteen days showed a general increase in delamination for fourteen days, then both appeared to have their delaminated area reduced. It is unlikely that this was actually the case. The decrease in measured double layer capacitance, directly proportional to the *measured* decrease in delamination is probably due to the build up of corrosion products on the steel. This is particularly likely to be the case for defilm6, with the acetate buffer electrolyte as at that pH (5.2) iron corrosion products are sparingly soluble. The reason for the build up of corrosion products on defilm9, which had 0.1M hydrochloric acid as an electrolyte is less clear. One possible reason could be due to the trapping of hydrogen under the coating from the cathodic reaction:

$$2H^+ + 2e^- \rightarrow H_2$$

Correlation of measured delamination with visual evidence

In order to attempt to assess the accuracy of the delamination measurements made using EIS, a sample of the damaged coatings were photographed after fifteen days immersion. As the coating was clear (none pigmented) the extent of delamination under the coating could be reasonably accurately estimated. Figure 3.13 shows a photograph made of defilm6 after fifteen days immersion in acetate buffer. The dark area observed at the base of the defect and spread out under the coating is probably magnetite (Fe_3O_4).

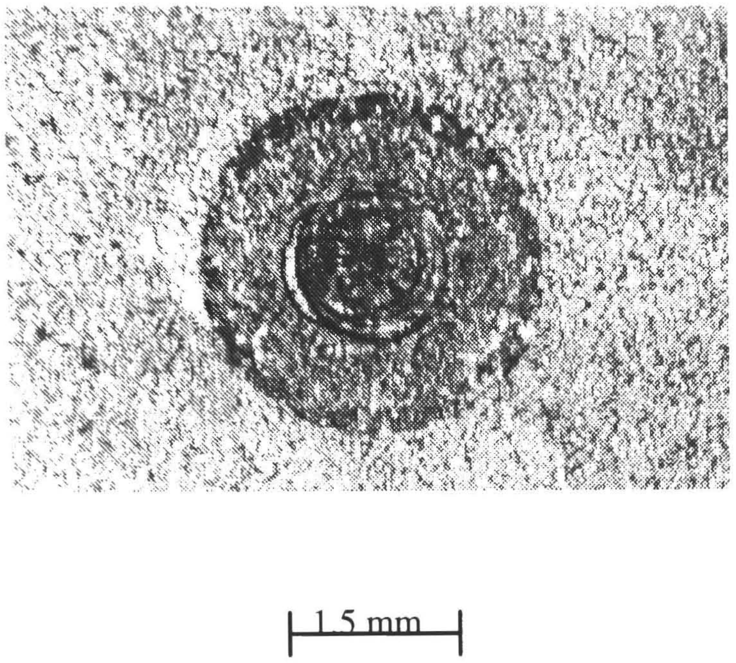

Figure 3.13 - Photograph of Mechanically Damaged Polymer and Associated Delamination after Fifteen Days Immersion in Acetate Buffer Electrolyte.

From figure 3.13 it is clear that the delamination is circular (Model 1) and quite extensive. The outer circle of darkened metal/polymer is *ca.* 0.9 mm greater in radius than the original drilled area.

Therefore:

Drilled area = 1.767×10^{-6} m^{2}.
Drilled + outer circle = 8.55×10^{-6} m^{2}.
Delaminated area; The area of polymer with evidence of electrolyte under it
(W - P) = 6.78×10^{-6} m^{2}.
= 0.0678 cm^{2}

Wetted metal area / Pore area ratio = **1: 4.8**

The EIS data using the capacitance ratios to calculate wetted metal area gave a value of Wetted metal area / Pore area as:

W / P = **1: 6.1**

And the area of delamination (W - P) = 0.0902 cm^{2}

Therefore it can be seen that the area of delamination calculated from visual inspection of the damaged coating is close to the value area of delamination calculated from the capacitance data obtained by EIS. This suggests that in general, for this type of analysis, EIS can be used to get a reasonably accurate value for wetted metal area under a coating.

3.6.3.2 Aluminium Substrate

Polyester coated aluminium was damaged by a drill in three ways. A 1.5 mm diameter hole was created, a 0.6 mm diameter hole was created and four 0.6 mm diameter holes were made. Two samples of each system were studied. The electrolyte was 0.1M H_2SO_4 with all measurements being made under nitrogen.

The calculation of wetted metal area is considerably more complex and more subject to error than on steel, due to the way the oxide film on aluminium changes with time. As a result, the wetted metal area has been calculated using the oxide film capacitance found from the uncoated aluminium measurements, made after different immersion times.

Experimental Results

The data collection and analysis is similar to that used for the mechanically damaged coatings on steel, apart from the values of C_{dlo} used to calculate wetted metal area (W), which instead of being constant, changes with immersion time in electrolyte.

N.B. For aluminium, the equation for wetted metal area:

$$W = \frac{C_{dl}}{C_{dlo}} \quad \text{is equivalent to:} \quad W = \frac{C_{ox}}{C_{oxo}}$$

C_{oxo} is the oxide film capacitance of the bare aluminium. C_{oxo} was calculated for the bare aluminium after different immersion times (3.4.3.3). Note, working electrode area is 4.9 cm^2.

The impedance results (R_{ox} and C_{ox}) are tabulated below (tables 7 to 12) with the derived quantities of porosity (P), wetted metal area (W) and delaminated area (W-P).

Time / d	R / KΩ	C / μF	W	W/P	W-P	W / cm^2	W-P / cm^2
0	9.24	2.11	0.0942	26.0932	0.0906	0.4616	0.4439
1	54.5	0.287	0.0040	1.0981	0.0004	0.0194	0.0017
2	43.9	0.366	0.0049	1.3682	0.0013	0.0242	0.0065
5	43.2	0.403	0.0047	1.3149	0.0011	0.0233	0.0056
6	64.9	0.206	0.0024	0.6567	-0.0012	0.0116	-0.0061

1.5 mm Hole on Q Al, 1 Hole.

Table 7: *Impedance results and calculated wetted area parameters for Mefilm1*

Time / d	R / KΩ	C / μF	W	W/P	W-P	W / cm^2	W-P / cm^2
0	37.5	1.64	0.0732	20.2810	0.0696	0.3588	0.3411
1	52.5	0.421	0.0058	1.6108	0.0022	0.0285	0.0108
2	57	0.362	0.0049	1.3533	0.0013	0.0239	0.0062
3	45.8	0.449	0.0058	1.5946	0.0021	0.0282	0.0105
6	220	0.156	0.0018	0.4973	-0.0018	0.0088	-0.0089
7	46.9	0.517	0.0059	1.6480	0.0023	0.0292	0.0115

1.5 mm Hole on Q Al, 1 Hole.

Table 8: *Impedance results and calculated wetted area parameters for Mefilm2*

Time / d	R / KΩ	C / μF	W	W/P	W-P	W / cm^2	W-P / cm^2
0	413	0.0301	0.0013	2.3248	0.0008	0.0066	0.0038
1	350	0.1070	0.0015	2.5569	0.0009	0.0072	0.0044
4	285	0.1380	0.0017	2.9622	0.0011	0.0084	0.0056
5	110	0.0546	0.0004	0.7680	-0.0001	0.0022	-0.0007
6	27.4	0.0636	0.0007	1.2662	0.0002	0.0036	0.0008
7	20	0.0300	0.0003	0.5973	-0.0002	0.0017	-0.0011

0.6 mm Hole on Q Al, 1 Hole.

Table 9: *Impedance results and calculated wetted area parameters for Mefilm3*

Time / d	**R / KΩ**	**C / μF**	**W**	**W/P**	**W-P**	**W / cm^2**	**W-P / cm^2**
0	281	0.034	0.00153	2.6415	0.0009	0.0075	0.0046
1	282	0.135	0.00186	3.2260	0.0013	0.0091	0.0063
4	319	0.167	0.00207	3.5847	0.0015	0.0102	0.0073
5	1000	0.030	0.00035	0.6113	-0.0002	0.0017	-0.0011
6	264	0.055	0.00063	1.0910	0.0001	0.0031	0.0003
7	869	0.026	0.00030	0.5196	-0.0003	0.0015	-0.0014

0.6 mm Hole on Q Al, 1 Hole.

Table 10: *Impedance results and calculated wetted area parameters for Mefilm4*

Time / d	**R / KΩ**	**C / μF**	**W**	**W/P**	**W-P**	**W / cm^2**	**W-P / cm^2**
0	205	0.1430	0.0064	2.7636	0.0041	0.0313	0.0200
1	157	0.2410	0.0033	1.4410	0.0010	0.0163	0.0050
4	155	0.4170	0.0052	2.2397	0.0029	0.0254	0.0140
5	113	0.5140	0.0061	2.6209	0.0037	0.0297	0.0183
6	112	0.3680	0.0042	1.8332	0.0019	0.0208	0.0094
7	120	0.4840	0.0056	2.4111	0.0033	0.0273	0.0160

0.6 mm Hole on Q Al, 4 Hole.

Table 11: *Impedance results and calculated wetted area parameters for Mefilm5*

Time / d	**R / KΩ**	**C / μF**	**W**	**W/P**	**W-P**	**W / cm^2**	**W-P / cm^2**
0	183	0.115	0.0051	2.2225	0.0028	0.0252	0.0138
1	134	0.321	0.0044	1.9194	0.0021	0.0217	0.0104
4	122	0.190	0.0024	1.0205	0.0000	0.0116	0.0002
5	49	0.149	0.0018	0.7597	-0.0006	0.0086	-0.0027
6	38	0.192	0.0022	0.9565	-0.0001	0.0108	-0.0005
7	20	0.100	0.0012	0.4982	-0.0012	0.0056	-0.0057

0.6 mm Hole on Q Al, 4 Hole.

Table 12: *Impedance results and calculated wetted area parameters for Mefilm6*

General Observations

The general tend seen from all the systems studied (tables 7-12) is that after approximately five days immersion, the delaminated area had changed substantially compared with the delaminated area measured at t=0. The change in delaminated area over the total immersion time appears to follow two distinct trends:

Mefilm 1 & 2 both show a large delaminated area on initial immersion, that rapidly drops off towards zero. The initially larger delaminated area is expected, as Mefilm 1 & 2 both were cut with larger defects (dia. 1.5 mm).

The other systems studied (Mefilm 3-6), all damaged with either one or four 0.6 mm diameter holes showed an initially small delaminated area, which increased slightly, before decreasing after about five days. This is illustrated in figure 3.16.

The delamination area is taken as the measurement of the wetted metal area on initial immersion (in contrast with mechanically damaged coated steel).

The properties of the six systems are summarised below in table 13:

System	Number of Defects	Diameter of each Defect	Relative Area
Mefilm1	1	1.5 mm	6.2
Mefilm2	1	1.5 mm	6.2
Mefilm3	1	0.6 mm	1
Mefilm4	1	0.6 mm	1
Mefilm5	4	0.6 mm	4
Mefilm6	4	0.6 mm	4

Table 13: *Size, number and relative areas of artificial defects*

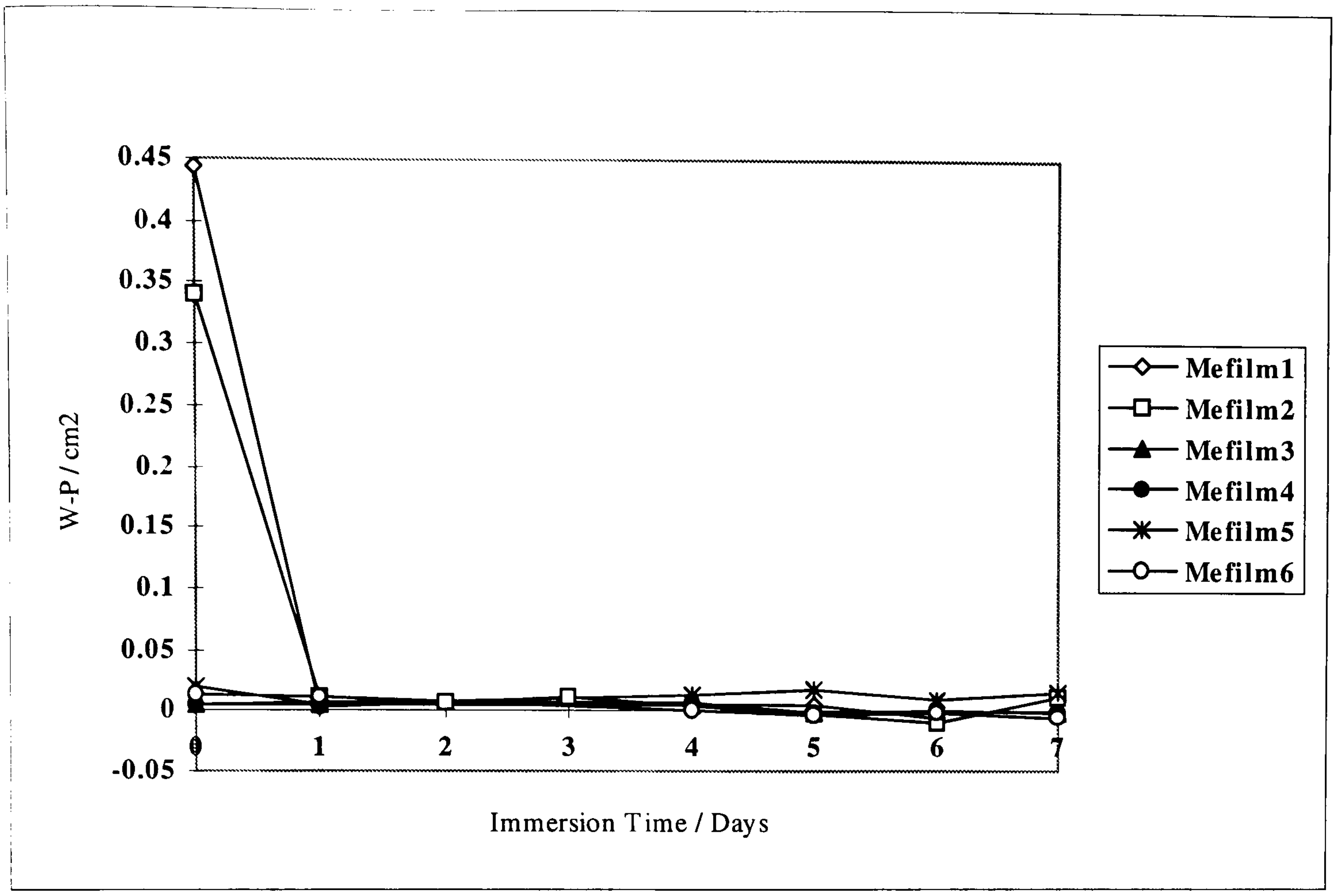

Figure 3.14 Graph showing the Change in the delaminated area (W-P) with immersion time in 0.1M H_2SO_4.

It is clear, therefore from tables 7 - 12 and figure 3.14 that although defects in the coating on aluminium, may initially have an area of delamination around them, especially on the larger defects, the delaminated area is reduced with time. The reason for this reduction in delaminated area is likely to be due to the different local chemical environment in the delaminated area under the coating compared with the bulk electrolyte. A likely cause of this is a low rate of diffusion of Al^{3+} from electrolyte in the delaminated area into the bulk electrolyte. This would cause a thickening of the oxide film on the aluminium under the delaminated coating so forcing out electrolyte and reducing the delaminated area.

Comparison of Initial Wetted Metal Area with Relative Areas of Defects

Table 13 shows the relative area of the artificial defects to each other. At initial immersion, it can be assumed that the measured capacitance is proportional to the area of delamination and defect area, as there will not have been significant build up of aluminium corrosion products. This is from the relationship, previously shown:

$$W = \frac{C_{ox}}{C_{oxo}}$$

Therefore, the ratio of relative wetted areas (relative to Mefilm4) between the three different systems on initial immersion, should be close to the defect area ratios, assuming each system has delaminated in a similar way (circular from the defect).

System	Number of Defects	Diameter of each Defect	Relative Area	W / cm^2	Relative Wetted Area	Diameter of delamination / mm
Mefilm1	1	1.5 mm	6.2	0.4616	69.9	7.67
Mefilm2	1	1.5 mm	6.2	0.3588	54.4	6.76
Mefilm3	1	0.6 mm	1	0.0066	1.0	0.92
Mefilm4	1	0.6 mm	1	0.0075	1.1	0.98
Mefilm5	4	0.6 mm	4	0.0313	4.7	0.99†
Mefilm6	4	0.6 mm	4	0.0252	3.8	0.89†

† Delamination around **one** defect.

Table 14: *Ratio of relative wetted areas of the three different defect systems (Measured at t=0)*

It can be seen from table 14, that comparing Mefilm3-6, that when the number of defects is quadrupled, there is a corresponding quadrupling of the wetted metal area. This suggests that the delaminated areas measured by EIS are consistent with the delamination measured by visual observation.

However, this does not hold true for Mefilm1 & 2, where a larger 1.5 mm defect was used. In this case the delamination diameter (diameter of wetted metal area), used to compare the relative degree of delamination is far in excess of the delamination measured on the smaller defects. The delamination diameter measured here was 7.2 mm (average), with a 2.1 mm radius of coating delaminated.

The coatings with smaller defects (Mefilm 3-6) had a delamination radius of 0.95 mm (average), with 0.35 mm radius of the coating delaminated. A similar degree of coating delamination would be, in principal, expected from the larger defect assuming a similar delamination mechanism was in place.

This huge difference in, what is effectively the rate of delamination suggests that a larger defect on a coating causes a larger scale failure in the adhesion of the polymer surrounding it, possibly due to the change in mechanical properties of the coating around the defect. For a small defect, there is probably a far smaller effect on the mechanical properties of the coating in the area of the defect, so giving a far smaller loss of adhesion.

3.7 Conclusions

1. DC measurements can be used to measure the corrosion rate of both steel and aluminium, although with aluminium, the intercept of the cathodic slope with the corrosion potential line should be used. The impedance parameters of bare aluminium are not constant, but change with immersion time.

2. Delamination under polymer coatings can be reasonably modelled by using resistance and capacitance components in a transmission line model. AC impedance measurements may underestimate the delaminated area.

3. Measurement of the delaminated area around a defect on polymer coated steel using AC impedance gave a good correlation with visual measurements of the associated corroding area. This suggests that AC impedance is effective at measuring delamination.

4. On polymer coated aluminium the delaminated area appears to *decrease* with time, probably due to the formation of a thick layer of corrosion products under the coating, due to a low diffusion rate of Al^{3+} from the corroding surface. The effective rate of delamination is different for defects with different areas. A larger defect area appears to give a greater rate of delamination of the surrounding coating.

5. The extent of delamination around defects of identical size but on different substrates (steel and aluminium) is different. On steel, the wetted area to defect area ratio (W/P) is 5.3 after eight days immersion, compared to aluminium with a W/P ratio of between 12.6 and 16.3 after immediate immersion. The difference in delamination is likely to be due to both the chemical delamination mechanism on the surface (anodic undermining *etc*.) and differences in the adhesion of the coating to the substrate.

References

[1] M. Stern, *J. Electrochem. Soc.*, **102**, 609, (1955).

[2] S. Evans, E.L. Koehler, *J. Electrochem. Soc.*, **108**, 509 (1961).

[3] A. Despic, V.P. Parkhutik, *Modern Aspects of Electrochemistry* **20**, 401, Plenum, (1989), Eds. Bockris, White & Conway.

[4] J.B. Bessone, D.R. Salinas, C.E. Mayer, M. Eber and W.J. Lorenz, *Electrochim. Acta* **37**, 2283, (1992).

[5] H.J.W. Lenderink, M. v.d. Linden, J.H.W. De Wit, *Electrochim. Acta,* **38**, 1989, (1993).

[6] C.M.A. Brett, *Corrosion Science* **33**, 203 (1992).

[7] R. Hirayama, S. Hauyama, *Corrosion* **47**, 952, (1991).

[8] J. Titz, G.H. Wagner, H. Spähn, M. Ebert, K. Jüttner, W.J. Lorenz, *Electrochim. Acta*, **37**, 2309, (1992).

[9] G.R.T. Schueller, S.R. Taylor, *J. Electrochem. Soc.* **139**, 3120, (1992).

[10] J. Hitzig, K. Jüttner, W.J. Lorenz, W. Paatsch, *Corrosion Science*, **24**, 945, (1984).

[11] J. O'M Bockris, J. McBreen, L. Nanis, *J. Electrochem. Soc,* **110**, 102, (1965).

[12] R.D. Armstrong, J.D. Wright, *Electrochim. Acta,* **38**, 14, 1799 (1993).

PAGE

NUMBERING

AS ORIGINAL

Chapter 4

A Study into the Effects of UV_b Weathering on Polyester Powder Coatings.

4.1 Introduction

One of the most common and serious failure modes of paint coatings, such as the polyester powder coatings investigated here, is due to the effects of sunlight. The high energy Ultra Violet (UV) component of sunlight is particularly destructive. UV light can cause a breakdown of the polymer binder at a molecular level via chain scission which leads to a macroscopic breakdown of the bulk coating.

In this chapter various methods of accelerated weathering are discussed, the mechanism of photo-degradation of polymer coatings and different techniques for the determination of the extent of coating degradation are discussed. The experimental work has investigated the effect of UV weathering on polyester powder coatings. Polyester powder coatings were prepared and applied to a mild steel substrate. These panels were weathered in a QUV_b weathering chamber (Chapter 2) for different periods of time. The weathered panels were removed and studied by EIS, SEM and gloss loss (light reflectance) to quantitatively and qualitatively determine the degree of breakdown of the surface [1].

4.1.1 Accelerated Weathering Methods

Much of this discussion is based on a review by Johnson and McIntyre [2]. The weathering of paint coatings under natural conditions can take a wide variety of different times depending on temperature, humidity, area of exposure, time of year and nature of polymer and substrate. In order to accurately predict the performance of a coating, it would in principle be necessary to follow the performance of the coating over its operational life. Clearly when developing new coatings, this kind of testing is unfeasible, since coatings can have an operational lifetime of 20 years or more, therefore accelerated test methods have been developed. Accelerated weathering methods, as well as reducing the exposure time of the coating, help to standardise the exposure conditions, such as humidity and temperature. The industry standard methods for calculating degradation with weathering time are currently gloss loss, colour retention and chalking. These are discussed later.

Accelerated weathering methods fall into two types;

1. Natural exposure. This method utilises sites with extremes of climate such as Florida and Arizona and intensified sunlight systems that use mirrors to intensify sunlight falling on a panel, known as EMMA (Equatorial Mounts with Mirrors for Acceleration) and EMMAQUA [3]. This intensifies natural sunlight to about 8 suns. It is known that one year of EMMAQUA is equivalent to about five years of Florida exposure, in terms of gloss loss / chalking etc. This is due to the virtually identical UV spectrum of natural sunlight and EMMAQUA light.

2. Artificial weathering. This utilises higher intensity and/or higher energy (shorter wavelength) radiation from light sources such as QUV, carbon arc and xenon arc. Both accelerated weathering methods can, in principle, be correlated with natural exposure times in different environments. The accelerated exposure method used in the work carried out for this thesis has utilised QUV_b exposure.

4.1.1.1 QUV_b Exposure

QUV_b light is produced from fluorescent tubes, and has a maximum intensity at around 313 nm, with high intensity of light between 290 nm and 270 nm, below the solar cut off [7]. Therefore QUV_b light provides a large degree of acceleration compared with natural exposure, but at the expense of inducing some 'unnatural' photochemistry, due to its output below the solar cut off.

4.1.1.2 Correlation of QUV_b exposure with Florida and EMMAQUA exposure

A comparison of the weathering experienced by polyester coatings when weathered by three different methods, QUV_b, Florida and EMMAQUA is given by Osmond in reference [3]. The degree of gloss loss between a polyester coating and an acrylic has been discussed by Osmond [3]. This shows after 400 hours QUV_b the polyester had only 12 % gloss retention, whilst the acrylic had 77 % gloss retention. However Florida exposure for 30 months and equivalent EMMAQUA exposure showed the acrylic to degrade the most with a gloss retention of 6 % and 9 % respectively for the two methods, compared to the polyester which showed a gloss retention of 38 % and 31 % respectively. In summary, the polyester was more sensitive to degradation from QUV_b light, whilst the acrylic was more susceptible to degradation from natural sunlight. It is therefore difficult to correlate time of QUV_b exposure with time of natural sunlight exposure for different coatings. Therefore it can be seen that QUV_b exposure is useful for testing the *relative* performance of similar systems, with the same resin chemistry, but does not correlate well with Florida exposure for different systems.

4.1.1.3 Correlation of UV_b / Condensation Weathering with Florida Exposure.

In the ASTM D-4587 test used in the work described in this thesis, QUV_b exposure is coupled with a condensation cycle. In work related to the ASTM D-4587 test, Grossman [8], looked at the correlation between UV_b exposure in a combined exposure / condensation test and Florida exposure. The degree of degradation was compared by the gloss retention values from light reflectance at 20° to the normal. Grossman found that the best coatings weathered by UV_b / condensation held their gloss better than the equivalent Florida test, whilst weak coatings degraded more from UV_b / condensation weathering than from Florida exposure. In all, it was found that the acceleration ratio (Florida compared to UV_b / condensation weathering) ranged from 8:1 for the strongest coatings to 25:1 for the weakest coatings with a median of 17:1, calculated from the median value of gloss retention after 500 hours UV_b / condensation. Overall, it would appear that trying to correlate the degradation of systems with different resin chemistries with natural exposure is subject to considerable problems, as concluded by Osmond [3]. It should also be noted that one year of Florida exposure, with its humid sub tropical climate is taken to be about 2.5 years of exposure in Europe [9].

4.1.2 Photochemistry of Organic Coatings

Organic coatings undergo photo-oxidation when exposed to UV light. In practice, for a coating to degrade it must generally contain a chromophore(s) that absorbs sunlight at wavelengths > 295 nm. The absorbed energy is dissipated through a free radical oxidation pathway, shown in figure 4.1 [4, 14].

Initiation

$\text{Polymer (P)} + \text{UV} \rightarrow \text{P}^*$

$\text{P}^* \rightarrow \text{P}\cdot$ (free radical polymer)

Chain Propagation

$\text{P}\cdot + \text{O}_2 \rightarrow \text{PO}_2\cdot$

$\text{PO}_2\cdot + \text{P-H (polymer)} \rightarrow \text{PO}_2\text{H}$

Chain Termination

$2\text{PO}_2\cdot \rightarrow \text{PO}_2\text{P} + \text{O}_2$

$2\text{P}\cdot \rightarrow \text{P-P} + \text{disproportionation}$

$\text{PO}_2\cdot + \text{P}\cdot \rightarrow \text{PO}_2\text{P} + \text{disproportionation}$

$2\text{PO}_2\cdot \rightarrow \text{ketones} + \text{alcohols}$ (disproportionation)

Degradation Processes

$\text{PO}_2\text{H} + \text{light (or heat)} \rightarrow \text{PO}\cdot + \text{HO}\cdot$

$\text{PO}\cdot \rightarrow \text{ketones} + \text{P}'\cdot$ (Chain Scission)

Figure 4.1

In figure 4.1 the polymer undergoes initial photochemical excitation to produce the highly energetic polymer species P*. This may undergo bond cleavage to form P· free radicals. P· then reacts with dioxygen to form the highly reactive peroxo species $\text{PO}_2\cdot$. This then undergoes a chain reaction with other polymer strands producing polymers with hydroperoxide species PO_2H or disproportionates to form ketones and alcohols. These hydroperoxides may then degrade via PO· in a chain scission reaction to form ketones and other, shorter polymer free radicals.

4.1.2.1 Photodegradation of Polyester Coatings

In practice, many commercially used polymers do not absorb near UV light in the 290 - 400 nm region. This would suggest that these polymers should be photochemically stable. However many commercially used polymers contain impurities and foreign particles incorporated into the coating mixture. These can act as *photosensitisers,* which absorb UV light and transfer the energy to the bulk polymer [5]. Photosensitisers are generally substances such as chains with extended conjugation, polyaromatic compounds, carbon particles and nitrous oxides.

Polyesters are thought to photo-degrade from an initial Norrish type 1 reaction, which gives chain scission to produce radicals. A model polyester, used by Rånby and Hult [5] has been used in order to study the photo-degradation of polymers. This model polyester is close in structure to that used as the binder in the polyester coatings experimentally used in this thesis. This is shown in figure 4.2:

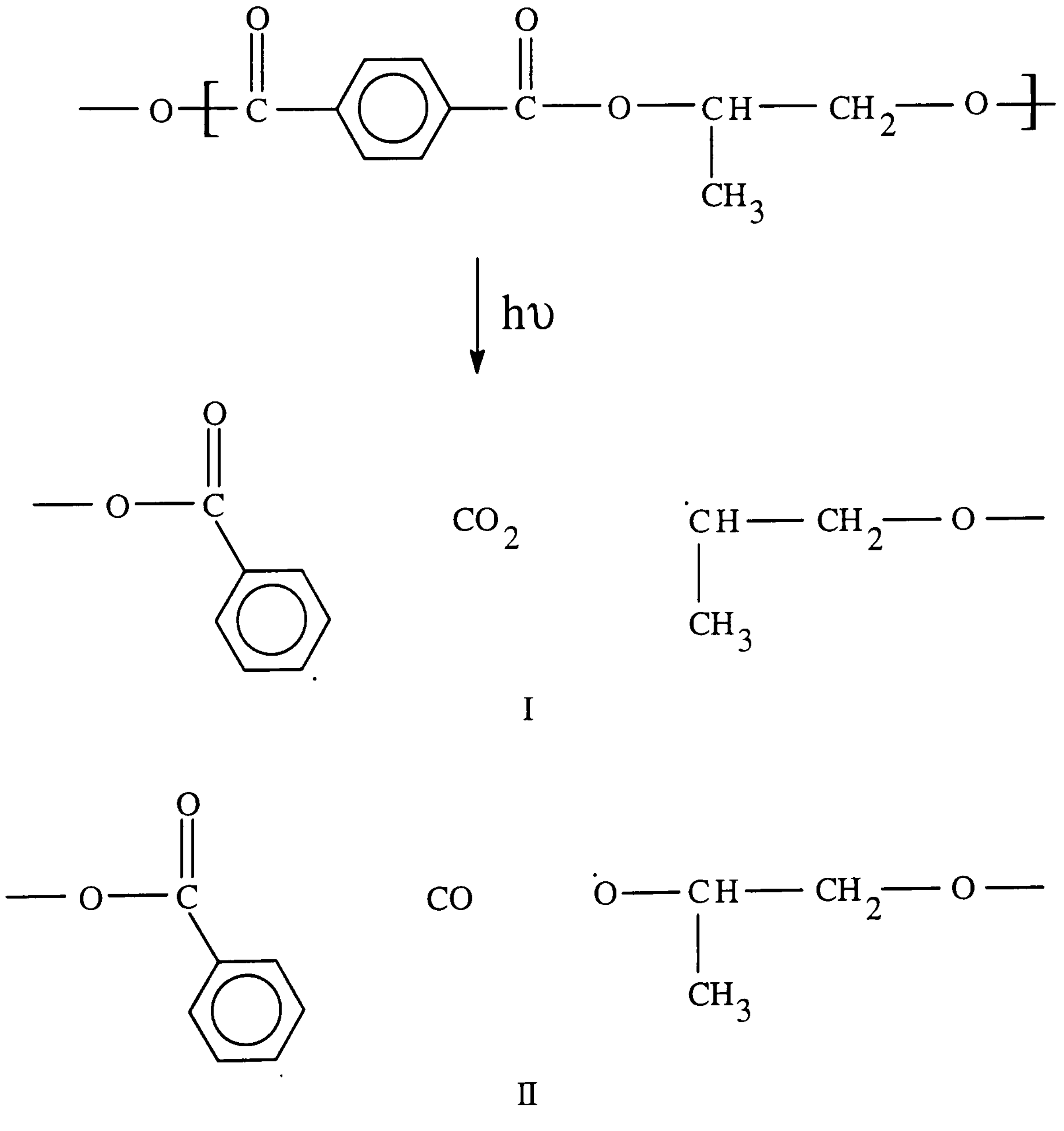

Figure 4.2 Norrish type I Chain Scission of a Polyester

The carbon monoxide and carbon dioxide formed in the above reaction were detected by gas analysis [5]. The phenyl radical produced above can then react with dioxygen to form a peroxy radical (A), which then abstracts hydrogen from other polymer chain end groups to form the hydroperoxide (B):

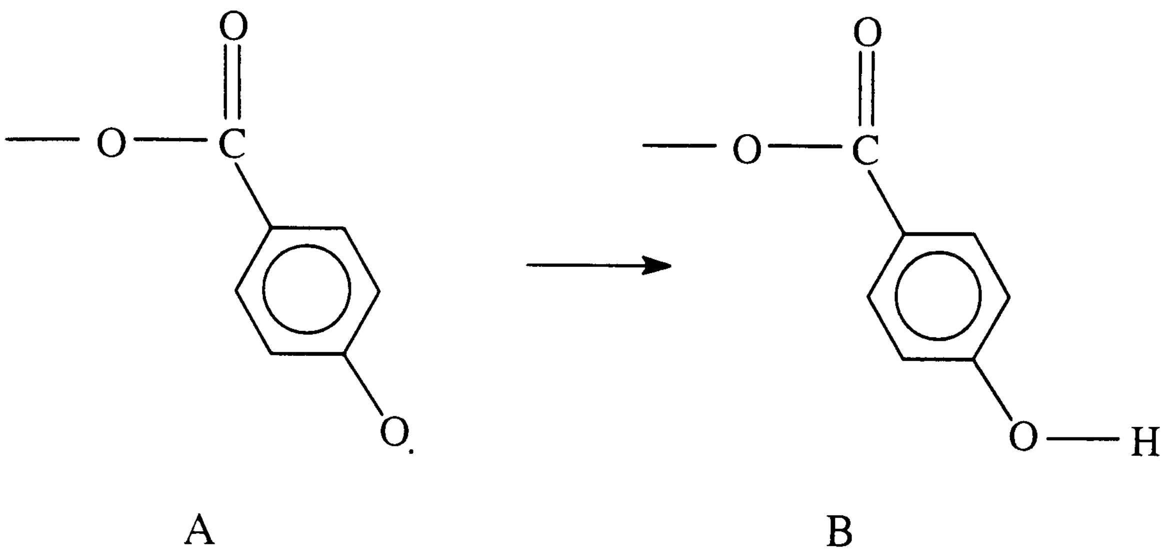

Figure 4.3 Formation of peroxy radical and subsequent H abstraction to form the hydroperoxide.

The discolouration of UV degraded pigmented coatings has been generally reported, indeed colour change is a used in assessing the durability of powder coatings. This is known as the Delta E requirement, set down by the AMMA [6]. The reason for this colour change is thought to be due to further reaction of the peroxy radical A to form quinones and diquinones [5]. These quinone groups have been shown to absorb UV and short wavelength blue light, giving a yellow colouration to the polymer.

4.1.3 Degradation Mechanisms of Bulk Polymer from UV light Exposure

So far, in considering the interaction of ultra-violet light with organic coatings, only the chemistry at a molecular level has been considered. However, the effects measured on UV weathered coatings by light reflectance or EIS are properties of the *bulk* coating. It is important to be able to relate the processes affecting the polymer chain, such as bond scission and polymer oxidation down to base ketone and alcohol units, to the breakdown of the bulk coating. The bulk degradation of clear and pigmented coatings will be considered separately, as they are distinct in terms of the mechanism of coating breakdown.

4.1.3.1 Bulk Degradation of Clear Coatings

When a coating is weathered by UV light, the polymer units in the resin start to undergo chain scission and degrade to low molecular weight alcohols and ketones, as stated previously. The effect of this is that as these degradation products are washed away, either by rain or in the condensation phase of a weathering chamber, the top part of the coating starts to loose its bulk, and embrittles. This loss of coating bulk can be measured as the 'loss of dry film thickness' (DFT) [9]. Measurements by Rehacek [10] on the loss of DFT in clear coatings weathered in Prague, Czech Republic has given losses of DFT at between 5 and 10 μm / year for three different alkyd coatings.

This loss of bulk and dry film thickness of UV weathered clear coatings takes place most in the top layer of the coating. The consequence of this is that while the top of the coating becomes thinner and more embrittled, the bottom part of the coating, near the substrate is relatively undamaged [10]. As the coating thermally contracts and expands, the top and bottom layers of the coatings have a different degree of thermal expansion and elasticity. This subjects the whole coating to great strain, which causes a general cracking and failure of the coating, as illustrated in figure 4.4.

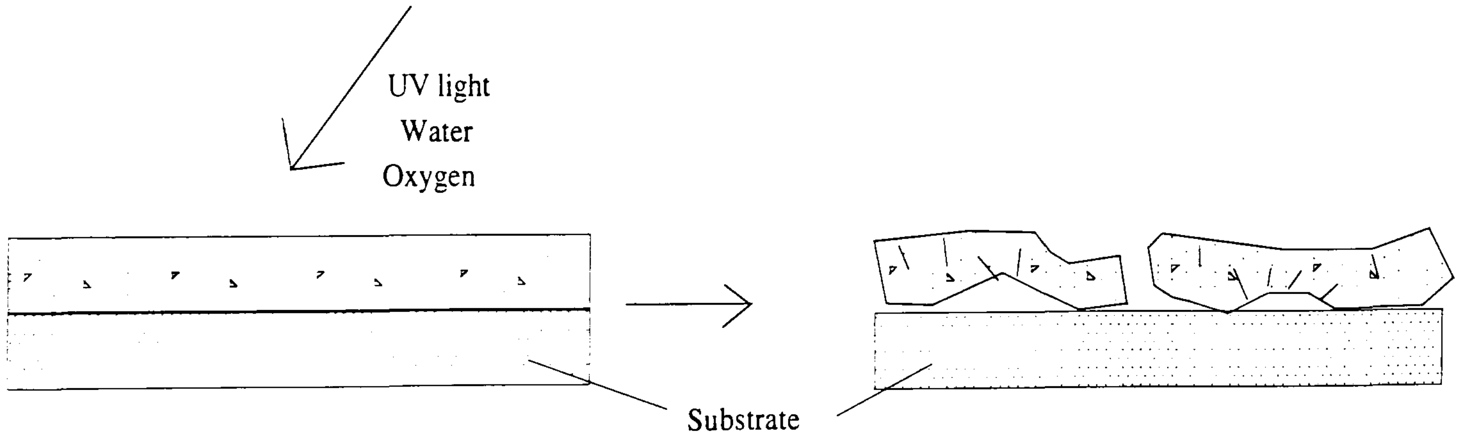

Figure 4.4 Cracking of a Coating Caused by Embrittlement of Top Layer of Coating by UV Weathering.

4.1.3.2 Bulk Degradation of Pigmented Coatings

The bulk breakdown mechanism of pigmented coatings is rather different than that of clear coatings. In terms of reduction of Dry Film thickness (DFT), the situation is far better than on the otherwise identical clear coatings. Rehacek [10] has tabulated the reduction in DFT / year for three systems, one a clear alkyd coating and two others being pigmented versions of the alkyd coating. DFT measurements showed a 10 μm /

year reduction for the clear coating, whilst the two pigmented systems showed between a 1.5 μm and 3 μm reduction / year.

The Pigment Volume Concentration (PVC) of a coating is the percentage volume of a coating that is pigment. The PVC of a coating has a critical effect on its elasticity [9,18]. The higher the PVC of a coating, generally the more brittle it is. A pigmented coating has the incident UV radiation concentrated in the top layer due to the pigment absorbing and reflecting UV light. The effect of this is to get a breakdown of the filler, (polymer resin) with polymer being lost as ketones / alcohols, in the same way as the clear coating. This increases the PVC in the top layer of the coating, causing embrittlement and cracking of the top layer of the coating. This cracking of the surface causes the coating deeper down to degrade, with larger cracks developing, eventually permeating through to the substrate [9]. The pigment itself can initiate photo-degradation if it has not been pre-treated. Titanium dioxide is photochemically active in its pure form, with UV light action capable of causing it to catalyse the formation of oxygen radicals, which can then lead to a polymer breakdown pathway. The titanium dioxide pigment utilised in the coatings considered in this thesis has been photochemically deactivated by coating the particles with an alumina coating.

4.1.4 Techniques for Measuring UV Degradation of Polymer Coatings

Measurement of the extent of degradation of a UV weathered coatings gives two principal items of information. 1. The degree of degradation at the moment in time the measurement was made, and importantly, 2. Predictive information on the likely extent of future coating failure. There are two principle approaches to measuring the effects of UV weathering on polymer coatings. One is to attempt to measure the photochemical oxidation reactions, or the products of (figure 4.1). This is looking at the degradation process at a *molecular* level. Another approach is to measure the changes in the bulk properties of the coating.

4.1.4.1 Measurement of Photochemical Oxidation Reactions: Measurements at a Molecular Level

Figure 4.1 shows the generally accepted reaction scheme for the photo-oxidation of polymers when exposed to UV light. It can be seen that the reactions involve radical intermediates and some of the principle reaction products are hydroperoxides. Therefore it should be possible to follow the reaction either by using ESR (Electron

Spin Resonance) spectroscopy, or by using iodometric titrations to measure hydroperoxide concentrations. In addition, a variety of other techniques can be used such as ^{13}C NMR , Infra-red spectroscopy [15], chemiluminesence [16] and oxygen uptake. For the purpose of this thesis, two techniques are considered:

Iodometric Titrations

Iodometric titrations have been used to measure the concentration of hydroperoxide species, formed in the degradation pathway of the polymer:

$$PO_2\cdot + \text{P-H (polymer)} \rightarrow PO_2H$$

Mielewski, Bauer and Gerlock [11] have measured hydroperoxide concentrations for different acrylic melamine and acrylic urethane compounds as a function of exposure time to a xenon arc UV weathering system. They measured hydroperoxide levels in the different polymers and achieved a correlation between the photo-initiation rate of the degradation reaction and the hydroperoxide concentrations present, although this correlation broke down after long exposure times. The photo-initiation rate was measured using ESR via a nitroxide decay assay. Mielewski *et.al* concluded that iodometric titrations, because of their correlation with the rate of initiation of free radicals might provide an effective measure of coating weatherability.

Electron Spin Resonance Spectroscopy

In reference [11] Mielewski *et.al* used ESR to measure the photo-initiation rate of acrylic urethane coatings by absorbing the nitroxide, 4-hydroxy-2,2,6,6-tetramethylpiperidinyl-1-oxyl into the weathered coating. On photolysis of the system, the decay rate of the nitroxide signal, proportional to the formation of radicals in the system was measured using ESR. This technique is similar to the study carried out by Gerlock, Bauer and Briggs [12], who used ESR to predict rates of coating photodegradation.

Sommer *et.al* have looked at a system for ultra fast weathering of polymers, where radical concentration can be measured as a function of time using ESR [13]. They were able to measure the effect of photostabilisers incorporated into the polymer, with a clear difference in the concentration of radicals formed between a stabilised and non-stabilised polymer being seen, during the first 200 minutes of light exposure. It would appear that in principle, ESR could be used as a 'fast answer' technique to determine the future UV resistance of a coating, with measurements being made in just a few hours.

Infra-red Spectroscopy (FTIR)

Fourier Transform Infra Red (FTIR) spectroscopy has been shown to be a sufficiently sensitive surface analytical technique to measure the concentration of photo-oxidation products in weathered polymer coatings. Work done by Mailhot and Gardette [15] has measured the change in the IR absorption maxima for the C=O absorption as ketone photo-oxidation products are formed. Derivatives of oxidation products were made by reaction of aldehydes and ketones with sulphur tetrafluoride (SF_4), acyl fluorides and alkyl fluorides. Acylfluorides give a distinct C=O absorption above 1800 cm^{-1}. Derivatives were also made with ammonia and methanol. By use of HPLC and using photolysis on the photo-oxidised coating, combined with FTIR the products of the photo-oxidation of polystyrene coatings have been identified and their relative concentrations found.

4.1.4.2 Measurement of Photochemical Oxidation Reactions: Measurements of Bulk Coating

The principle methods of physical determination of coating degradation after weathering are three specified by the AAMA [6]: Colour Retention, Chalk Resistance and Gloss Retention. These have specific ASTM specifications:

Colour Retention:	ASTM D 2244-85
Chalk Resistance:	ASTM D 659
Gloss Retention:	ASTM D 523-85

In addition there are various other techniques such as measuring the change in coating thickness with weathering such as Contact Angle of water on the surface, Electrochemical Impedance Spectroscopy, Scanning Electron Microscopy and techniques that measure the mechanical properties of the coating such as Dynamic Mechanical Analysis (DMA).

Colour Retention

The yellowing of white pigmented coatings has been previously mentioned in section 4.1.2.1 is due to the formation of conjugated quinone groups as the product of reactions of the hydroxyperoxide photo-oxidation products. Fading of paint colour is often due to chalking.

Chalk Resistance

Chalking of a weathered coating takes place because of the release of non-bound pigment powder from the surface of a weathered coating [9]. This comes about as a result in the dry film thickness (DFT) of the coating, during weathering, (so called 'shrinkage') which leaves non-bound pigment particles on the surface.

Gloss Retention

The gloss of a paint coating measures the degree of surface break-up of the coating [9]. Gloss is the percentage of visible light reflected from the surface at a specified angle to the normal (generally 20° and 60°). The two angles give different degrees of scattering of light, with the 20° angle always giving a greater degree of scattering than the 60° angle. These angles are specified by the ASTM D 523-85. Gloss is measured relative to a standard black glass surface, equated as 100% gloss). Gloss loss, like chalking comes about as the coating looses filler, exposing pigment particles on the surface. On non-pigmented coatings, the microcracking of the surface, caused by the effects previously discussed reduces the gloss as more reflected light is dispersed.

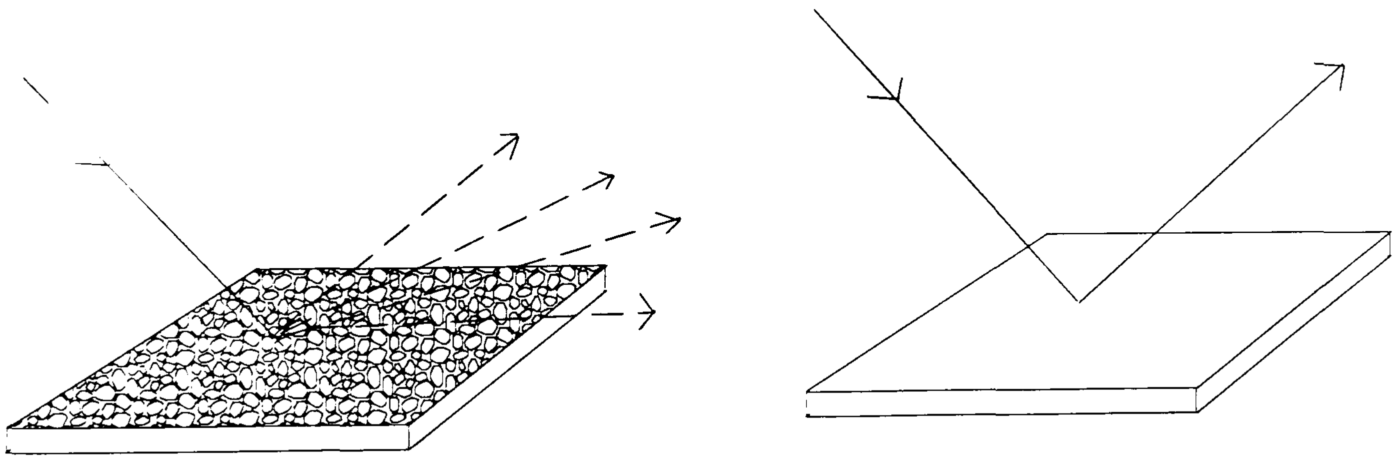

Low Gloss - Surface broken up, dispersing incident light

High Gloss - Smooth surface reflecting mos incident light

Figure 4.4 Diagram illustrating Light Reflection on the Surface of a Paint Coating

Gloss Retention is expressed as:

(Gloss of weathered Panel / Gloss of non-weathered Panel) x 100

In practice, it is common for coating specifications to be given for the time for a coating to reach 50% of its original value [2].

Electrochemical Impedance Spectroscopy (EIS)

EIS can be used to measure the change in porosity of a coating and the corroding area of metal underneath. The principle to EIS has been discussed in detail in Chapter 1. The use of EIS in measuring weathered paint coatings is discussed later in this chapter and in reference [1].

Scanning Electron Microscopy

SEM can be used to view, at very high magnification the weathered paint coating. It has been deployed in the work described in this chapter and in reference [1]. Its principle disadvantages are that it is destructive, as the electron beam damages the surface, and is non-quantitative. Visual microscopy can get around the difficulties of beam damage, although at the expense of magnification.

4.2 Aims and Experimental Summary

4.2.1 Aims

The aim of the work described in this chapter was to measure the degree of coating breakdown experienced by two polyester coatings when subjected to weathering in a QUV_b weathering apparatus. EIS does not appear to have been used previously to measure degradation of UV weathered coatings although it has been used to measure immersion effects of coatings in aqueous solutions [17]. EIS measurements were used to estimate the degree of underfilm corrosion taking place, and to compare with SEM and Gloss loss measurements.

4.2.2 Experimental

The experimental background to the study described in this chapter can be found in Chapter 2, especially section 2.7. To briefly summarise:

Two polyester powder coatings were made and applied to mild steel panels:

Coating 1: Clear, Polyester cross linked with multifunctional amide PRIMID®.

Coating 2: As coating 1, but incorporating deactivated titanium dioxide pigment. (White in colour)

These two coatings will be referred to as the clear and pigmented coatings respectively. The electrolyte was 0.1M hydrochloric acid, and the a silver / silver chloride reference electrode was used. The weathering times are given later. The QUV_b weathering apparatus was operated on a cycle of four hours QUV_b and four hours condensation. A sample of the two coating systems were subjected to four hourly thermal cycling between 20 and 50 °C (4h at 20 °C followed by 4h at 50 °C) and analysed using EIS in order to determine if the thermal differences experienced in the QUV_b weathering apparatus contributed towards coating degradation.

4.3 Experimental Results

The experimental results and discussion is divided into the three sections, referring to the EIS results, SEM results and Gloss loss.

4.3.1 Electrochemical Impedance Results

In order to calculate the values of porosity and wetted metal area, using the equations and method shown in Chapter 2 (2.4.6), it was necessary to find the values of charge transfer resistance and double layer capacitance of the bare steel immersed in 0.1M hydrochloric acid (under nitrogen).

These values are:

R_{cto} (Bare metal charge transfer resistance) = 75Ω
C_{dlo} (Bare metal charge transfer resistance) = 210 μF

All impedance values are for a working electrode area of 4.9 cm^2.

The value of the theoretical bulk resistance of a coating with 100% pores (R_{bt}) is dependent on the thickness of the coating. The general equation to find R_{bt} has been given in Chapter 2. In these experiments the conductivity of 0.1 M HCl is 0.042 Ω^{-1} cm^2. Therefore R_{bt} can be calculated by:

$$R_{bt} = \frac{d}{116.67}$$

Where d is the coating thickness in cm.

4.3.1.1 Measurement of Potential Thermal Degradation

As the ASTM D-4587 QUV weathering standard consists of a 4 hourly cycle between QUV_b (at approximately 55 °C) and water condensation (at approximately 40 °C) it is possible that the effect of thermal cycling could be responsible for causing coating breakdown. Hence, both types of coatings were exposed to a 4 hourly thermal cycling regime between 50 °C and 20 °C for time periods of up to 450 hours and their impedance responses monitored. In no case did this thermal cycling regime result in any deviation from the capacitive behaviour exhibited by the original unexposed coatings. The stability of polyesters over a wider temperature range has also been reported by Kinoshita *et.al* [19] who conducted a thermogravimetric / Fourier Transform Infra Red analysis of two polyesters, similar to those used in this work. They found no evidence of degradation products at temperatures below 350 °C.

4.3.1.2 Clear Coating Impedance

Before exposure to QUV_b radiation all coatings gave a purely capacitive impedance response indicating a lack of conducting pathways through the coating. These coatings remained capacitive for time periods of over 11 days immersion in electrolyte. The capacitance values typically lying within the range 60 - 120 pF cm^{-2}.

Upon exposure to QUV_b radiation there was a clear change in the impedance response of the coatings, changing from the original capacitive behaviour to give a Nyquist semicircle indicating the coating was beginning to fail. This is an important result as it clearly demonstrates that upon exposure to a QUV_b/condensation cycle the polyester coating systems are affected in such a way that transport pathways through the coating are formed.

The results presented in table 1 illustrate how the impedance behaviour of a typical weathered polyester clear-coat system used in this work varies with time of immersion in 0.1 M HCl.

Immersion Time / days	R_b / MΩ	C_g / pF	Porosity	R_{ct} / MΩ	C_{dl} / nF	Wetted Area
0	∞	288	-	-	-	-
1	94	263	2.88×10^{-10}	-	-	-
4	35	343	7.75×10^{-10}	-	-	-
5	35	336	7.75×10^{-10}	9.9	156	7.4×10^{-4}
7	30	341	8.90×10^{-10}	8.5	387	1.8×10^{-3}
8	22	348	1.25×10^{-9}	9.0	146	7.0×10^{-4}
10	20	376	1.34×10^{-9}	4.8	134	6.4×10^{-4}

Note - All resistance and capacitance values are given for the electrode area, which was 4.9 cm^2.

Table 1: Changes in the low and high frequency impedance response of a clear polyester powder coating (after 190 hours QUV_b exposure) with immersion time in a 0.1 M HCl electrolyte. System C4.

In 0.1 M HCl at pH 1 the corrosion products of iron are likely to be soluble, hence pore or channel blocking is not likely to occur and the impedance response (high frequency) will be that of the coating itself (not coating + blocked pores). In the same way, the low frequency response, when seen, will represent the active (or exposed) wetted metal area beneath the coating. As immersion time increases the electrolyte penetrates the pores in the coating. This causes the coating's bulk resistance to fall, an effect which is clearly seen in table 1. Eventually, the electrolyte at the base of the pores begins to spread beneath the coating, resulting in an increased wetted metal area which is seen as a second semi-circle in the Nyquist plot.

Although in all cases the coatings developed measurable porosity upon irradiation, there was no apparent correlation between the magnitude of the porosity and QUV weathering time, as shown in table 2. This may be because of the difficulties associated with producing coatings of the same thickness, especially the pigmented coatings. Coating thicknesses have been tabulated for comparison.

System	QUV Exposure Time / Hours	Porosity (2 Days)	Porosity (12 Days)	Coating Thickness
C1	0	$<1 \times 10^{-11}$	$< 1.1 \times 10^{-11}$	43 μm
C2	90	4.7×10^{-10}	8.7×10^{-9}	53 μm
C3	120	2.1×10^{-10}	1.4×10^{-9}	53 μm
C4	190	2.9×10^{-10}	1.3×10^{-9}	56 μm
C5	450	3.2×10^{-11}	2.0×10^{-10}	55 μm
C6	450	2.0×10^{-10}	1.6×10^{-10}	55 μm

Table 2: Variation in porosity of clear polyester powder coatings with QUV_b exposure time (after 2 days and 12 days immersion in 0.1 M HCl).

4.3.1.3 Pigmented Coating Impedance

Contrary to the unpigmented coatings, all of the white pigmented polyester coatings exhibited a measurable bulk resistance (hence porosity) prior to any exposure to QUV_b (table 3). This is expected as the incorporation of pigment into a coating generally results in pathways through the coating for ions, oxygen and water, in particular via the pigment/binder interface. This is further supported by the generally higher bulk capacitance (C_g) values obtained from the pigmented coatings, which is likely to arise due to a higher level of water in the coating.

System	R_b / MΩ	C_g / pF	Porosity	Coating Thickness
P1	149	903	1.2×10^{-10}	36 μm
P2	188	502	1.1×10^{-10}	47 μm
P3	149	518	1.6×10^{-10}	51 μm
P4	131	525	1.9×10^{-10}	51 μm
P5	117	548	1.4×10^{-10}	37 μm
P6	131	765	1.2×10^{-10}	38 μm

Table 3: Initial impedance characteristics of white polyester powder coatings before exposure to a QUV_b environment (after 1 day in 0.1 M HCl).

Unlike the clear coatings, there was little time dependence of the porosity upon immersion time in the HCl electrolyte after the first day for the pigmented coatings. The fact that the pigmented systems reach equilibrium before the clear systems suggests that the transport pathways in the clear system are narrower, hence more time is required for electrolyte percolation. It is important to note that the 'porosity' measurement calculated only gives an indication of the *total* defect area per unit area of coating and not the *number* and *size* of individual defects.

After QUV_b weathering there was very little change in the impedance properties of the pigmented coatings until exposure times of over 125 hours had been achieved, after which a clear increase in porosity was observed. From table 4 it is obvious that after a given exposure period a very significant increase in porosity occurs, which can be explained in terms of surface embrittlement and crack propagation.

System	QUV Exposure Time / Hours	Porosity	Wetted Area	Coating Thickness
P1	53	1.1×10^{-10}	-	36 μm
P2	122	1.6×10^{-10}	-	47 μm
P3	172	2.9×10^{-10}	-	51 μm
P4	216	9.0×10^{-10}	2.6×10^{-5}	37 μm
P5	304	4.8×10^{-6}	7.3×10^{-4}	38 μm
P6	304	1.0×10^{-7}	4.2×10^{-4}	38 μm

Table 4: Impedance characteristics of pigmented polyester powder coatings after exposure to a QUV_b environment (after 1 day in 0.1 M HCl).

Initially the incident UV radiation will only penetrate the surface of the white pigmented polyester coating to a depth of several microns. When the UV strikes the surface of the pigmented coating, the binder gradually degrades via a chain scission mechanism. This has the effect of causing the surface layer to become significantly more brittle, resulting in a coating which consists essentially of a thin brittle layer over a thicker, more elastic layer. Once this situation has been reached there is a propensity for deep cracking to occur [9]. If these cracks penetrate the coating, a significant increase in porosity similar to that observed would result. Figure 4.5 shows the way the coating rapidly fails (manifested as increase in coating porosity) after about 200 hours weathering.

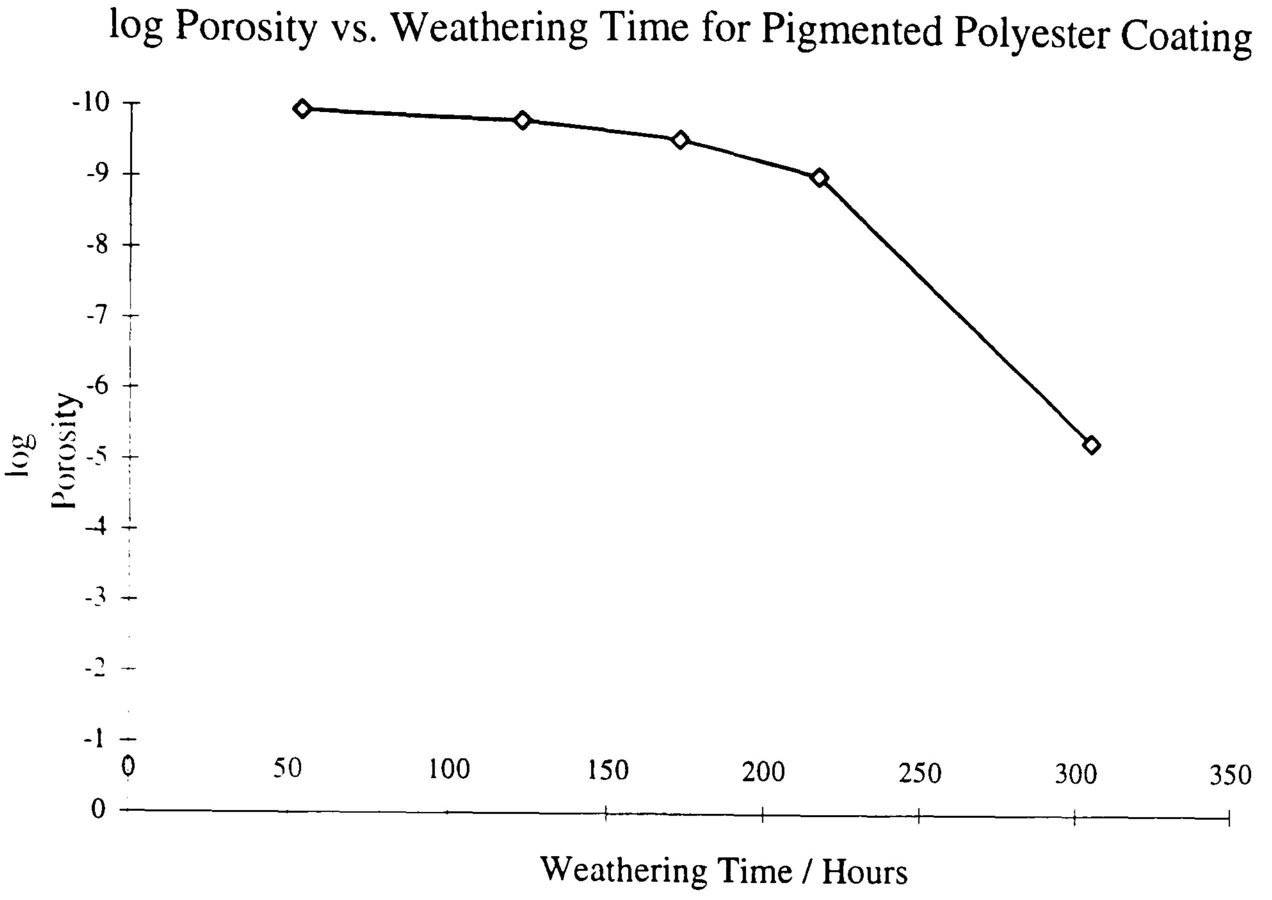

Figure 4.5: Change in Porosity of Pigmented Coatings with Weathering Time

This situation is different to the clear coat case, in which an initial increase in porosity is observed which does not appear to develop in the same catastrophic way. This is because, in the case of the clear coatings, the depth of penetration of the UV_b radiation is much greater. Thus, although degradation of the polymer does occur (as seen by the appearance of porosity), the embrittlement of the coating changes in a more gradual way with depth. Therefore in the case of the clear coating, the likelihood of catastrophic cracking through to the substrate is significantly reduced.

4.3.2 Scanning Electron Microscopy

Scanning Electron Microscopy showed up clear evidence of degradation on the weathered coatings. The lack of quantitative information provided by SEM has already been mentioned, however SEM does show the way in which the surface of the coating changes with weathering. All coatings were coated in a thin layer of gold prior to examination, to provide a conducting surface.

4.3.2.1 Clear Coating (Non-Pigmented)

Figure 4.6a shows that the non-weathered coating is fairly smooth and featureless:

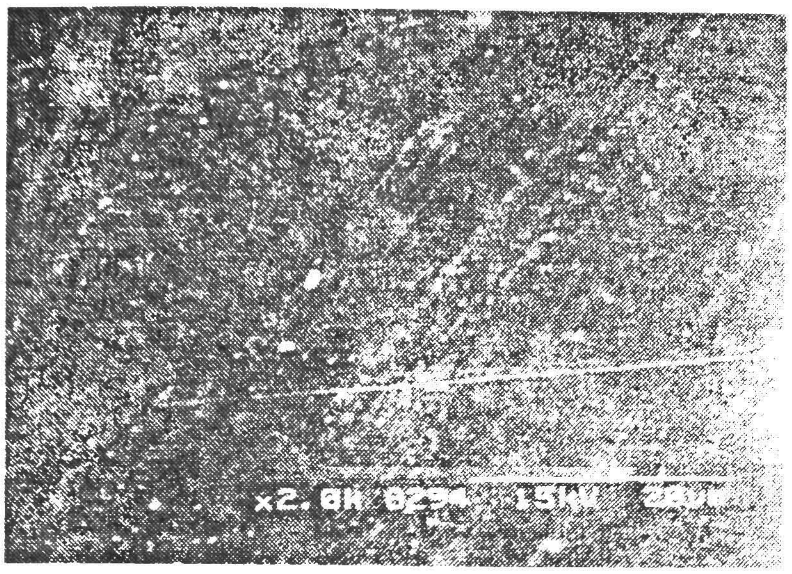

x 2000

Figure 4.6a Non-weathered

Evidence of coating break-up on the clear coatings was seen after 90 hours weathering (figure 4.6b). At high magnification a fine cracking of the surface is observed:

Figure 4.6b x 20,000
90 Hours weathering

After 190 hours of weathering, surface break-up is clearly seen even at low magnification. figures 4.6c (i & ii) shows the development large cracks and fissures in the surface. White deposits are observed on the surface of the coating - which is the beginning of chalking, resulting from photo-oxidation of the polymer.

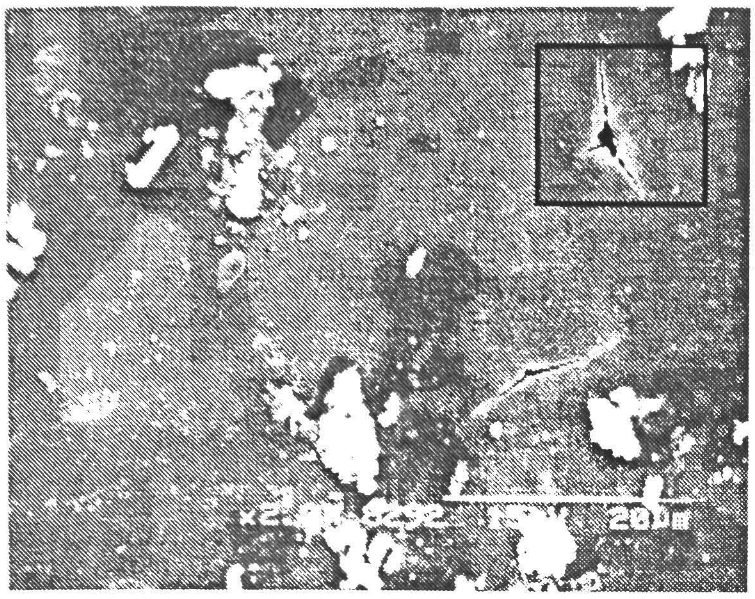

Figure 4.6c i x 2000 190 hours weathering

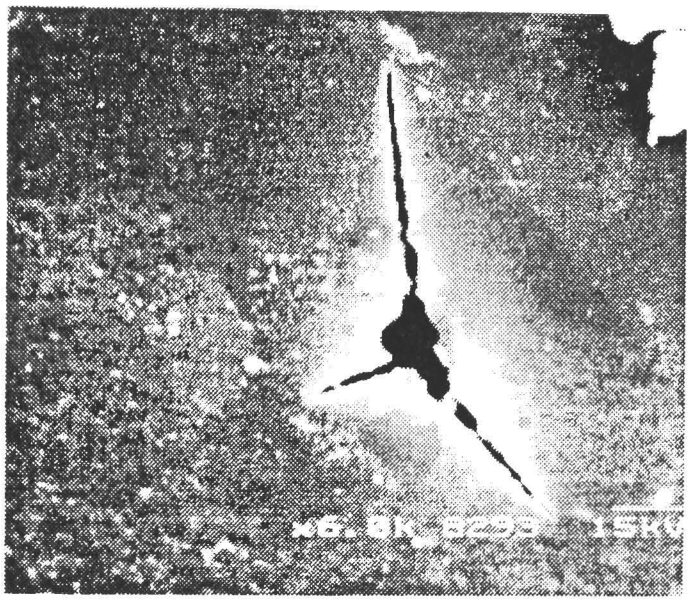

Figure 4.6c ii x 6000. Magnification of crack.

Figure 4.6d shows the extent of coating breakdown after 2500 hours weathering. At the low magnification of 2000x it is clear that the surface of the coating is broken down, with the formation of pores and defects in the coating. This coating was not analysed with EIS. A pore entrance is clearly visible in the centre of the picture.

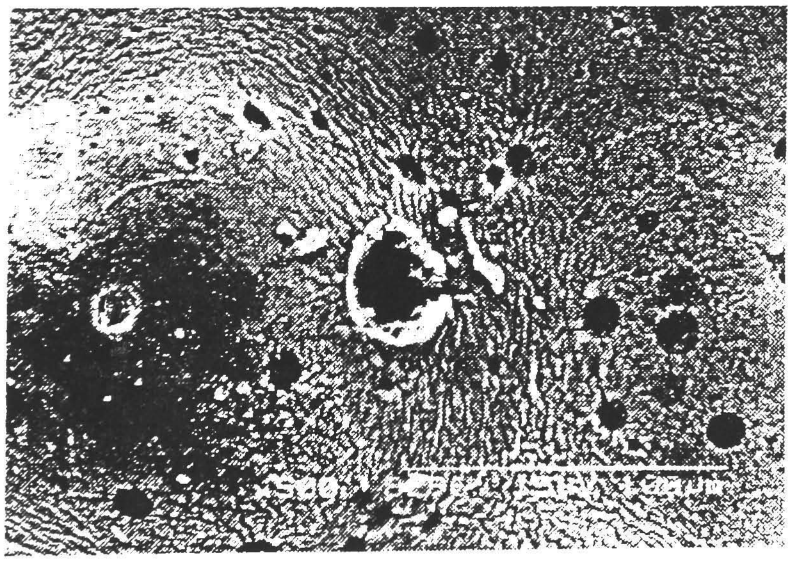

x 500

Figure 4.6d 2500 hours weathering

4.3.2.2 Pigmented Coatings

Degradation of the pigmented films in the form, of cracking was harder to observe than in the unpigmented films due to the pigment (TiO_2) particles scattered on the surface. What is evident from the SEM micrographs is the way in which the coating loses filler (polymer) leaving pigment on the surface. Also the development of pores is evident.

The non-weathered coating (figure 4.7a) shows the pigment distributed across the surface. There is some evidence to suggest that the area around pigment particles may be responsible for the measured porosity of the unweathered coatings with darker areas. suggesting depressions in the surface adjacent to pigment particles. This is shown clearly in figure 4.7b, where the area around a pigment particle has been magnified.

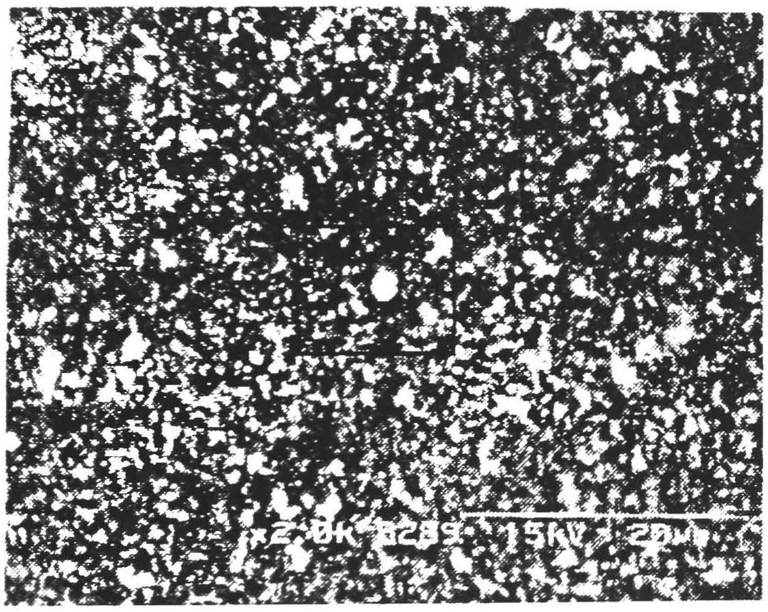

Figure 4.7a Pigmented Coating at x 2000 magnification.

Figure 4.7b Zoom of figure 4.7a 10000x magnification - looking at a pigment particle on the surface.

After 172 hours of weathering there appears to be the development of pores on the coating which may be enlargements of the depressions observed in the unweathered coating. This is seen in figure 4.7c, with the possible pore magnified in figure 4.7d.

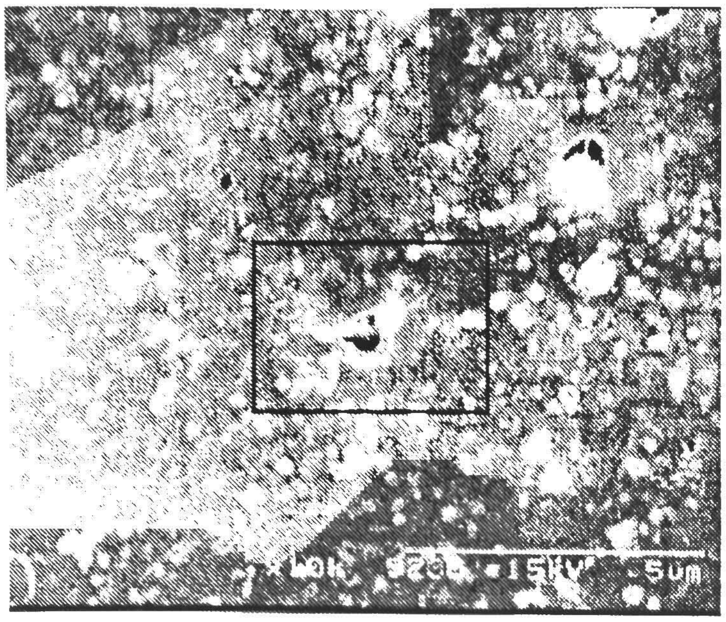

Figure 4.7c x10,000

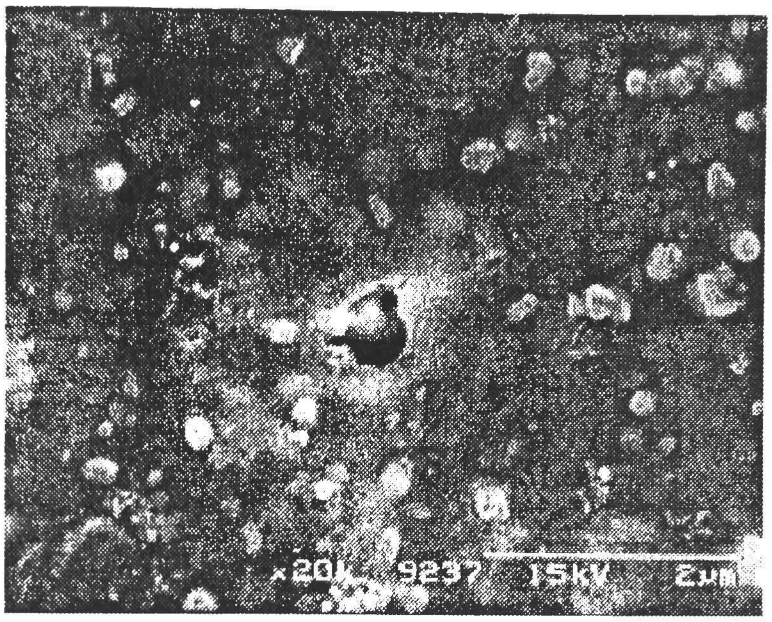

Figure 4.7d Zoom of figure 4.7d, looking at pore. x 20,000

The SEM micrographs of the coating weathered for 216 hours shows increased levels of debris on the surface, which is likely to be chalking, as pigment particles are left behind as the filler degrades. This is clearly seen in figures 4.7d & e. There is evidence of a substantial loss of filler around the pigment particles.

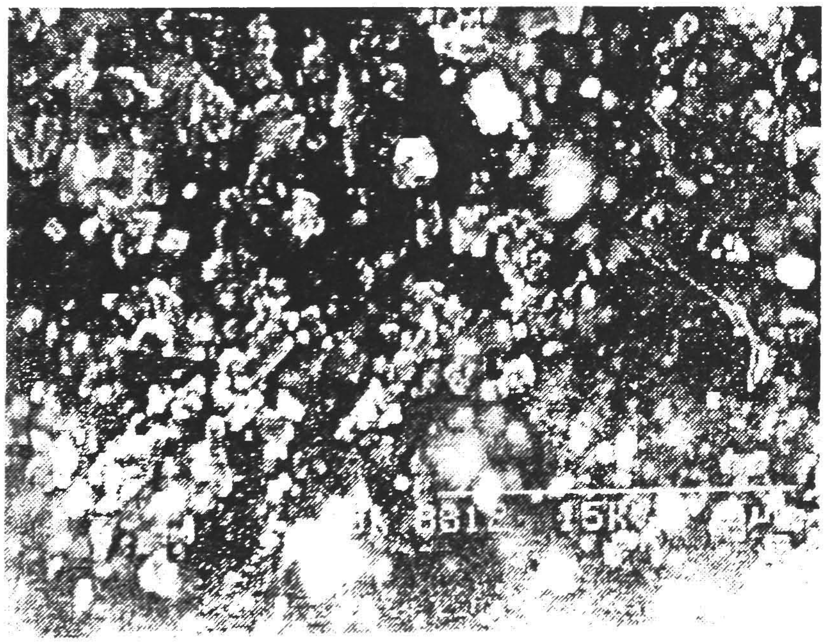

Figure 4.7d x 10,000

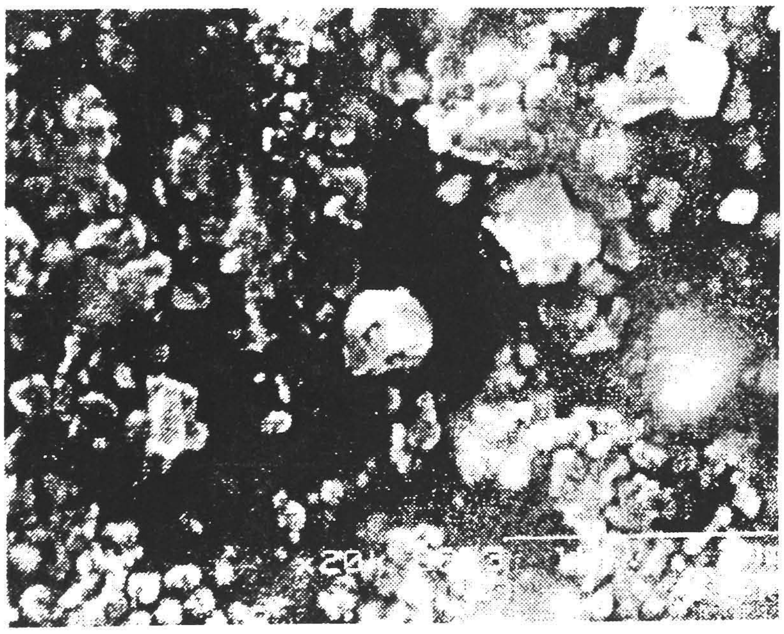

Figure 4.7e Zoom of degraded area in figure 4.7e x 20,000

4.3.3 Gloss Loss Measurements

Gloss measurements were only made on the pigmented coatings, due to failure of instrumentation when the measurement of the non-pigmented coatings was due to be made. Gloss retention at the two reflection angles (20° & 60° to the normal) is plotted with the change in retention of porosity against weathering time in figure 4.8.

% Porosity retention = (Porosity at zero weathering time / Porosity at time) x 100

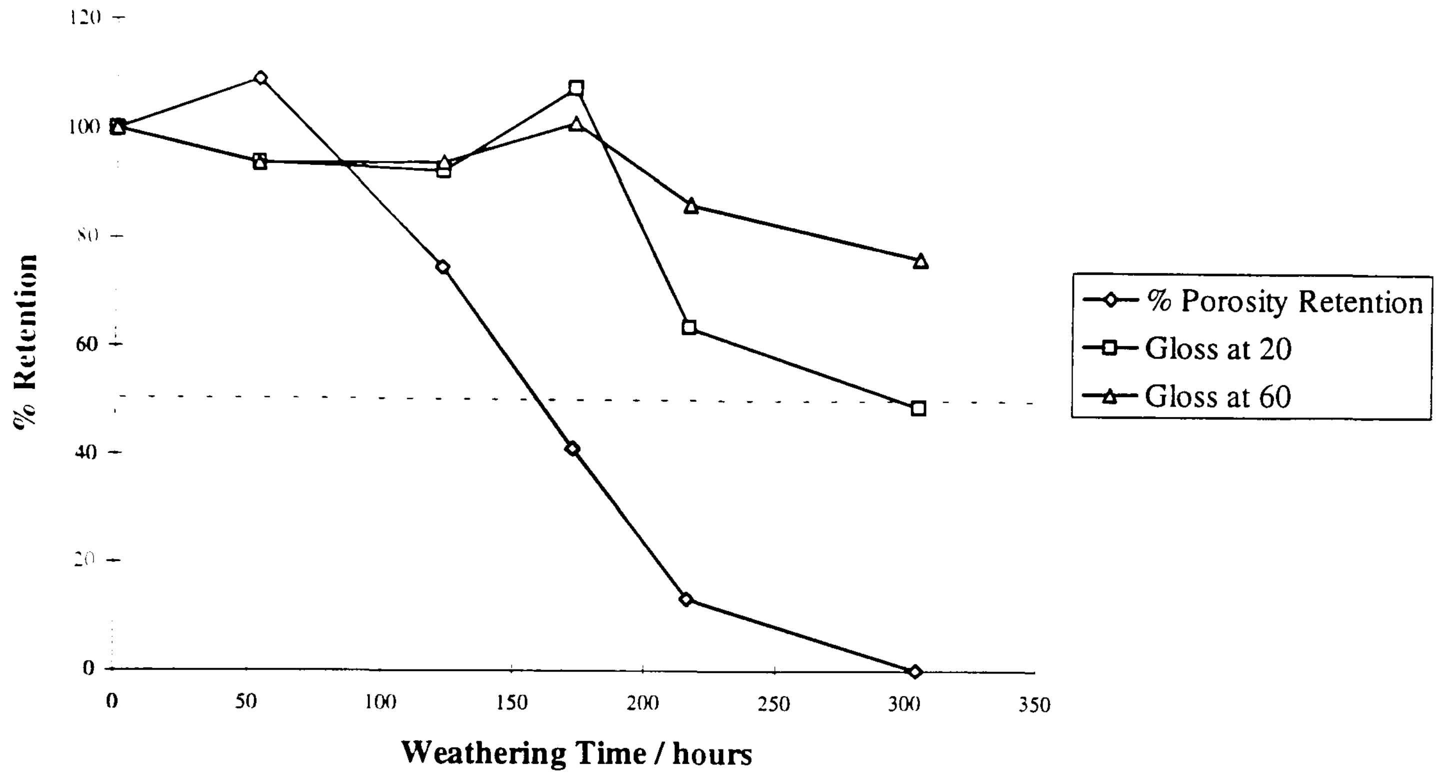

Figure 4.8 Graph of change in retention of porosity and gloss with weathering time.

In practice the benchmark failure point taken for durability evaluation of protective coatings is time taken to reach 50 % gloss reduction. It can be seen from figure 4.8 that porosity retention changes significantly before the gloss retention changes. This suggests that measurement of porosity retention may give an effective early warning of coating failure.

4.4 Conclusions

Exposure of powder polyester protective coatings to QUV_b radiation results in a degradation of the coating, generally observed as a decrease in gloss. This breakdown of the coating has been successfully followed in this work using EIS to quantify the extent of porosity generated as a result of QUV weathering. Qualitative information highlighting the changes in surface appearance of the films with increasing exposure time has also been obtained using SEM. It appears that EIS detects a breakdown in coating porosity at a time considerably before gloss loss measurements. SEM also shows coating degradation at a fairly early stage, although the qualitative nature of this technique makes it difficult to compare with measurements made by EIS or gloss measurements.

The difference in the EIS and SEM response of the pigmented and non-pigmented coatings gives further evidence of the difference in degradation mechanisms of such coatings. This was most clearly illustrated in the difference in the measured porosity with weathering time of the two coatings. The clear coating started to fail after a short weathering time, but did not increase in porosity significantly with time after the initial coating failure. The pigmented coating showed a gradual increase in porosity with weathering time. The non-pigmented coatings are penetrated to a greater depth by the UV light than the pigmented coatings, which results in a gradual increase in brittleness of the top layer and eventual coating failure. The pigmented coatings, with their low depth of UV penetration have the energy from the UV light concentrated in top layer of the coating. This causes a highly brittle top layer overlying a relatively elastic bottom layer which results in catastrophic coating failure, of the type measured on the pigmented coating after 300 hours weathering.

References

[1] R.D. Armstrong, A.T.A. Jenkins, B.W. Johnson, *Corrosion Science*. **37**, 1615, (1995).

[2] B.W. Johnson, R. McIntyre, *XXth Int. Conf. Org. Coat. Sci & Tech.*, Athens, 205, July 4-8 1994.

[3] M. Osmond, *J.O.C.C.A. Surface Coat. Int.,* **76**, 402, (1993).

[4] S. Peter Pappass, *Prog. Org. Coat.,* **17**, 107, (1989).

[5] B. Rånby & A. Hult, *Org. Coat. Sci. & Tech.* Vol. 7, eds. G.D. Parfitt, A.V. Patsis.

[6] American Architectural Manufacturers Association standard 605.2-92.

[7] Bulletin L-816, The Q Panel Company, Salford, Manchester M5 3EL.

[8] G.W. Grossman, *J. Coat. Tech.,* **49**, 45, (1977).

[9] E.V. Shmid, *Exterior durability of Organic Coatings,* F.M.J. Int. Publ. Ltd. 1988.

[10] K. Rehacek *et.al*, *Proc. FATIPEC-Congress,* part III, 5, (1980).

[11] D.F. Mielewski, D.R. Bauer & J.L. Gerlock, *Poly. Degrad. & Stab.* **33**, 93, (1991).

[12] J.L. Gerlock, D.R. Bauer, L.M. Briggs, *Xth Int. Conf. Org. Coat. Sci. & Tech*, Athens, 37, 9-13 July 1984.

[13] A. Sommer, E. Zirngiebl, L. Kahl & M. Schönfelder, *Prog. Org. Coat.,* **19**, 79, (1991).

[14] S.M. Halliwell, *RAPRA Review Reports 53,* **5**, (1992).

[15] B. Mailhot & J.L.Gardette, *Macromolecules*, **25**, 4119, (1992).

[16] R.H. Fleming & A.Y. Craig, *Poly. Degrad. & Stab.* **37**, 173, (1992).

[17] E.P.M. Westing, J.H.W. De Wit, G.M. Ferrari, *Corrosion Science* **36**, 957, (1994).

[18] L.A. Simpson, *Tioxide Ltd. Technical Service Report*, D 9150 GC.

[19] R. Kinoshita, Y. Teramoto, T. Nakano, H. Yoshida, *J. Therm. Anal.*, **38**, 1891, (1992).

PAGE

NUMBERING

AS ORIGINAL

Chapter 5

A Study into the Role of the Aluminium Substrate in Filiform Corrosion.

5.1 Introduction

The aim of the work described in this chapter is to attempt to understand the role of the substrate in influencing filiform corrosion. In order to do this the electrochemical behaviour of bare aluminium has been considered in detail and the aluminium substrate analysed both electrochemically and by non electrochemical techniques. Filiform corrosion was induced on two different aluminium substrates. Filiform corrosion was measured when the substrates were coated with polyester powder coatings. Measurement of growth rate of filiform corrosion on the two substrates has been made, and differences attributed to differences in the two aluminium substrates.

Filiform corrosion is a form of localised underfilm corrosion that is characterised by thread like filaments, generally growing away from a cut edge, or discontinuity in the paint coating. The growth rate of filiform corrosion is influenced by both the nature of the substrate on which the corrosion is actually taking place and the nature of the overlying paint coating. In this chapter the role of the substrate in affecting the rate of filiform corrosion is considered. In Chapter 6, the role of the paint coating is considered. The overall aim of the work described in both Chapters 5 & 6 is to try and gain a better understanding of the mechanism of filiform corrosion, and as a result to be able to suggest active steps to prevent or lessen filiform corrosion.

5.1.1 Description of Filiform Corrosion

There are certain distinct characteristics of filiform corrosion:

- Filiform corrosion filaments have two main parts: a tail composed mainly of corrosion product and a head that contains liquid, which is the active corroding medium (Fig. 5.1).

- Filiform corrosion filaments do not cross each other, and will not cross breaks in the coating.

- Filiform corrosion activity has to be initiated by salts - often chlorides, in the case of aluminium. Chloride is continuously present in the head, water and oxygen are used up in the corrosion reaction and need to be continuously replenished.

- Filiform corrosion has been observed on iron, aluminium and magnesium substrates.

- A humid atmosphere is required for filiform corrosion advance, but at greater than 95% relative humidity (R.H.), filiform corrosion stops and blistering occurs.

- Oxygen and water are required for filiform corrosion growth.

Figure 5.1 shows the probable location of anodic and cathodic sites and the general features of filiform corrosion.

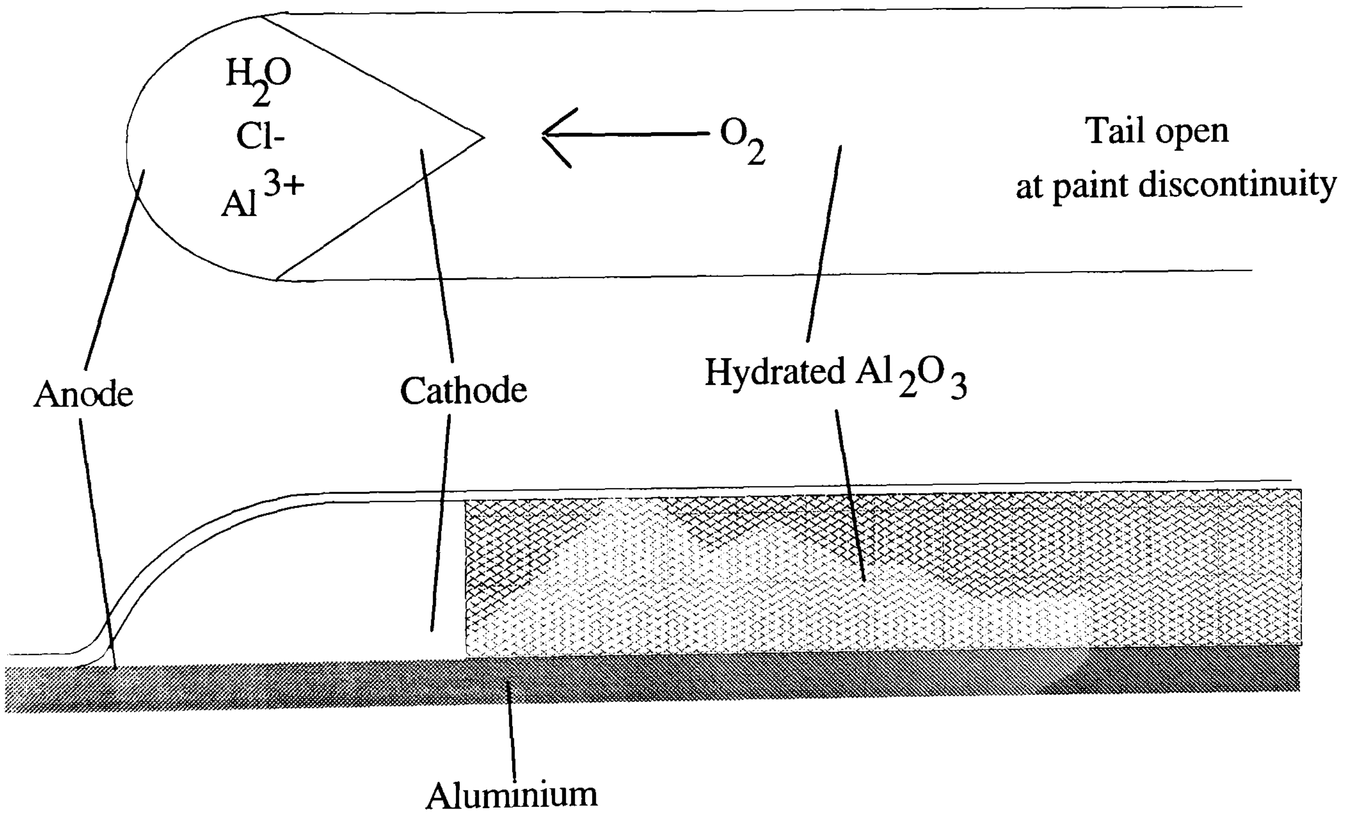

Figure 5.1 Diagram of the head and tail of a filiform corrosion filament.

A low resolution SEM micrograph shows the main visual characteristics of filiform corrosion (Fig. 5.2). The crack running horizontally across the top of micrograph is a paint discontinuity, cut into the coating. The way the paint coating has been pushed up by the filiform corrosion filament is clearly seen:

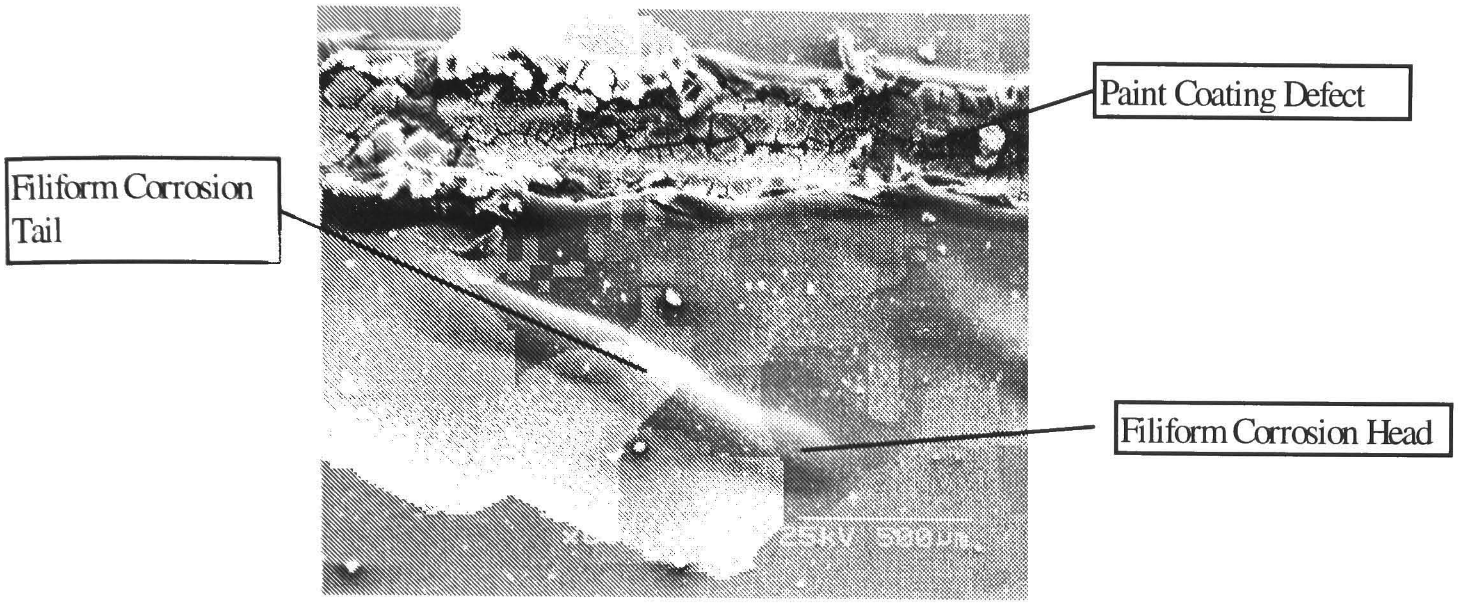

Figure 5.2 Low Resolution SEM of a Filiform Corrosion Filament at x 60 magnification.

5.1.2 Mechanism of Filiform Corrosion: A Review of the Literature

Filiform corrosion was first described in the literature in 1944 by Sharman [1]. Filiform corrosion trails consist of a tail section, containing hydrated corrosion products *i.e.* $Al_2O_3.nH_2O$ and a head, that contains liquid, and is the corrosion front where the filiform corrosion advances. This can be seen diagramatically in figure 5.1.

Filiform corrosion has been observed mainly on aluminium and steel substrates, and usually starts at cut edges on polymer coated panels, although Schofield *et.al* have initiated filiform corrosion at areas of salt contamination on paint films [4].

It is generally accepted in the literature that the filiform corrosion head has discrete anodic and cathodic regions. This is due to a non-uniform supply of oxygen to the head, with a higher oxygen concentration at the back of the head, where oxygen is supplied from the tail, which is itself open the atmosphere (a differential aeration cell). In addition, there is some evidence from Scanning Electron Microscopy of the corroded substrate of intermetallic impurities in the substrate forming localised cathodic areas [9]. The separation of cathodic and anodic regions is thought to give filiform corrosion its directionality. Should the differential supply of oxygen fail, with oxygen being uniformly available in the head, then its is likely that the filiform head will loose its directionality and form a blister.

Measurements of the potential difference between the front of the head and the tail are given by Slabaugh *et.al* [11], who measured a potential difference of 25 mV with microcalomel electrodes between the area immediately in front of the head (anodic) and the tail (cathodic). Measurements of pH in the head by Slabaugh *et.al* [11] have indicated that the fluid in the head has a pH of 1, although they were unable to distinguish between any change in pH across the cell. Ruggeri and Beck [12] have estimated that the pH in the front of the head is around 1 and the pH at the back of the head higher, at around 4-5.

There are two main theories for the mechanism of delamination of the coating above the head. One is osmotic disbondment. Several researchers [2,7,8] accept the possibility that the formation of salts and existence of ions in the filiform head can cause osmotic transfer of water across the film. Slabaugh [7] and van der Berg [8] claim that this osmotic pressure inside the head is sufficient to cause delamination of the polymer above the metal. However this suggestion is refuted by Funke [3], who maintains that insufficient osmotic pressure can build up since the tail of the filiform corrosion filament is open to the surroundings at one end.

There has been recent evidence from Scanning and Transmission Electron Microscopy studies of sections through filiform corrosion filaments that the mechanical force from hydrated corrosion products may have an important role in causing delamination, and filiform corrosion advance, especially on substrates which give better adhesion to the overlying coating. This cause of delamination was originally proposed by Van Loo *et.al* [10] and has been confirmed by Nisancioglu *et.al* [9].

The degree of adhesion between the metal and coating is likely to be of importance when considering filiform growth, as this will affect the ease of delamination. In some work done by van der Berg [8], it was found that slower filiform growth was observed on rough, sand blasted steel compared to growth on smooth steel that was only degreased.

The effect of reducing the corrosion activity of the substrate has been investigated [9]. It has been found that using a chromate conversion coating on the substrate can substantially inhibit filiform corrosion growth.

5.2 Experimental

A general description of the work carried out here is given in Chapter 2. Experimental work described in this chapter consists of:

- An electrochemical study of the bare aluminium substrates, both A & Q.

- Measurement of surface of two aluminium substrates using SEM and laser profilometry.

- Coating of A and Q aluminium with a polyester powder coating, and measurement of the rate of filiform growth rate, following pretreatment (discussed in Chapter 2).

Both aluminium substrates were pre-treated by immersion in 1M sodium hydroxide for five minutes, then washed with high purity water. The powder coatings applied to the two substrates were polyester cross linked with PRIMID®, one clear and one pigmented, grey in colour. The relative difference between the two coating types are not compared here, but in Chapter 6. The two coatings referred to are given the coding G1 (Pigmented) and W1 (non-pigmented). The precise composition of these coatings can not be revealed for reasons of commercial confidentiality.

5.3 The Corrosion and Electrochemistry of Aluminium

5.3.1 Introduction

An understanding of the way in which aluminium corrodes integral to an understanding of the role of the aluminium substrate in filiform corrosion. In this work, two aluminium substrates were studied, Q aluminium and A aluminium. The two substrates were analysed by linear sweep voltammetry, EIS, EDX, SEM and laser profilometry.

5.3.2 Aluminium Corrosion [17]

Aluminium has a passive oxide film covering its surface. Aluminium corrodes via dissolution of the oxide film. The formation of the oxide film is thermodynamically favoured with a free energy of -864.6 kJ mol^{-1} under standard conditions for the reaction:

$$Al + 3H_2O = Al_2O_3 + 3H_2$$

In acidic media the oxide layer can breakdown by:

$$1/2Al_2O_3 + 1/2\ H_2O + H^+ \rightarrow Al(OH)_2^+$$

$$Al(OH)_2^+ + H^+ \rightarrow Al(OH)^{2+} + H_2O$$

$$Al(OH)^{2+} + H^+ \rightarrow Al^{3+} + H_2O$$

and in alkaline solution:

$$1/2Al_2O_3 + 1/2H_2O \rightarrow Al(OH)_3$$

$$Al(OH)_3 + OH^- \rightarrow AlO_2^- + 2H_2O$$

These reactions take place on the oxide / solution interface. As the oxide layer dissolves, the equilibrium across the metal / oxide interface is simultaneously changed causing more metallic aluminium to be oxidised. Overall, aluminium corrosion takes place over both the two interfaces.

The overall corrosion potential that aluminium takes up in a solution is a combination of the two half reactions:

		Standard Potentials
	$Al \rightarrow Al^{3+} + 3e^-$	$E^\circ = -1.67$ V
and	$O_2 + 4H^+ + 4e^- \rightarrow 2H_2O$	$E^\circ = 1.23$ V
or	$2H^+ + 2e^- \rightarrow 1/2\ H_2$	$E^\circ = 0.00$V

The reduction reaction that dominates will depend on the availability of oxygen in the system. In a study done by Brown *et.al* [19] on the growth of conversion coatings on aluminium, the oxygen reduction reaction on aluminium was considered to take place by electron tunnelling across the aluminium oxide film reducing oxygen on the oxide surface (in the absence of conducting channels through the oxide).

In a deaerated solution at unit concentrations of corrosion products the corrosion potential of the aluminium corrosion system will lie between -1.67 V and 0.00V. However it is not fixed and will drift considerably when measured experimentally depending on electrolyte, gas purge conditions, impurity ions and surface pretreatment.

This is unlike iron, which has a fairly fixed corrosion potential. The effect of oxygen on the corrosion potential taken up by aluminium is clearly demonstrated in the following experimental results.

5.3.3 The Solution Electrochemistry of Aluminium

The potential of the aluminium anodic reactions given in section 5.3.2 are only correct if the concentration of the reactants are at unit activity and at a temperature of 25° Celsius. In a corrosion situation, the concentration of Al^{3+} will be limited by the solubility product of the reaction:

$$Al(OH)_3 = Al^{3+} + 3OH^-$$

The solubility product of aluminium oxide is: 1×10^{-33} $mol^4\ dm^{-12}$. Therefore the concentration of Al^{3+} in the electrolyte can be calculated, given that:

At pH 1 (0.1M H_2SO_4), $[OH^-] = 10^{-13}$ M.

So: $[OH^-]^3 = 10^{-39}\ M^3$

Which gives a theoretical concentration of Al^{3+} of 10^6 M. This is calculated thermodynamically, and does not take into account the rate of dissolution of the aluminium.

Using this calculated concentration of Al^{3+}, it can be seen that the standard oxidation potential of aluminium is modified by the Nernst equation:

$$E = E^o + \frac{2.3RT}{nF}\log(a_{M^{n+}})$$

Giving a value for the oxidation potential of aluminium as:

$$E = E^o + \frac{2.303RT}{3F}\log[Al^{3+}]$$

$$E = -1.67 + 0.020 \times 6$$

$$\mathbf{E = -1.55\ V}\ \textit{vs.}\ \mathbf{SHE}$$

The reduction potentials of oxygen and H^+ are also pH dependent, related by the Nernst equation. This has been discussed in Chapter 1 (1.5).

The potential taken up by the corroding aluminium depends on potentials of the anodic and cathodic reactions, as discussed, and the relative gradients of the potential - current polarisation curve in the potential region close to the corrosion potential.

5.3.4 Linear Sweep Measurements on Bare Aluminium (Theory)

Work done by Evans and Koehler [16] has demonstrated that the Tafel equation can be applied to the aluminium corrosion situation. However, the aluminium dissolution curve (anodic reaction) did not exhibit Tafel type behaviour. They therefore used the intercept of the cathodic Tafel line with the corrosion potential to calculate the corrosion current. This is demonstrated in Figure 5.3.

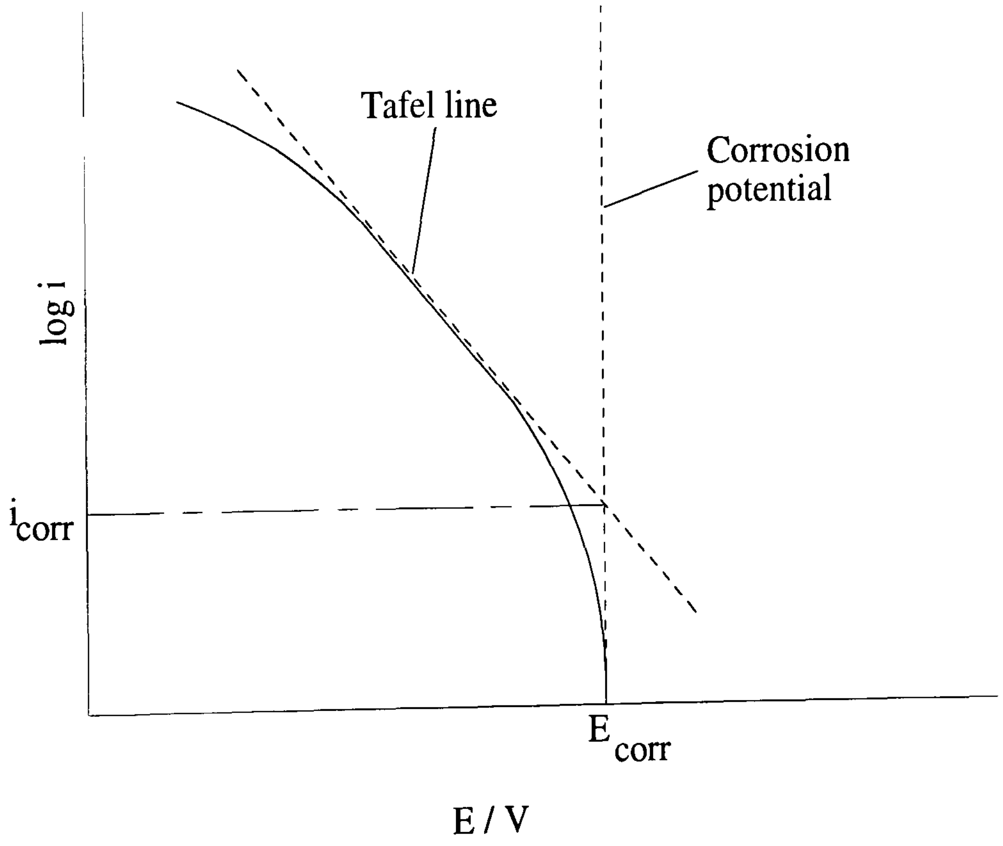

Figure 5.3 - Determination of corrosion current from cathodic Tafel line intercept with corrosion potential.

The anodic current / potential line does not obey Tafel type behaviour because the thickness of the oxide layer changes with potential. The anodic current becomes potential independent as the current becomes limited by the rate of dissolution of the oxide layer. At positive higher potentials the oxide film will be thicker than at lower potentials so inhibiting the anodic reaction.

5.3.5 Tafel Analysis Results of Bare Aluminium

The linear sweep voltammograms have been re-plotted as Tafel plots to allow a direct comparison of the effect of oxygen in the electrolyte on rest potential and corrosion current. The aim of this work was to try and discern a significant difference in the corrosion rates of the two substrates, and to attempt to quantify the affect that oxygen has on the relative corrosion rates of the two substrates. This information is important, as it is related to the rate of filiform corrosion on the two substrates which is considered later. If the two substrates show very different immersed corrosion rates then this could be related to any difference in measured filiform corrosion rate. In figure 5.4 and 5.5 tangents have been added to the plot, showing the cathodic Tafel line / corrosion potential intercept.

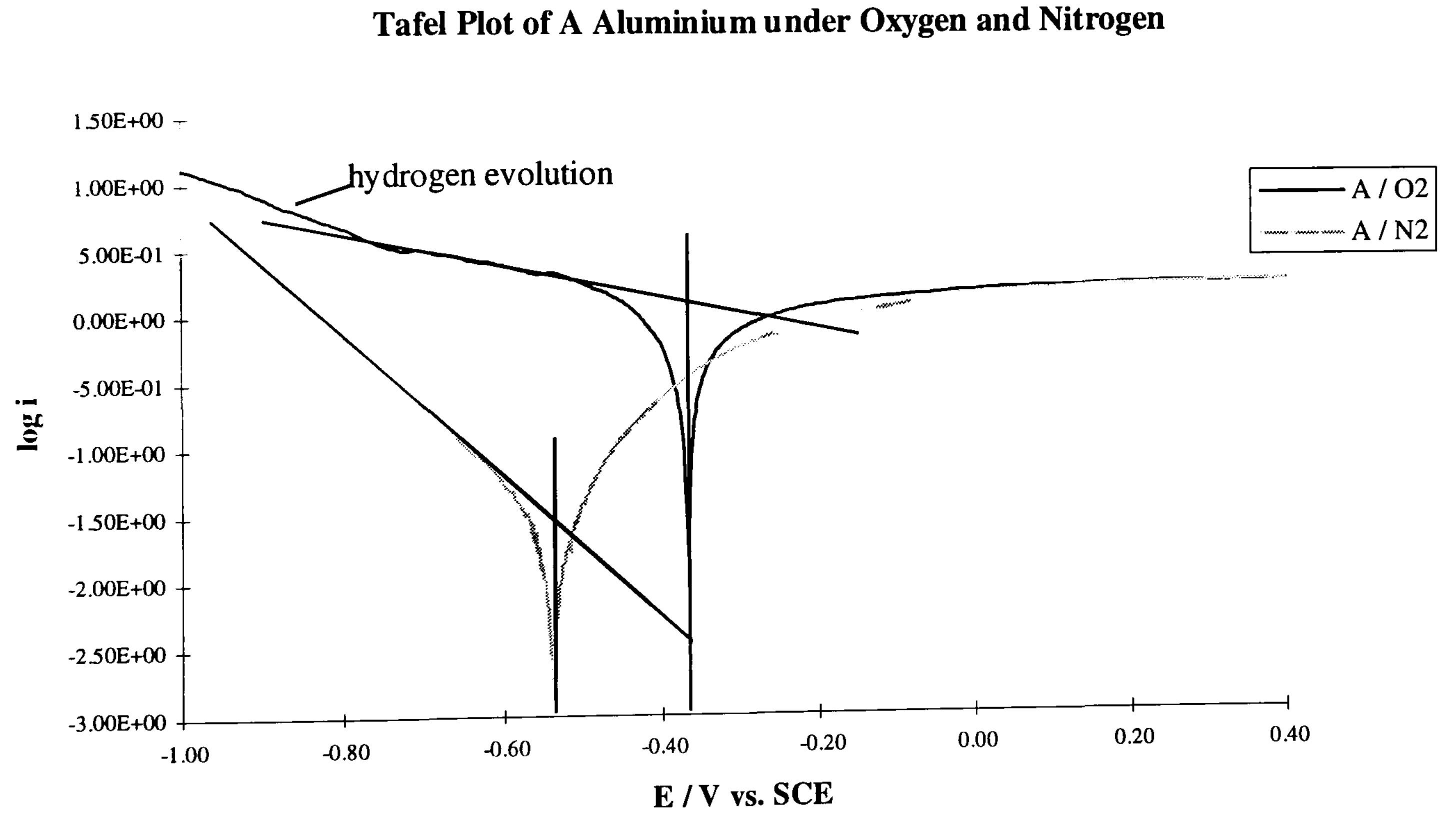

Figure 5.4 A aluminium under nitrogen and oxygen:

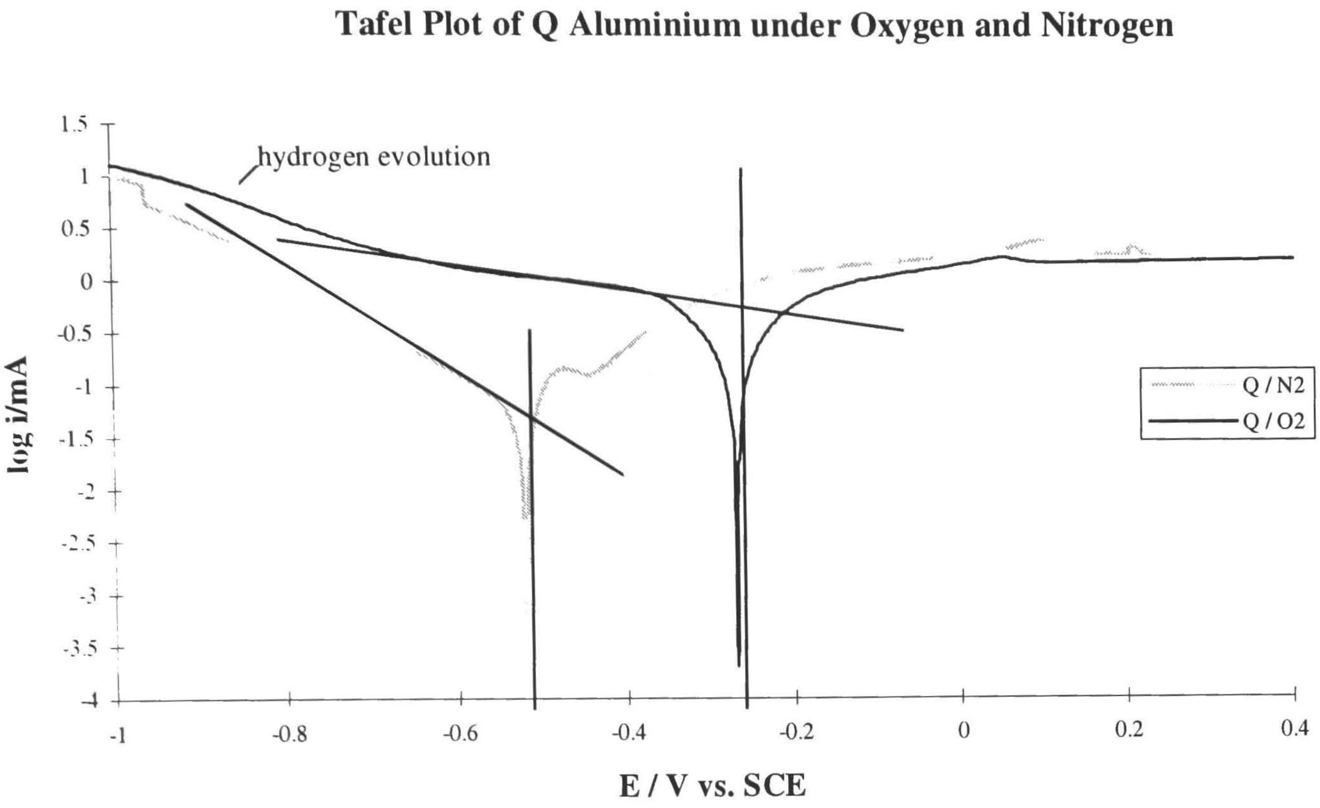

Figure 5.5 Q aluminium under nitrogen and oxygen:

The deviation from Tafel behaviour of the anodic reaction is clearly seen. The anodic reaction becomes potential independent, as the oxide layer thickens. This is because the anodic reaction becomes limited by the rate of dissolution of the oxide layer.

The Tafel gradients and corrosion potentials are tabulated below for the different systems:

	A Aluminium	**Q Aluminium**
E_{corr} / Nitrogen	-550 mV	-510 mV
E_{corr} / Oxygen	-360 mV	-270 mV
Cathodic Tafel gradient / Nitrogen	180 mV decade^{-1}	200 mV decade^{-1}
Cathodic Tafel Gradient / Oxygen	780 mV decade^{-1}	560 mV decade^{-1}
Corrosion Current / O_2	0.32 mA cm^{-2}	0.13 mA cm^{-2}
Corrosion Current / N_2	0.0051 mA cm^{-2}	0.013 mA cm^{-2}

Table 1 - DC measurements of the two aluminium corrosion systems.

Table 1, and figures 5.4 and 5.5 show clearly the difference in the cathodic Tafel gradient of aluminium under oxygen and nitrogen. The Tafel gradient of the systems under oxygen is much greater than under nitrogen, partially accounting for the more positive corrosion potential of aluminium under oxygen. The corrosion currents of the two substrates, which are related to the corrosion rates, are different. A aluminium corroded faster under oxygen than Q aluminium, although both substrates corroded faster under oxygen than nitrogen. Q aluminium corroded faster under nitrogen than A aluminium under nitrogen. This can be attributed to the fact that oxygen is, in principle, a more powerful electron acceptor than H^+. In oxygenated 0.1M sulphuric acid both the effect of oxygen reduction and hydrogen evolution can be seen on the Tafel plot, as shown in figures 5.4 and 5.5..

5.4 EIS Response of Aluminium

Aluminium was polarised at -500 mV *vs.* SCE and the EIS spectrum measured. As the corrosion potential is very unstable, -500 mV *vs.* SCE was chosen in order that the EIS response of the bare aluminium could be compared with the EIS response of the coated aluminium. -500 mV *vs.* SCE was reasonably close to all the measured corrosion potentials of the two substrates under oxygen and nitrogen. The approximate polarisation resistance of the aluminium has been determined. The aim of this work was to obtain the impedance parameters of the bare aluminium for comparison with the linear sweep measurements and in order that the porosity and wetted metal area of the coated aluminium could be calculated later (Chapter 6). This is shown in figure 5.6. The difference in the resistance of the system under nitrogen and oxygen is clear. Note that the inductive loop has been omitted.

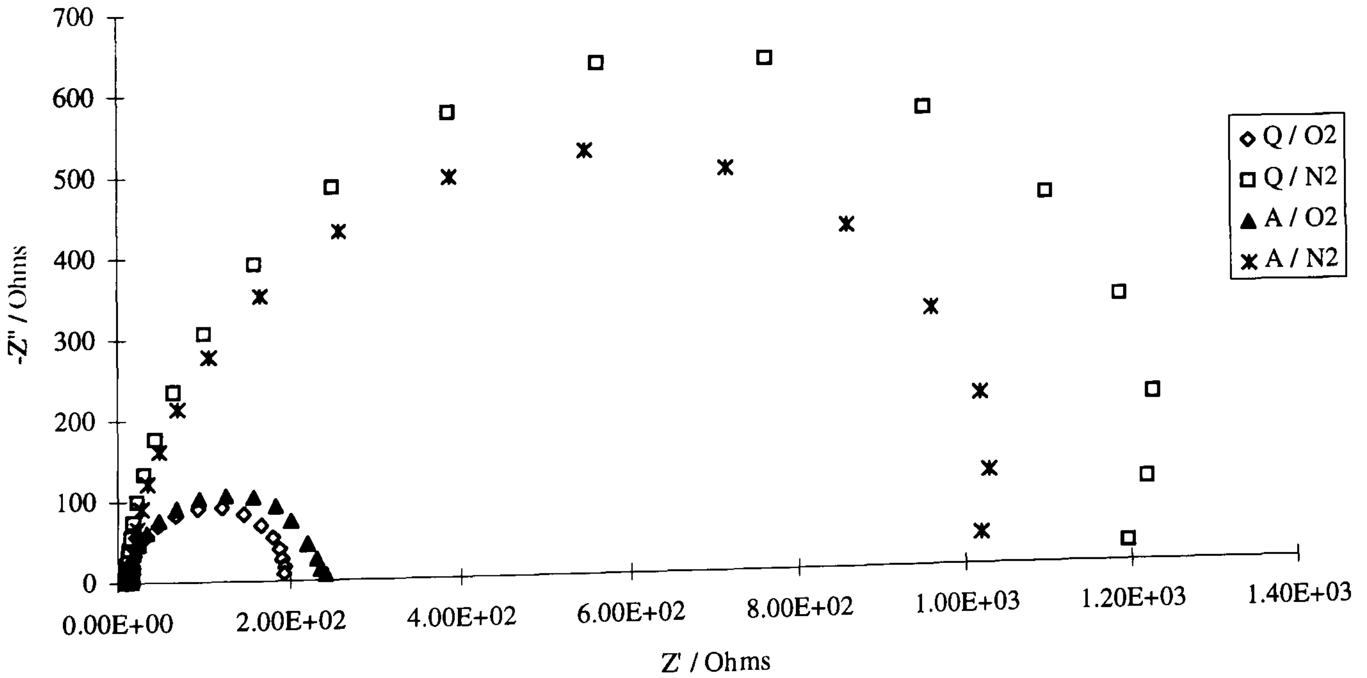

Figure 5.6 EIS Response of Q and A Aluminium Polarised at -500 mV *vs.* SCE under Nitrogen and Oxygen.

The resistance and capacitance values of the four systems are tabulated below in Table 2:

Q / O_2		Q / N_2		A / O_2		A / N_2	
R / KΩ	**C / μF**	**R / KΩ**	**C / μF**	**R / KΩ**	**C / μF**	**R / KΩ**	**C / μF**
0.184	51.8	1.23	36.6	0.232	36.4	1.04	37.8

All measurements are for a working electrode area of 4.9 cm^2.

At potentials close to the corrosion potential, the measured resistance is the polarisation resistance. This is related to the gradient of the polarisation line by [13]:

$$R_p = \frac{dE}{di} \approx \frac{\Delta E}{\Delta i}$$

Which comes from the Stern-Geary equation discussed in Chapter 1 [14]. The Stern-Geary equation relates the polarisation resistance with the corrosion current of the substrate (Chapter 3, 3.3.3). This shows that the corrosion current is inversely proportional to the polarisation resistance.

$$R_p \propto \frac{1}{I_{corr}}$$

Therefore the impedance results shown in figure 5.5 confirm that aluminium corrodes more slowly under nitrogen than oxygen, although the relative rates of corrosion (inversely proportional to polarisation resistance) of the two substrates are different compared with the linear sweep measurements. Q aluminium has a lower polarisation resistance under oxygen and A aluminium has a lower polarisation resistance under nitrogen. The reason for this discrepancy is probably due to the fact that the EIS measurements of aluminium were not done at the corrosion potential but at -500 mV *vs.* SCE. In this work, the measurements of the Tafel intercepts to measure corrosion rate have been taken as the most accurate way of measuring the relative corrosion rates of the two substrates.

5.5 Non Electrochemical Analysis of Aluminium

The morphology of the surface of the aluminium has been studied using Scanning Electron Microscopy (SEM), Laser profilometry and EDX. Metallic impurities in the surface of the aluminium have been determined using EDX (Energy Dispersive X-ray Spectroscopy).

5.5.1 Scanning Electron Microscopy of Aluminium

The results of the measurements of surface roughness show that the A aluminium is significantly smoother than the Q aluminium. The SEM images shown in figure 5.7 show a small area of the metal (*ca.* 100 x 100 µm). The A aluminium is noticeably smoother, with extrusion lines running vertically down the picture. The Q aluminium has a more disordered surface. Intermetallic particles on both substrates are clearly seen on the surface.

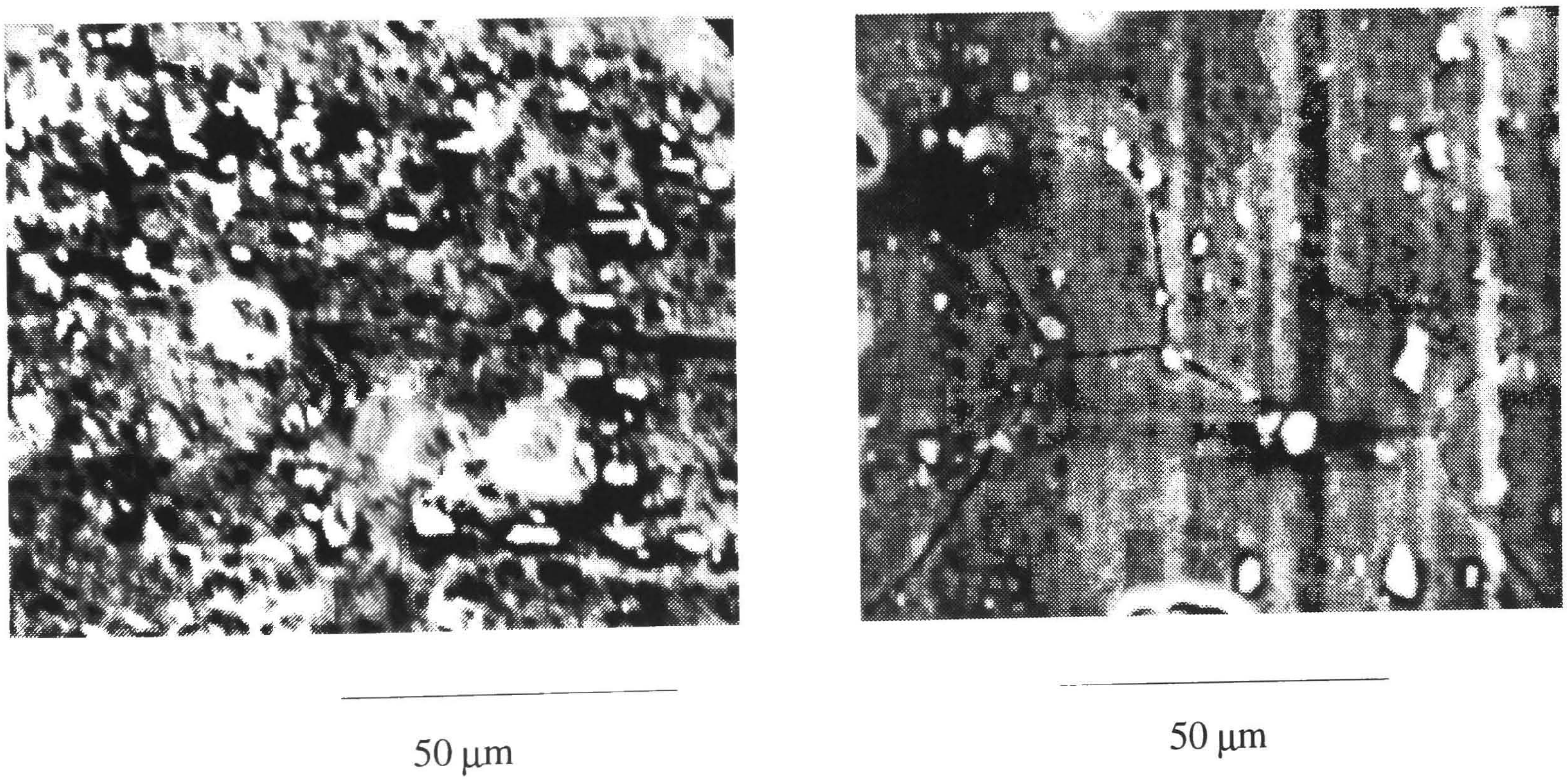

1. Q Aluminium

2. A Aluminium

Figure 5.7 SEM images of the bare aluminium substrates

5.5.2 Laser Profilometry [18]

The laser profilometer operates using an infra-red semiconductor laser (1). A simplified diagram is given in figure 5.8. This beam is passed through a beam splitter

(4) with the intensity being measured on a photodiode (2). This incident beam is focussed through an objective lens (5) to a spot about 1 μm in diameter on the surface being measured. The reflected laser light, from the surface, is put through a beam splitter (4) and imaged onto a second differential photodiode (3). The instrument compares the illumination of the relected light on the second photodiode (3) with the illumination of the incident light on the first photodiode (2). The instrument is calibrated such that when the objective lens is at precise focal length from the surface, the photodiodes are illuminated equally. As the beam moves across the surface, the distance between the objective lens and the surface changes resulting in unequal illumination of the photodiodes. The height of the objective lens over the surface is then moved to keep the photodiodes equally illuminated. By the laser scanning over an area, the surface can be imaged in three dimensions.

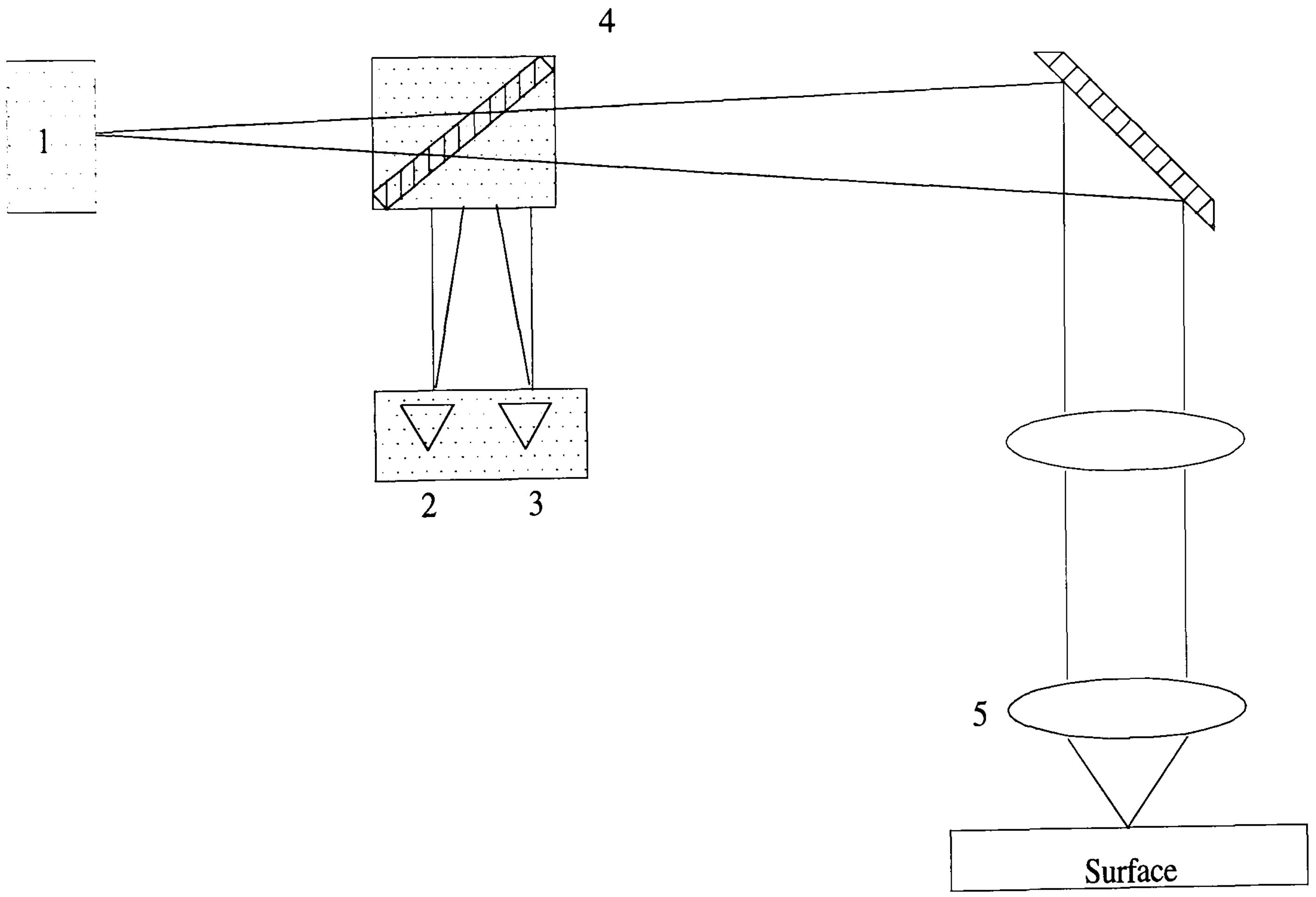

Figure 5.8 Simplified Diagram of Laser Profilometer

The laser profilometer results give a value for the roughness parameter, R_a of the substrate are seen in figure 5.9. This is defined as the arithmetic mean of fluctuations in the peak to trough height.

Q Aluminium: $R_a = 0.33$ μm A Aluminium: $R_a = 0.26$ μm

Showing that the Q aluminium is rougher than the A aluminium.

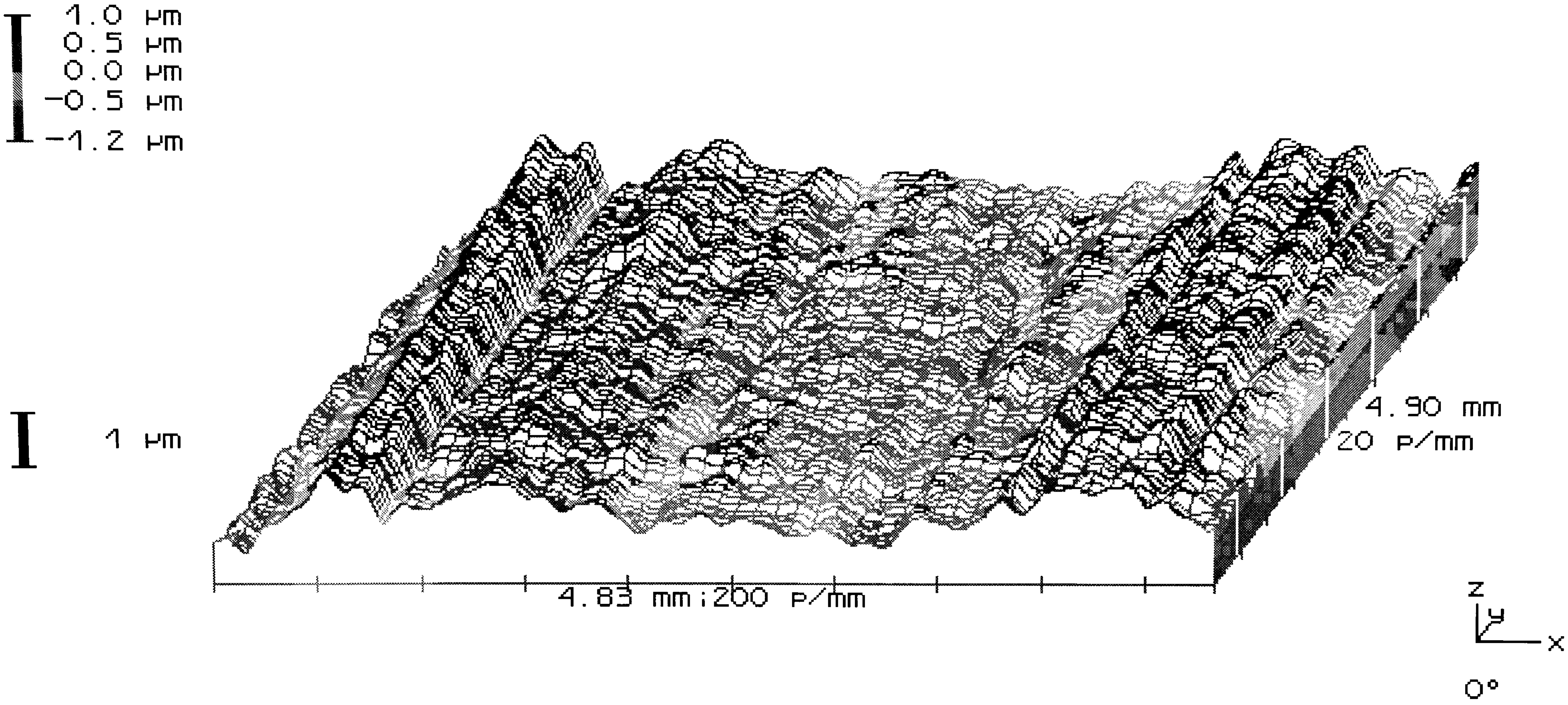

A Aluminium

Figure 5.9a Laser Profilometry images of an A aluminium substrate.

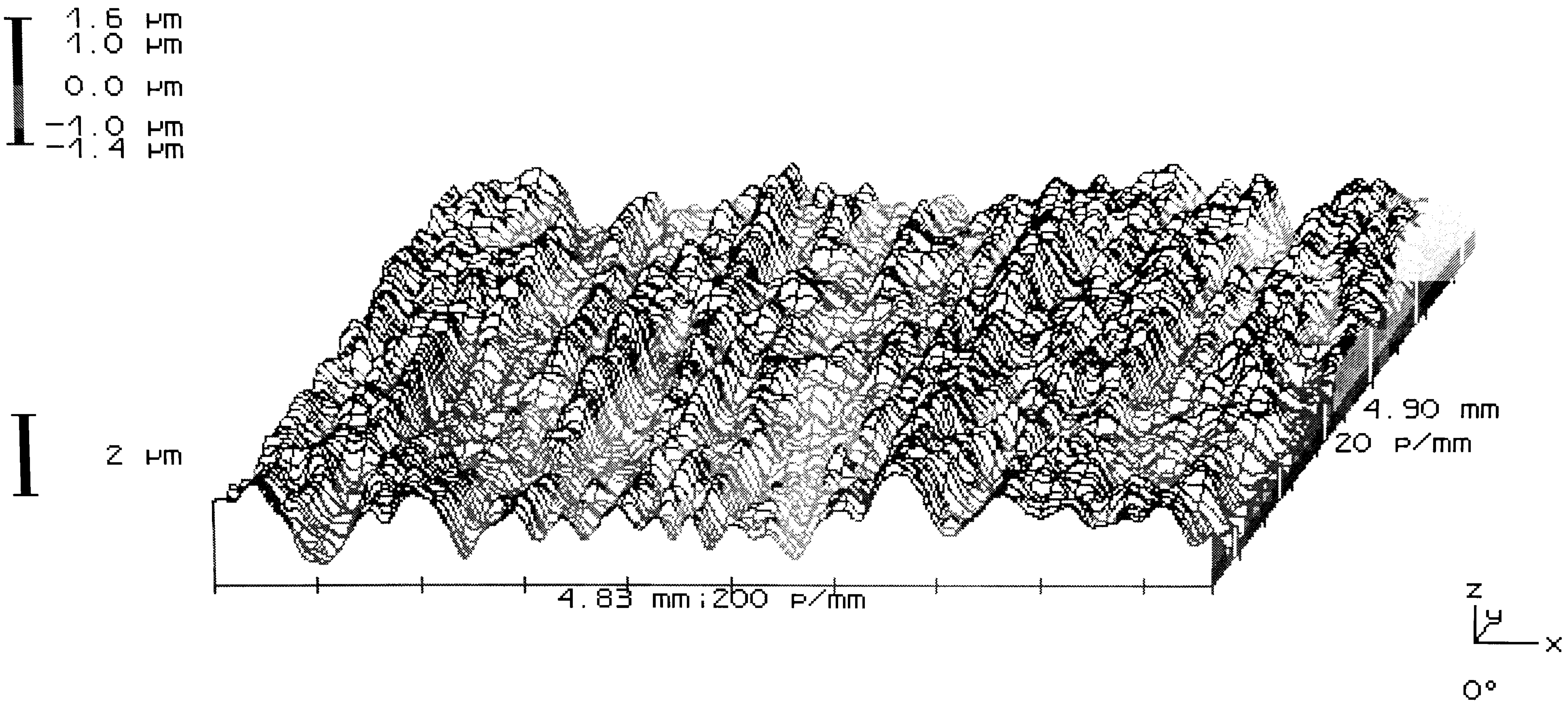

Q Aluminium

Figure 5.9b Laser Profilometry images of a Q aluminium substrate.

5.5.3 EDX Analysis of Aluminium

EDX analysis of the two aluminium substrates showed the main impurities in the Q aluminium to be iron (0.7 %) and manganese (1 - 1.5 %), whilst in the A aluminium to be just iron (0.5 %). The Q aluminium has a milled finish, the A aluminium had surface extrusion lines running vertically along the length of the panel.

5.6 Filiform Corrosion Experiment Results

Filiform corrosion was initiated on four systems. Two substrates had two different coatings applied. This has been described in more detail in Chapter 2, but to summarise:

Q Aluminium
→ Clear Coating, W1
→ Pigmented Coating, G1

A Aluminium
→ Clear coating, W1
→ Pigmented Coating, G1

The aim of the work described in this chapter is to study the effect of substrate on filiform corrosion. The principle way of doing this is to look at the growth rate of filiform corrosion.

5.6.1 Growth Rate Measurements

Selected filiform corrosion filaments, taken as representative of the system were measured after 55 days. The results are summarised in figure 5.10. Figure 5.10 shows a clear difference in the growth rate of filiform corrosion on the two different substrates. Differences in growth rate between the two different coatings on identical substrates are also discernible, this will be discussed in Chapter 6. The aim of the study subsequent to finding this difference in growth rate on the two substrates was to attempt to find out what on the substrate was causing this difference.

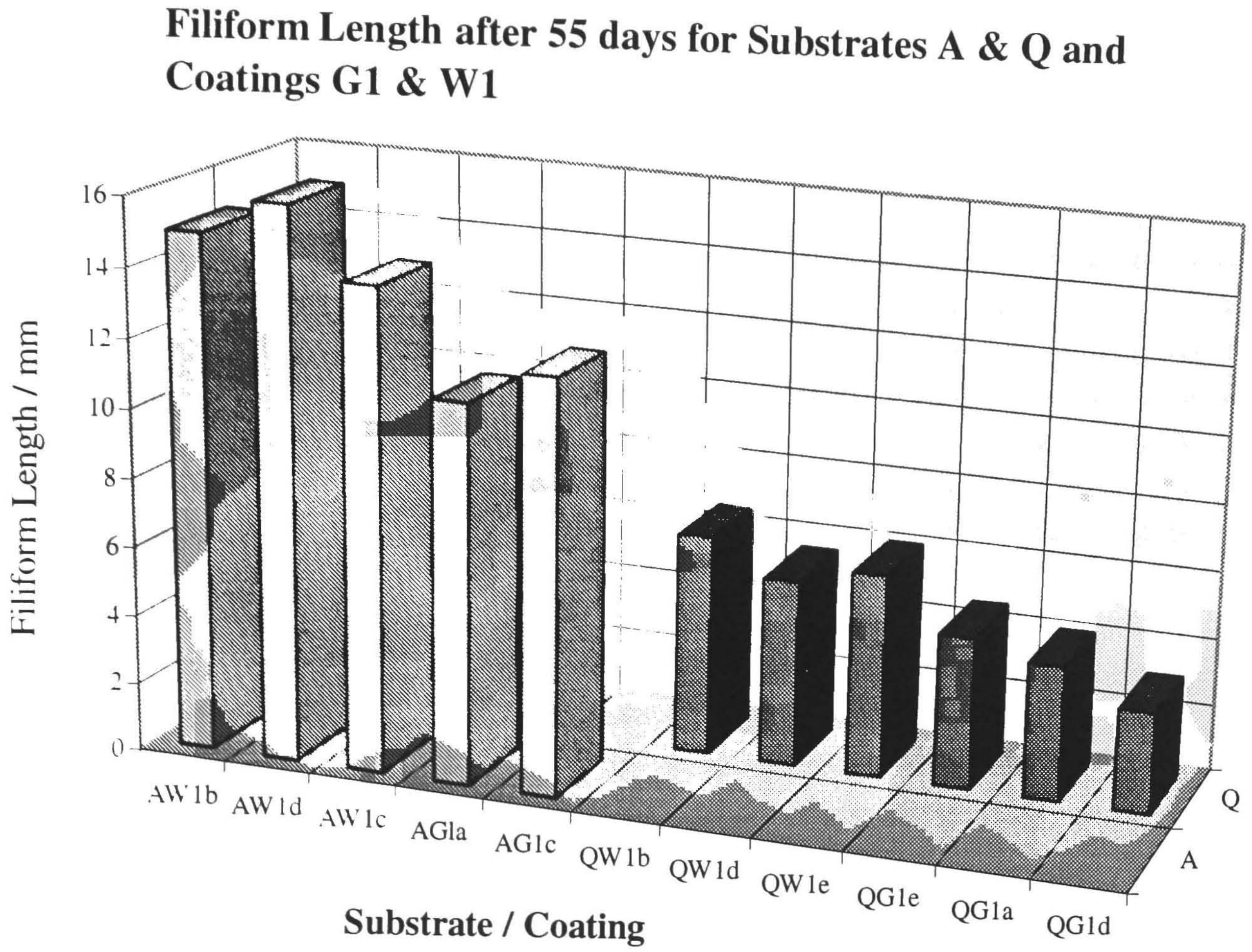

Figure 5.10 Filiform corrosion length after 55 days after initiation at 40° Celsius, 80 % relative humidity.

5.6.1.1 Factors Which Control the Rate Of Filiform Corrosion

In order to understand why filiform corrosion proceeds at different rates on different substrates (as shown in figure 5.10) it is important to look at the factors which inhibit filiform corrosion advance and the mechanism of filiform corrosion. The corrosion system envisaged is shown in figure 5.1.

Role of Oxygen

Experiments done by Slabaugh *et.al* [11] have shown that an oxygen containing atmosphere is essential for filiform corrosion growth. This is to be expected as the aluminium corrosion reaction requires oxygen. Oxygen can, in principle, reach the active filiform corrosion head both through the tail and through the coating. The supply of oxygen through the coating will depend on the barrier properties of the coating and how these change when the coating is stressed, *i.e.* where the coating is pushed up by underlying corrosion products. This will be discussed in more detail in Chapter 6. The supply of oxygen through the tail has been studied by Ruggeri and Beck [12] who have calculated the flux of oxygen is up to ten times greater from the open end of the tail to the head than from through the coating. However, work carried out for this thesis has shown that sealing of the open end of the filiform corrosion tail at the score in the coating does not appear to stop filiform corrosion (Chapter 6). It is generally considered that the hydrated aluminium oxide that forms at the back of the filiform corrosion head has gel like properties and forms a semi permeable membrane which prevents the diffusion of ions in the head back into the tail, but allows oxygen into the head.

Role of water

Water is required in the head as it is an integral part of the corrosion reaction. Experiments done for this thesis have shown that filiform corrosion stops when removed from a humid atmosphere:

Samples of all of the four different filiform corrosion systems were removed from the humidity cabinet after 1 week. they were put in a desiccator containing silica gel and kept at 40° Celsius, the same temperature as the filiform corrosion systems in the humidity cabinet. The filiform corrosion stopped advancing.

Water is used in the formation of the aluminium oxide corrosion products contained within the tail, and so needs continued replacement. It seems likely that it enters the filiform head as a vapour in the same way as oxygen: through the open end of the tail, or through the coating.

Role of the corrosion activity of the substrate

A substrate with a higher corrosion rate should in principle, have a greater corrosion activity. A study done by Nisancioglu *et.al* [9] has shown that anodising the aluminium and/or pre-treating with chromate conversion coatings has a significant effect on reducing filiform corrosion activity. They found that substrates with intermetallics on the surface had significant corrosion around intermetallic particles which acted as localised cathodic sites.

In the linear sweep voltammetry experiments reported earlier in section 5.3.3 it was found that A aluminium had a corrosion current in 0.1M sulphuric acid under oxygen of 0.32 mA cm^{-2} where as the Q aluminium in the same conditions had a corrosion current in oxygen of 0.13 mA cm^{-2}. This suggests that A aluminium corrodes at over twice the rate of Q aluminium, when exposed to oxygen (as in a filiform corrosion cell). These results have to be treated with care, as they are subject to some degree of experimental error, but would appear to suggest one reason why the filiform corrosion filaments were so much longer on the A aluminium than the Q aluminium after 55 days.

The increased corrosion rate found on A aluminium is unexpected considering the greater percentage of impurities on the Q aluminium (iron 0.7 %, manganese 1 - 1.5%) with the A aluminium having iron as its principle measurable impurity at 0.5 %. This measurement having been done by EDX. However, these results are subject to inaccuracies, as local areas of impurity metals can distort the results and the limit of detection of impurities is rather low.

Role of the Substrate Roughness

Powder coatings, such as used in this thesis adhere to substrates when the applied powder is heated and cured. In this process the powder melts and undergoes a rheological transformation where the powder particles coalesce then flow onto the substrate surface. The molten coating flows into the surface and 'anchors' the coating to the substrate, shown in figure 5.11.

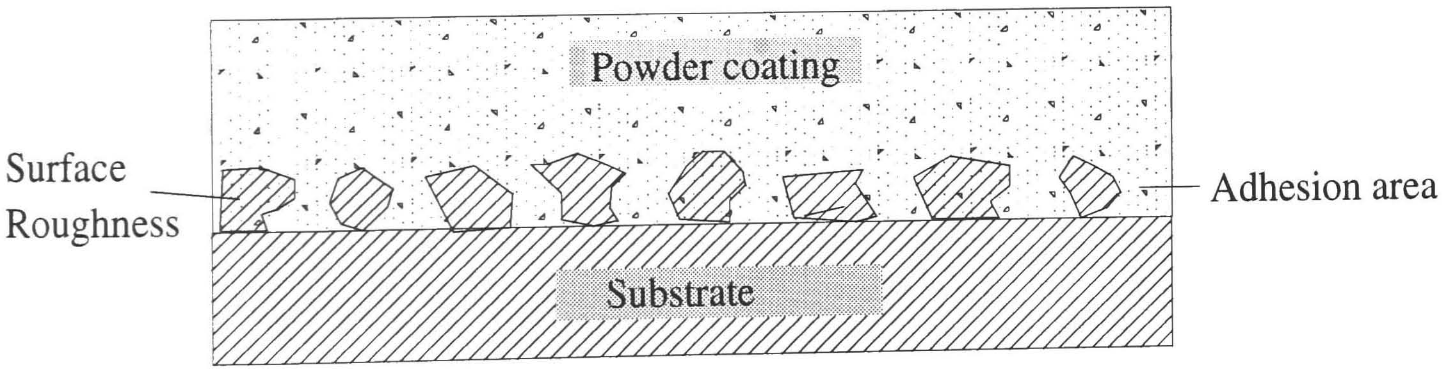

Figure 5.11 Model of adhesion of a powder coating to substrate

The role of adhesion in filiform corrosion has been discussed in section 5.1 [8,9].

Measurement of the substrate roughness using laser profilometry in section 5.5.2 has shown that the A aluminium is rougher than the Q aluminium, a finding that appears to be confirmed by the SEM micrographs of the surface. This difference in surface roughness is likely to be significant in giving different degrees of adhesion of the coating to the substrate, with the coating adhering better to the rougher Q aluminium. The difference in surface roughness and as a consequence adhesion seems likely to at least partially account for the difference in observed filiform corrosion activity on the two substrates [15].

5.7 Conclusions

There is evidence from analysis of the growth rate of filiform corrosion that surface morphology of the substrate may have an important role in governing the rate of filiform corrosion advance. It was seen that the rougher Q aluminium had significantly slower rate of filiform advance than the smoother A aluminium. The reason for this difference is likely to be, at least partially, due to the difference in adhesion of the coating to the two different substrates. In addition to the difference in substrate roughness was the difference in corrosion current of the two substrates. The A aluminium had a corrosion current 2.5 times greater than the Q aluminium when both substrates were immersed in 0.1M sulphuric acid under oxygen. It is uncertain whether the effect of surface roughness or corrosion rate (current) is the most important factor in inhibiting or enhancing filiform corrosion. It is likely that both are important.

References

[1] C. Sharman, *Nature*, **153**, 621 - 622. (1944).

[2] H. Leidheiser, *Corrosion* **38,** 374, (1982).

[3] W. Funke, *Prog. Org. Coat.* **9,** 29, (1981).

[4] M.J. Schofield *et.al, Proc. 8th Int. Cong. Metal. Corr.* **2,** 1047 (1981).

[5] R.D.Armstrong, J.D.Wright, *Electrochimica Acta* **38**, 1799, (1993).

[6] Deutsches Institut für Normung e. V. , Number 65 472.

[7] W.H. Slabaugh, M. Grotheer, *Industrial and Engineering Chemistry* **46,** 1014, (1954).

[8] W. van der Berg *et.al, Proc. 3rd. Int. Conf. Org. Coat. Sci. and tech. - Athens.* p. 188, (1977).

[9] K. Nisancioglu, H. Leth-Olsen and O. Lunder, *Proc. Corr. Prev. Org. Coat.* Cambridge, (1994).

[10] M. Van Loo, D.D. Laiderman, R.R. Bruhn, *Corrosion,* **9**, 277, (1953).

[11] W.H. Slabaugh, W. Dejager, S.E. Hoover, L.I. Hutchinson, *J. Paint. Tech.,* **44**, 76, (1972).

[12] R.T. Ruggeri, T.R. Beck, *Corrosion,* **39**, 452, (1983).

[13] J. Bessone, C. Mayer, K. Jüttner & W.J. Lorenz, *Electrochim. Acta,* **28**, 171, (1983).

[14] M. Stern, A.L. Geary, *J. Electrochem. Soc.*, **104**, 56, (1957).

[15] A.T.A. Jenkins, R.D. Armstrong, *Corrosion Science*, submitted January 1995.

[16] S. Evans, E.L. Koehler, *J. Electrochem. Soc.*, **108**, 509 (1961).

[17] A. Despic, V.P. Parkhutik, *Modern Aspects of Electrochemistry,* **20**, 401, Plenum, (1989), Eds. Bockris, White & Conway.

[18] UBM Messtechnik GmbH, Application notes, Ottostraße 2, D7505 Ettlingen, Germany.

[19] G.M. Brown, K. Shimizu, K. Kobayashi, G.E. Thompson and G.C. Wood, *Corrosion Science*, **35**, 253 (1993).

PAGE

NUMBERING

AS ORIGINAL

Chapter 6

A Study into the Role of the Coating in Filiform Corrosion.

6.1 Introduction

This chapter studies the role of the paint coating in affecting filiform corrosion. Filiform corrosion is affected by the substrate and coating. Chapter 5 has looked at how the substrate affects the rate of filiform corrosion. In this chapter the aluminium coating system studied in Chapter 5 is re-examined, this time studying the role of the coating. In addition a new filiform corrosion system is examined, looking at the effect of varying the glass transition temperature of the coating, on a single substrate type (Q aluminium). Electrochemical Impedance Spectroscopy (EIS) is used extensively to quantify the way in which the barrier properties of the coating overlying filiform corrosion changes. Scanning Electron Microscopy is used to look at the morphology of the coating overlying filiform corrosion filaments. Information gained on the coating is compared with growth rate figures of filiform corrosion filaments.

6.2 Coating Effects on Filiform Corrosion - The Background

The effect of coatings on filiform corrosion has not been reported widely in the literature. Sharman, who first reported on filiform corrosion stated that on highly pigmented paints filiform corrosion could not be observed [1]. This observation does not appear to have been replicated else where in the literature, or in the work reported in this chapter. In a study done by Van Loo *et.al* the effect of pigment loading on filiform corrosion activity was determined [2]. Permeability of paint coatings increases with pigmentation above the Critical Pigment Volume Concentration (CPVC). At the CPVC the barrier properties of the paint start to degrade, as insufficient binder exists between pigment particles. This effect of pigment on the performance of coatings has been discussed in Chapter 4. Van Loo found that on enamelled substrates that had not been pretreated with rust inhibitive primers that filiform corrosion was *not* observed above the CPVC. This was attributed to the coating being too porous. The effect of high porosity in this situation would be that large amounts of oxygen would be available through the coating, thus preventing the creation of a differential aeration cell, essential for filiform growth. Van Loo also found that thicker coatings gave wider filiform corrosion filaments, although he does not comment on why this should be so. Van Loo does state that the coating must be semi-permeable *i.e.* will allow some oxygen through it. A study by Slabaugh *et.al* has found that increasing coating thickness has decreased filiform corrosion activity on coated aluminium [6] They found that water vapour (and presumably oxygen) need to be transported through the coating for filiform corrosion to take place.

In terms of the effect of coating elasticity on filiform corrosion Van Loo states that the coating must be sufficiently elastic to allow deformation over the filiform corrosion products in the tail. In the work reported in this thesis it was found that although a totally inelastic coating *may* prevent filiform corrosion growth, this is very much a limit. Coatings examined in this chapter are all relatively brittle and, at room temperature are well below their glass transition temperature. There is evidence that they have deformed extensively in the areas overlying filiform corrosion, and this may aid the advance of filiform corrosion [3].

In a review of a report on filiform corrosion, it was reported that filiform corrosion was found to increase above the glass transition temperature, when the polymer was in a viscoelastic state [4,5].

Ruggeri and Beck [7] claim that water and oxygen are not transported through the coating and that filiform corrosion is relatively independent of coating properties.

In summary, it can be seen that in the literature there are essentially two views regarding the effects of coating on filiform corrosion. The first view [2,7] is that generally the coating has little effect on filiform corrosion activity. The second view is that the coating is permeable to oxygen and water and therefore variations in the coating will affect filiform corrosion.

Evidence is given in this thesis that the coating overlying filiform corrosion is made highly porous, and as such, in principle allows a ready route for oxygen and water to get to the filiform corrosion head [1]. It would therefore seem highly likely that the properties of the coating will influence filiform corrosion.

6.3 Experimental

6.3.1 Impedance Measurements of Filiform Corrosion

Two filiform corrosion systems have been studied in this chapter. The first is the system described in Chapter 5, with pigmented (G1) and non-pigmented (W1) coatings on two separate substrates. The second is of two similar blue coloured pigmented coatings (D200 & D42), but with different glass transitions temperatures, both applied to Q aluminium.

Impedance measurements were made by gluing cells on the coated substrate. For this study, cells with a different dimension were used, giving a working electrode diameter of 10 mm, area of 0.785 cm^2. A smaller working electrode areas used so that the coating overlying the filiform corrosion filament could be more accurately examined. This is shown in a plan view of the system, figure 6.1. It should be noted that the approximate area of filiform corrosion, as a proportion of the total coating area measured (where the coating above filiform corrosion was measured) is around 1:20, or 5%. Porosity results have not been normalised to reflect this, but are the measured porosity at the base of the cell. Measurements were made after one days immersion in electrolyte.

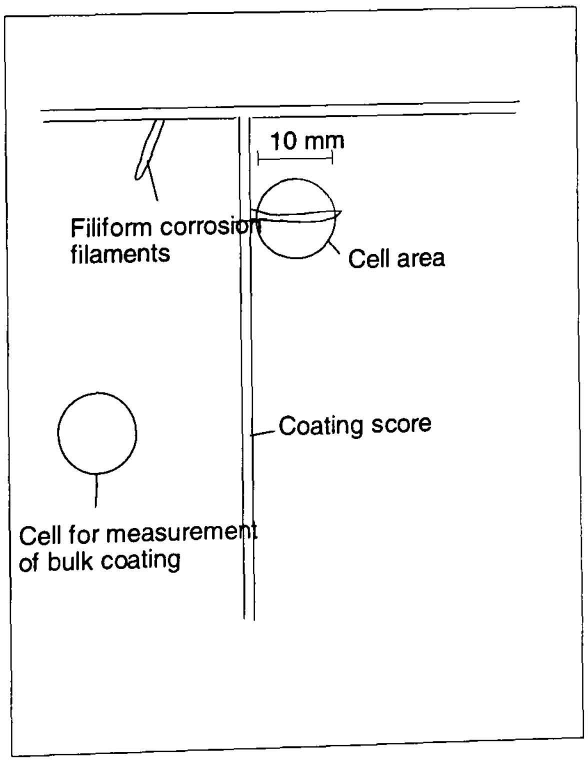

Figure 6.1 Plan view of Placement of Impedance Cells on Coated Aluminium

6.3.2 Non Electrochemical Measurements of Coatings

6.3.2.1 Glass Transition Temperature Measurement

Differential Scanning Calorimetry measurements were made on a Perkin Elmer DSC7. The glass transition temperature of all the coating systems was measured using Differential Scanning Calorimetry (DSC). DSC operates by varying the rate of heating of a sample to give a constant increase in its temperature [8]. The heating of the sample is measured against a reference. As the sample heats up it undergoes reactions or phase changes, that may be exothermic or endothermic. The differential of the heating rate with temperature becomes non-zero when the polymer changes phase *i.e.* where a polymer goes through its glass transition temperature. The differential of the heat supplied (power) is positive for an endothermic reaction and negative for an exothermic reaction.

6.3.2.2 Water Vapour Permeation

This involves measuring the rate of water vapour transport through a coating. It was achieved by applying samples of the coatings to non-stick substrates, curing in the normal way, then removing and attaching to a sample bottle containing ultra-pure water in a dissector containing silica gel (Fig. 6.2). The coating and bottle were weighed regularly on a sensitive balance to determine the weight loss due to water permeation with time.

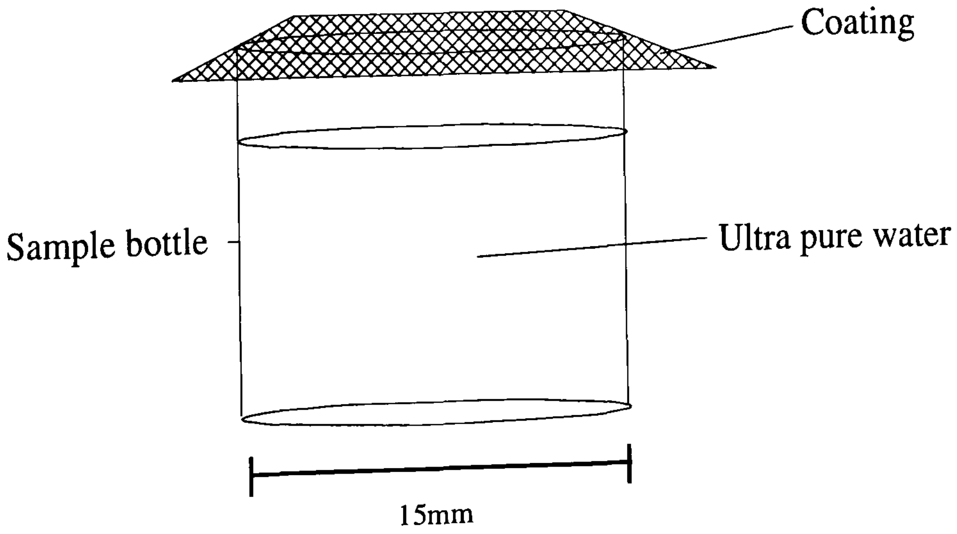

Figure 6.2 - Experimental setup for water permeation experiment.

The area of coating exposed to water permeation is 1.767 cm^2.

All exposed coatings were the same area.

6.4 Experimental Results

In this section the experimental results obtained on the coatings W1 and G1 and D200 and D42 are given. The implications of these experimental results are discussed separately in section 6.5.

6.4.1 Growth Rate Measurements

6.4.1.1 Coatings G1 and W1

The growth rate measurements for filiform corrosion on two different substrates have been given in Chapter 5. Here the growth rate data is re-presented in-order to attempt to show the difference between the two coatings more clearly. These coatings were measured every few days, the measurements given here are after 55 days at 40° Celsius, 80 % R.H.

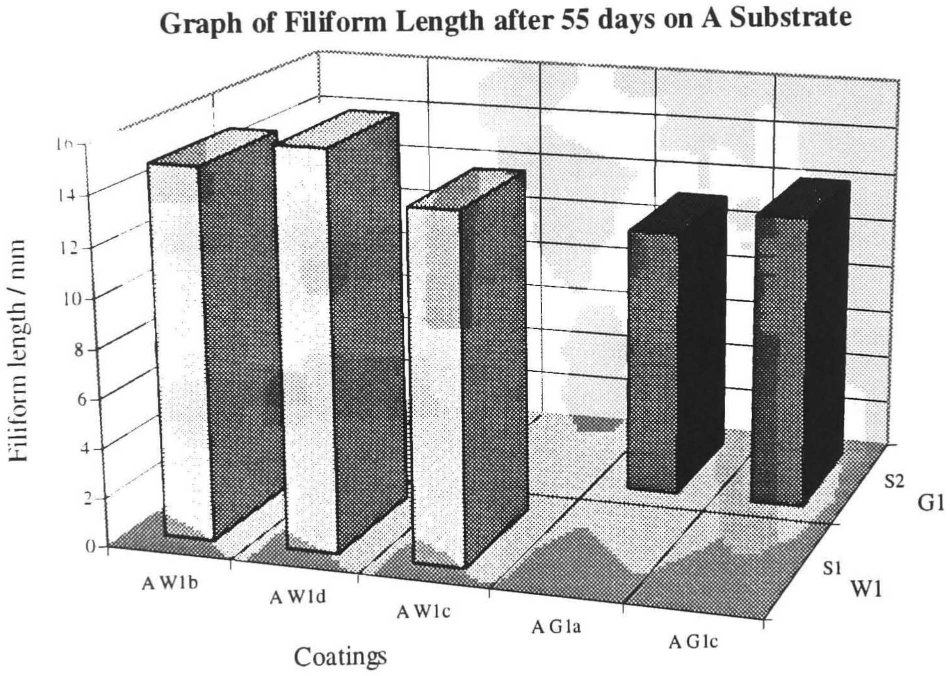

Figure 6.3a Comparison of Filiform Corrosion Filament Length under Coatings G1 and W1 after 55 Days

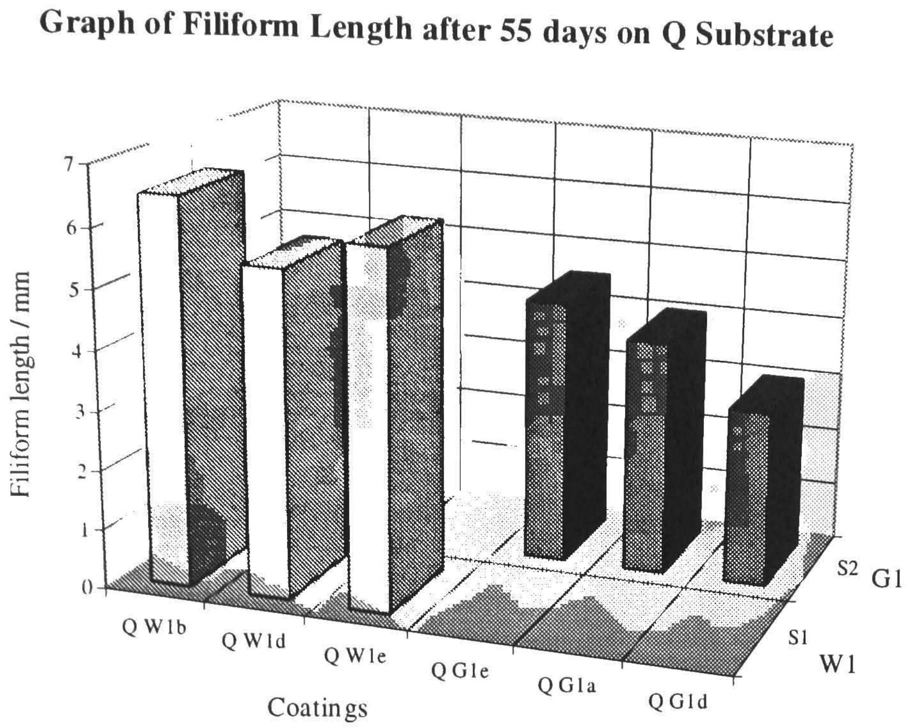

Figure 6.3b Comparison of Filiform Corrosion Filament Length under Coatings G1 and W1 after 55 Days

The growth rate measurements made on the coatings G1 and W1 show that coating W1 has longer filiform corrosion filaments than coating G1 after 55 days at 40° Celsius, 80% R.H.. This has been observed on both the substrates to which the coatings were applied (Figures 6.3a and 6.3b). This difference in the growth rate of filiform corrosion of the two coatings must be attributable to the properties of the coatings since the substrates were identical. Further experiments were performed in order to try and determine which properties of the coatings were different, and what might explain the differences in filiform corrosion growth rate. In addition experiments were done in order to study the way the coating changes when overlying filiform corrosion filaments.

6.4.1.2 Coatings D200 and D42

The difference in filiform corrosion lengths under the coatings D200 and D42, both on Q aluminium substrate is shown in figure 6.4. These coatings were treated and measured in the same way as coatings G1 and W1, except the final measurement was made after 48 days at 40° Celsius, 80 % R.H. Coatings G1 and W1 were selected on the basis of their difference in glass transition temperature, T_g.

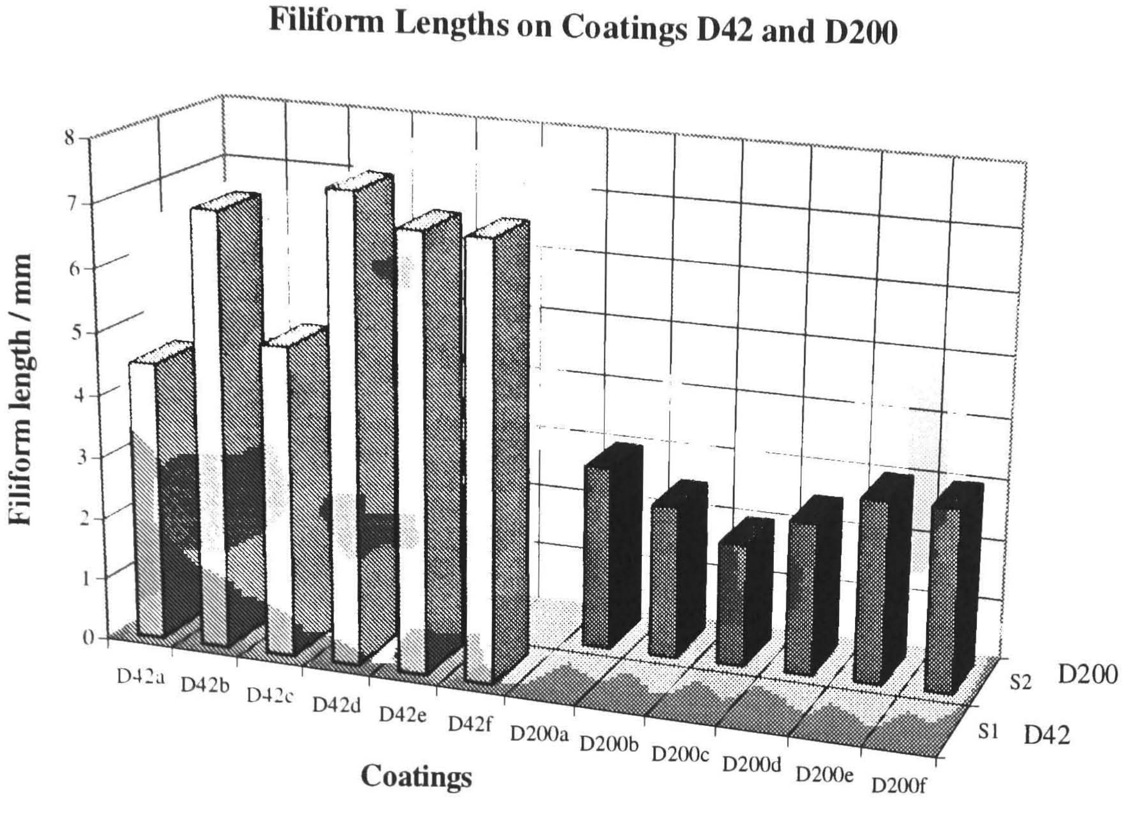

Figure 6.4 Comparison of Filiform Corrosion Filament Length under Coatings D200 and D42 after 48 Days

In a similar way to the coatings G1 and W1 the coatings D200 and D42 show considerable differences in filiform corrosion rate, with D42 being significantly more susceptible to filiform corrosion.

6.4.2 Impedance Measurements on Coatings

The porosity of the coatings, both in the none filiform corrosion areas and filiform corrosion areas have been tabulated in table 1 and table 2. Table 1 gives the impedance results for coatings W1 and G1, table 2 for coatings D200 and D42. Porosity and wetted metal area have been calculated using the method shown in Chapter 1 and Chapter 3. It is clear from the table 1 and table 2, that the coating overlying filiform corrosion filaments is significantly more porous *i.e.* broken down than the none corroded bulk coating. In addition there are differences in the degree of porosity between the different coatings. Note: A porosity of $< 10^{-11}$ indicates that the coating gave either a purely capacitive impedance, or a bulk resistance of a magnitude greater than could be accurately measured (generally > ~ 1000 MΩ).

6.4.2.1 Coatings G1 and W1

A Aluminium

Coating	Thickness / µm	R_b / MΩ	Porosity	C_{dl} / nF	Wetted metal area
W1bi - F	80	8.63	2.47×10^{-8}	0.083	1.44×10^{-5}
W1bi - NF	80	>1000	$< 10^{-11}$	-	-
W1bii - F	80	0.105	2.03×10^{-6}	-	-
W1bii - NF	80	>1000	$< 10^{-11}$	-	-
W1a - F	106	0.078	3.62×10^{-6}	74.5	0.013
W1a - NF	106	>1000	5.91×10^{-10}	-	-
G1a - F	112	184	1.62×10^{-9}	-	-
G1a - NF	112	>1000	$< 10^{-11}$	-	-
G1c - F	84	33.3	6.72×10^{-9}	3.93	6.87×10^{-4}
G1c - NF	84	>1000	$< 10^{-11}$	-	-
G1di - F	78	1291	1.61×10^{-10}	-	-
G1di - NF	78	>1000	$< 10^{-11}$	-	-
G1dii - F	78	185	1.15×10^{-9}	-	-
G1dii - NF	78	>1000	$< 10^{-11}$	-	-

F = Measurement made on coating overlying filiform corrosion

NF = Measurement made on non-corroded coating.

Q Aluminium

Coating	Thickness / µm	R_b / MΩ	Porosity	C_{dl} / nF	Wetted metal area
G1j - F	70	44.1	4.23×10^{-9}	-	-
G1j - NF	70	>1000	$< 10^{-11}$	-	-
G1f - F	60	126	1.26×10^{-9}	-	-
G1f - NF	60	>1000	$< 10^{-11}$	-	-
W1ai - F	70	0.05	3.72×10^{-6}	446	0.078
W1ai - NF	70	>1000	$< 10^{-11}$	-	-
W1aii - F	70	0.088	2.10×10^{-6}	183	0.032
W1aii - NF	70	>1000	$< 10^{-11}$	-	-
W1d - F	55	1.46	1.00×10^{-7}	-	-
W1d - NF	55	>1000	$< 10^{-11}$	-	-

F = Measurement made on coating overlying filiform corrosion

NF = Measurement made on none corroded coating.

Table 1

The difference in porosity of the coatings overlying filiform corrosion compared with the bulk coating is highly significant (Table 1). It is clear from these measurements that there is a clear path through the coating for water and oxygen to reach the active filiform corrosion head. This contradicts the view of Ruggeri and Beck [7], who claim that the oxygen and water are transported to the head solely through the tail.

In order to facilitate easier comparison of the two coating systems, the porosity of the coating overlying the filiform corrosion has been plotted as -log porosity against coating type in figures 6.5 and 6.6. Graphs are given for both substrates, with similar trends appearing in each. N.b. log = $\log_{10}$.

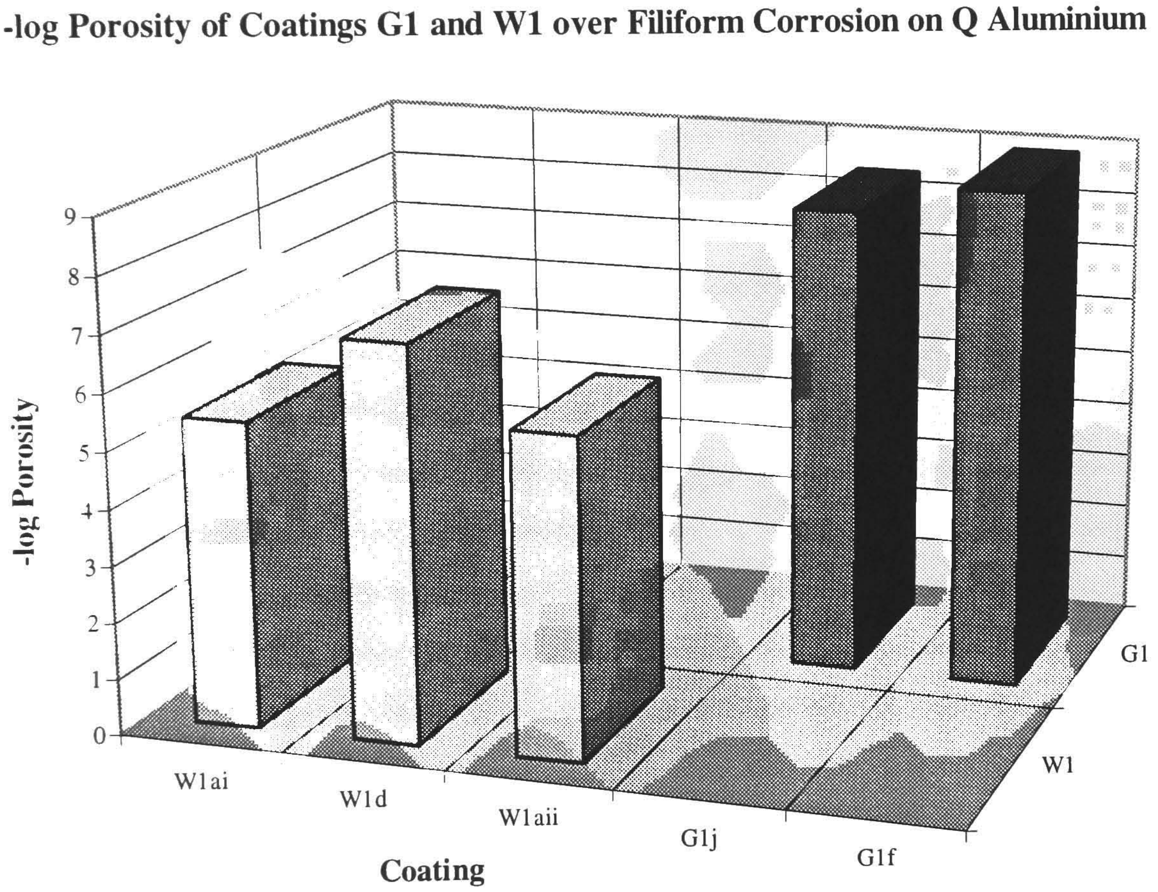

Figure 6.5

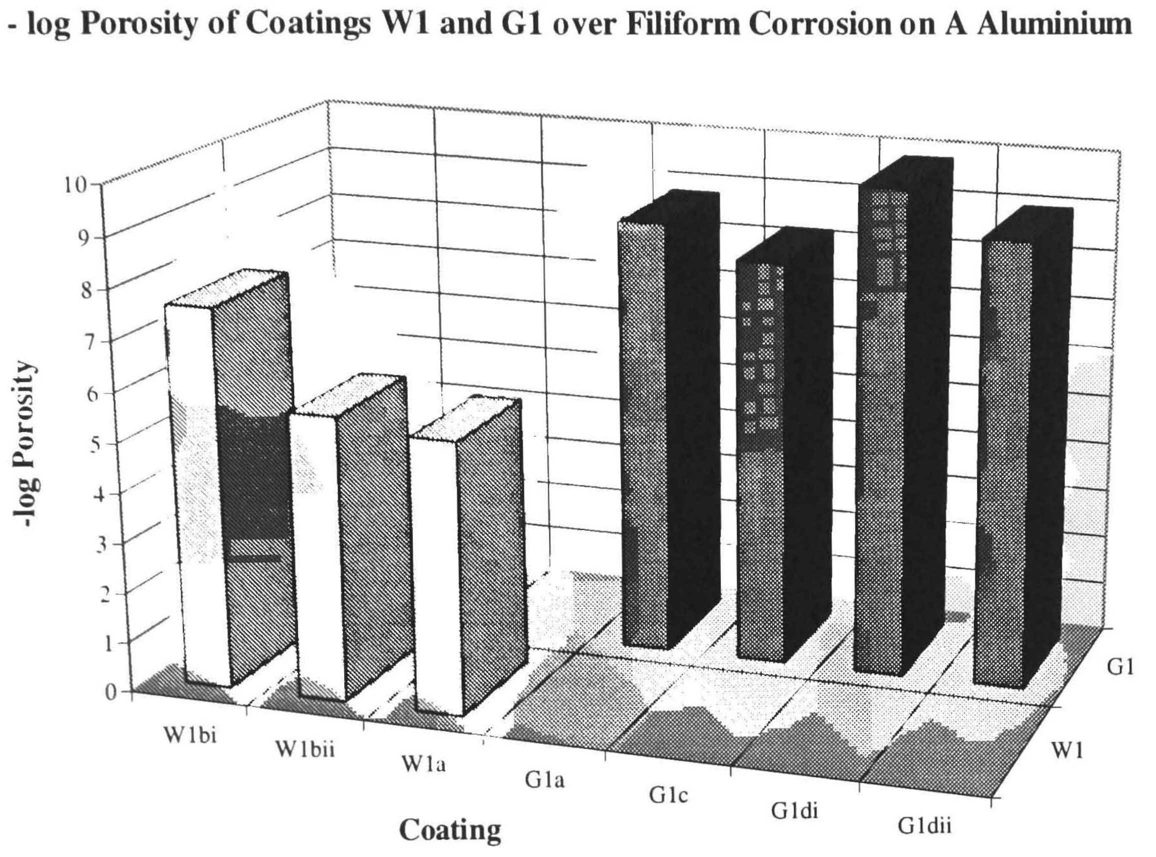

Figure 6.6

It is clear that the coating W1 has a significantly greater degree of coating breakdown, by at least an order of magnitude. This large (orders of magnitude) difference suggests that the difference in measured porosity is 'real' and not due to differences in the area of filiform corrosion measured or experimental artefacts.

6.4.2.2 Coatings D200 and D42

The two coatings with different glass transition temperatures: D200 having the lower T_g, D42 having the higher T_g. Table 2 shows a breakdown in the coatings properties (manifesting itself as an increase in porosity) of the coating overlying filiform corrosion filaments. This is similar to the measurements made on coatings G1 and W1, given in table 1.

Coating	Thickness / µm	R_b / MΩ	Porosity	C_{dl} / nF	Wetted metal area
D42b - F	66	0.111	1.586×10^{-6}	29.9	5.22×10^{-3}
D42b - NF	66	>1000	$< 10^{-11}$	-	-
D42d - F	35	1.80	5.18×10^{-8}	0.66	1.15×10^{-5}
D42d - NF	35	>1000	$< 10^{-11}$	-	-
D42e - F	70	4.48	4.15×10^{-8}	1880	0.330
D42e - NF	70	>1000	$< 10^{-11}$	-	-
D42c - F	48	15.14	8.44e-9	-	-
D42c - NF	48	>1000	$< 10^{-11}$	-	-
D200a - F	70	0.030	6.20×10^{-6}	1286	0.224
D200a - NF	70	>1000	$< 10^{-11}$	-	-
D200b - F	45	0.026	4.61×10^{-6}	2340	0.408
D200b- NF	45	>1000	$< 10^{-11}$	-	-
D200c - F	48	15.62	8.19×10^{-9}	-	
D200c - NF	48	>1000	$< 10^{-11}$	-	-

F = Measurement made on coating overlying filiform corrosion

NF = Measurement made on none corroded coating.

Table 2

The porosity of the coatings overlying filiform corrosion filaments has been plotted with respect to the coating type. This is shown in figure 6.7.

- log Porosity of Coatings D200 & D42 over Filiform Corrosion on Q Aluminium

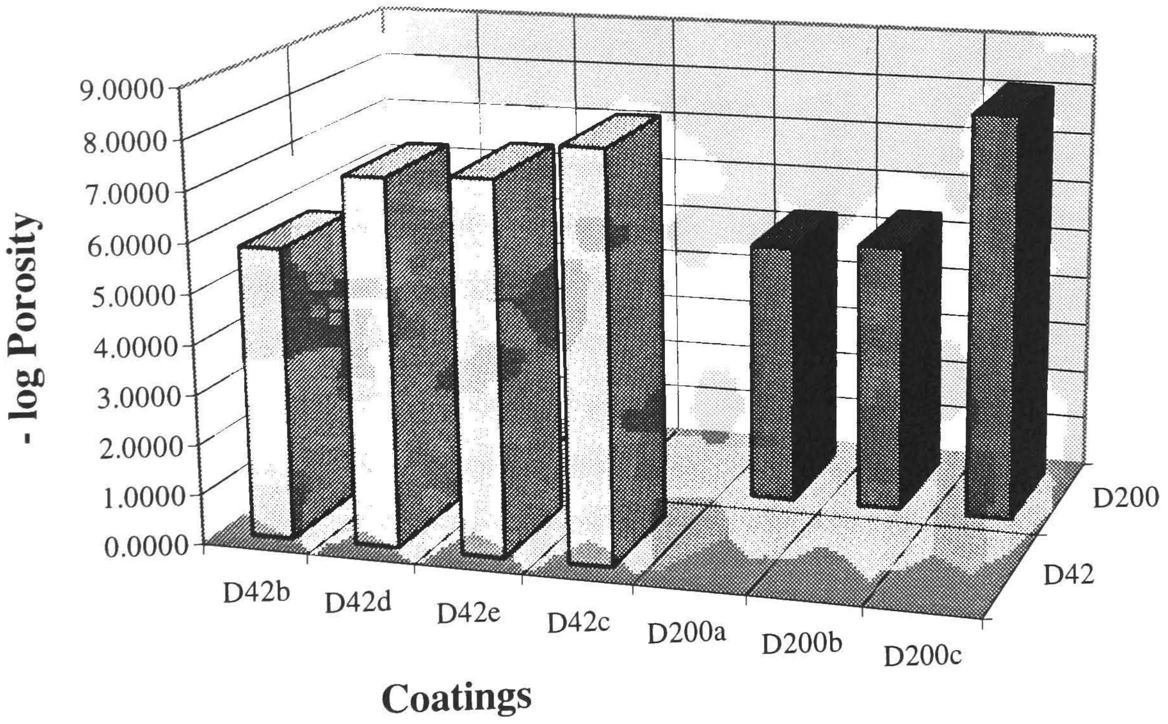

Figure 6.7

Figure 6.7 shows that there is not a definite difference in the porosity of coatings D200 and D42, or, any significant difference has not manifested itself on this number of measurements. The fact that the coatings exhibited very different filiform corrosion growth rates initially suggested that, on the basis of the previous work done, there should be some clear differences in the impedance of the two coatings. This is because more brittle, high T_g coatings would be expected to crack more easily when under stress, as in a filiform corrosion situation. A further study of the role of T_g on coating breakdown above filiform corrosion, on a larger number of samples would be of interest.

6.4.3 Scanning Electron Microscopy Results

These SEM images given here confirm the EIS results, in that there is evidence of cracking of the coating where it has been pushed up by the filiform corrosion underneath. The disadvantage of SEM is that it is almost purely a surface technique, and gives no information on the nature of the cracks below the surface of the coating. In addition the qualitative nature of SEM results makes direct comparison with other experimental results more difficult. However the SEM results presented here show a reasonable correlation with the measurements made using EIS, which show a breakdown in the barrier properties of the coatings overlying filiform corrosion filaments.

6.4.3.1 Coatings G1 and W1

The SEM micrographs of filiform corrosion under these coatings are shown in figures 6.8 and 6.9.

100 µm

Figure 6.8 SEM Image of Coating G1

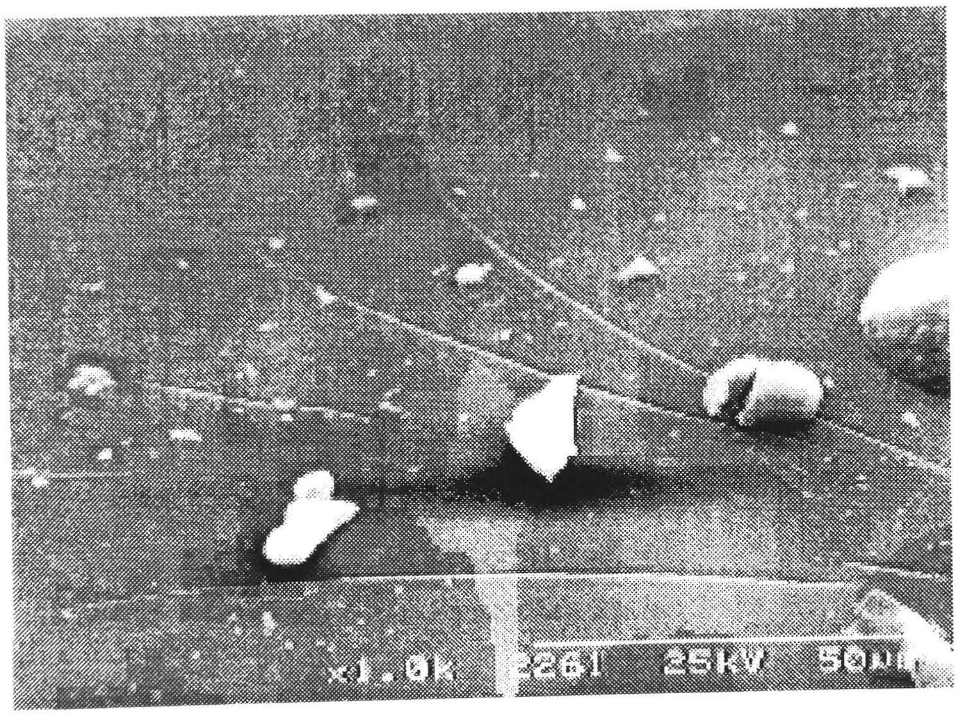

50 µm

Figure 6.9 SEM Image of Coating W1 (Clear Coating)

Figures 6.8 and 6.9 show essentially longitudinal cracks running along the coating covering the filiform corrosion filament with the cracks radiating out over the head section. The debris seen on the surface in figure 6.9 is probably dust or other contamination of the sample. Superficially it would appear that coating G1 (figure 6.8) has undergone a greater degree of cracking. However, it is probably 'dangerous' to conclude this as no information is given on the depth of the cracks observed on the surface. In both figure 6.8 and 6.9 the non filiform corrosion affected coating can also be seen.

6.4.3.2 Coatings D200 and D42

The SEM micrographs of filiform corrosion under these coatings are shown in figures 6.10 and 6.11

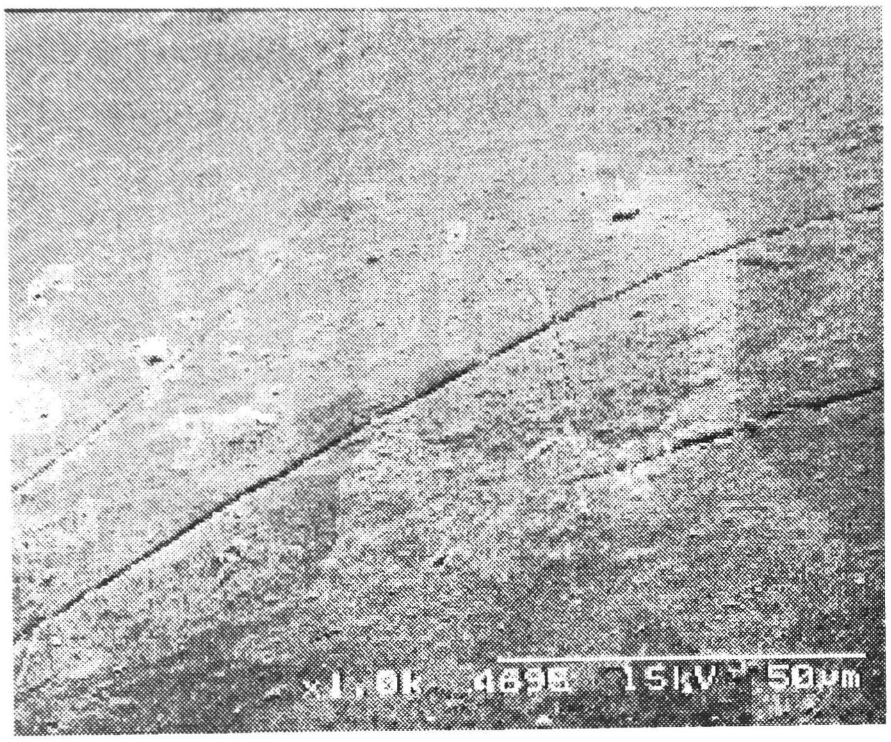

50 µm

Figure 6.10 SEM Image of D200

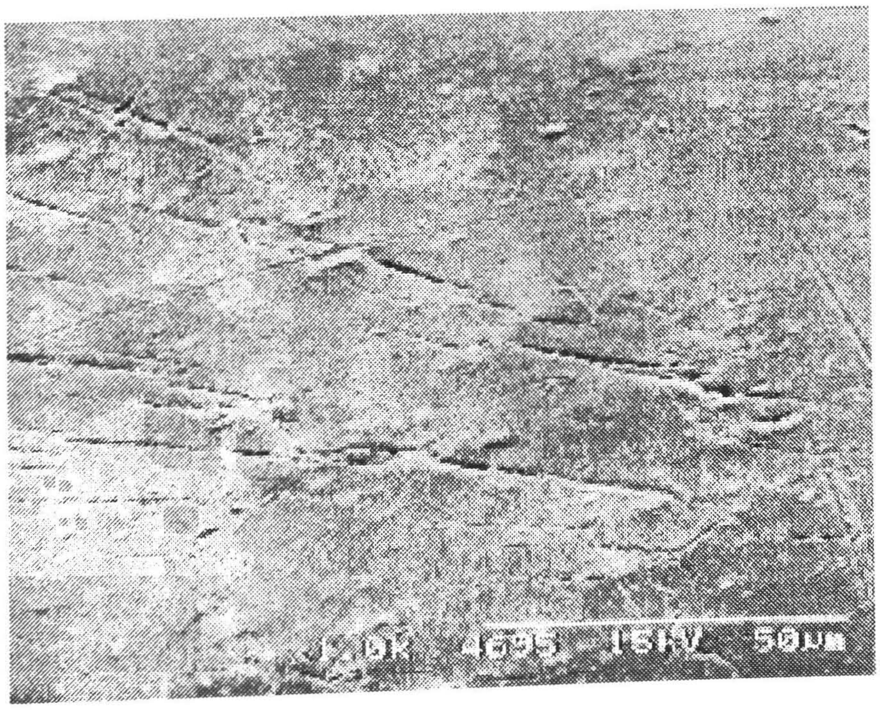

50 µm

Figure 6.11 SEM Image of D42

The degree of cracking on the coatings overlying filiform corrosion on coatings D42 and D200 appear less severe than on coating G1. However, as has been previously stated, SEM does not give any information on the depth of the cracks on the coating. Overall, SEM has given useful information on the how the measured increase porosity of the coatings overlying filiform corrosion has actually manifested itself.

6.4.4 Water Vapour Permeation

Water vapour permeation measurements were made by measuring the change in mass of the sample bottle, water and coating. As water permeates through the coating the mass of the system decreases. The results are shown in figures 6.12 and 6.13.

6.4.4.1 Coatings G1 and W1

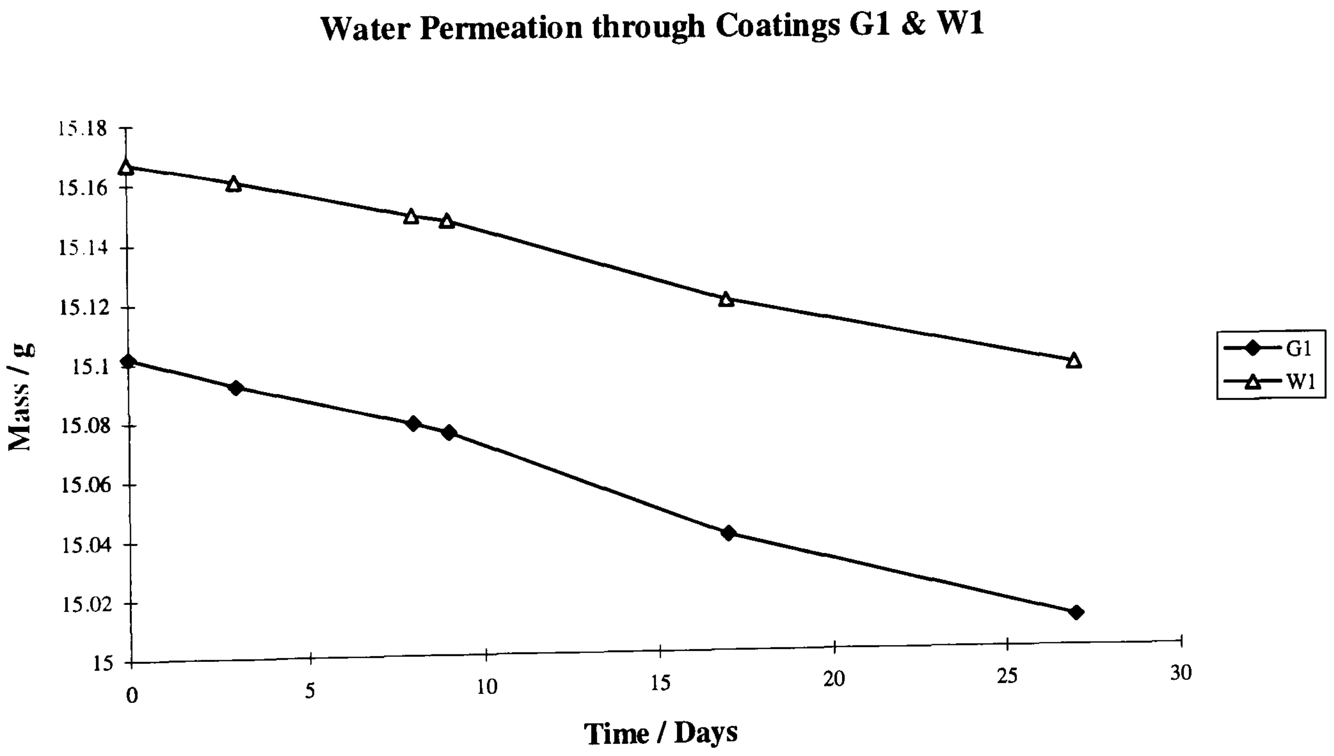

Figure 6.12 Graph showing Mass Loss due to Water Permeation through Coatings G1 and G2

Fitting a straight-line, using a linear regression program to the above points has given the following gradients:

G1:	3.482 mg day^{-1}	2.05 mg day^{-1} cm^{-2}
W1:	2.686 mg day^{-1}	1.58 mg day^{-1} cm^{-2}

This shows that the vapour permeation rate through coating G1 is over 77 % greater than coating W1. This is likely to be due to the pigmentation of coating G1.

6.4.4.2 Coatings D200 and D42

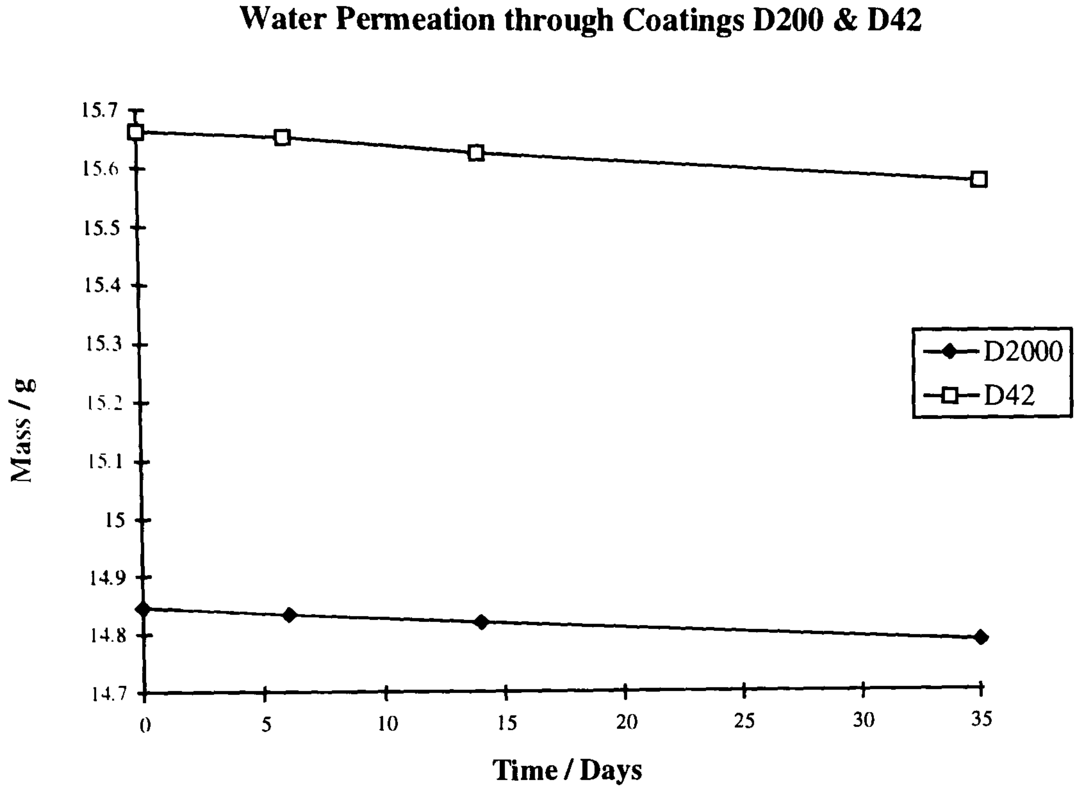

Figure 6.13 Graph showing Mass Loss due to Water Permeation through Blue Coloured Pigmented Coatings D200 and D42.

The change in mass due to water permeation through pigmented coatings D200 and D42 is shown in figure 6.13.

Fitting a straight-line, using a linear regression program to the above points has given the following gradients:

D200:	-1.697 mg day^{-1}	1.04 mg day^{-1} cm^{-2}
D42:	-2.341 mg day^{-1}	1.38 mg day^{-1} cm^{-2}

It can be seen that the rate of water permeation through coating D42 is over 70 % greater than coating D200.

It should be noted that these water permeation rates are relevant for the unstressed coating, which is not being subjected to mechanical force in the way it would do in a filiform corrosion situation. Therefore these vapour permeation results *may* not be relevant to the propagation of filiform corrosion.

6.4.5 Glass Transition Temperature

Coatings G1 and W1:

G1: 76.5 ° Celsius
W1: 77.4 ° Celsius

Coatings D200 and D42

D42: 82.4 ° Celsius
D200: 63.9 ° Celsius

The T_g measurements show that all the coatings at the temperature of filiform corrosion advance (40° Celsius) and of impedance measurements (room temperature) are all below their T_g's and therefore in a relatively rigid non elastic state. The lower the glass transition temperature the more 'rubbery' and flexible will be the coating. Hence Coating D200 will, in principle be less susceptible to brittle failure than coating D42. All the coatings overlying filiform corrosion are subjected to mechanical delamination and uplifting from the substrate as aluminium corrosion products are formed.

6.4.6 Effect of Sealing Score

On both filiform corrosion systems a sample of the coated panels were removed after 8 days at 40° Celsius / 80% R.H. and the score sealed with quick drying epoxy adhesive. The coatings were then immediately returned to the temperature / humidity cabinet. It was found that the sealing of the score on the paint coating did not measurably change the growth rate of filiform corrosion on the coating. This suggests, once again, that the permeation of oxygen / water through the coating to the filiform corrosion head is of great importance in filiform corrosion growth. Therefore, in the case of these powder coatings, it appears that transport of water and oxygen through the coating is of considerably more importance than transport from the cut edge of the coating through the tail.

6.5 Conclusions

6.5.1 Relationship between Coating Breakdown and Filiform Corrosion Rate.

The initial conclusion made from the EIS measurements made on the coatings was the way the coating barrier properties breakdown on the coating over-lying filiform corrosion. The implications of this, providing a route for oxygen and water to reach the filiform corrosion head has been discussed. This breakdown of the coating has been observed by SEM.

The relationship between coating breakdown (porosity increase) and the rate of filiform corrosion shows some interesting relationships. Coating W1 has a greater rate of filiform corrosion advance than coating G1. Coating W1 also shows the degree of porosity of the coating overlying the filiform corrosion filament 2 - 3 orders of magnitude greater than on coating G1. This suggests that the greater the degree of coating breakdown the greater the filiform corrosion rate, probably due to a greater supply of oxygen and water to the active filiform corrosion head.

The situation with the two coatings D42 and D200 is less clear. Whilst there is a clear difference in filiform corrosion growth rate between the two coatings (which is largely attributed to difference in T_g), with coating D42 exhibiting a filiform corrosion rate roughly twice that of coating D200, there is no clear, reproducible difference in coating porosity. As stated previously, a far larger study of the role of T_g in influencing coating breakdown in filiform corrosion situations would be of great interest.

6.5.2 Relationship Between Coating Glass Transition Temperature (T_g) and Filiform Corrosion Growth Rate

Coatings D42 and D200 have different glass transition temperatures. Coating D200 has the lowest T_g and will be therefore less susceptible to brittle failure. The fact that coating D200 also has a lower filiform corrosion growth rate suggests there may be a link between the two, with more flexible 'rubbery' coatings having greater filiform corrosion resistance. The mode of failure of the coating when under stress may relate to the ease of de-adhesion of the coating and the breakdown in the barrier properties of the coating. However the porosity measurements made on the coatings do not show increase coating breakdown on the higher T_g coating D42, in fact the converse is true.

6.5.3 Water Vapour Permeation Experiments

The degree to which water vapour permeation rates on the free, none stressed coating relate to the coating overlying filiform corrosion is questionable, particularly as it has been shown that the physical properties of the coating overlying filiform corrosion filaments are very different than the bulk coating. Coating W1 has a lower rate of vapour permeation than coating G1 (1.58 mg day^{-1} cm^{-2} compared to 2.05 mg day^{-1} cm^{-2}) although coating W1 exhibits a greater filiform corrosion rate. Coating D42 has a higher water vapour permeation rate than coating D200 (1.04 mg day^{-1} cm^{-2} compared to 1.38 mg day^{-1} cm^{-2}) , and a higher filiform corrosion rate. This is the opposite to coatings G1 and W1 and is more expected.

6.5.4 Epilogue

It is clear from the results presented in this chapter that the nature of the coating does have a role in determining the rate of filiform corrosion. However, apparently contradictory results from the experiments detailed here make it hard to determine the *precise* role of the coating. It seems likely that the mechanical properties of the coating, especially when stressed are important. It would be of interest to find if filiform corrosion could be eliminated by employing a coating with low porosity when deformed under mechanical stress and with good adhesion to a substrate.

References

[1] C.F. Sharman, *Nature*, **153**, 621, (1944).

[2] M. Van Loo, D.D. Laiderman, R.R. Bruhn, *Corrosion,* **9**, 277, (1953).

[3] A.T.A. Jenkins, R.D. Armstrong, *Corrosion Science*, Submitted January 1995.

[4] G.D. Steele, *Filiform Corrosion on Architectural Aluminium - A Review*, International Paints Ltd, Internal report.

[5] Filiform Corrosion - its Origins, Prevention and Repair on Coated Aluminium Elements, Forshungsinstitut für Pigmente und lacke E.V. Stuttgart.

[6] W.H. Slabaugh, W. Dejager, S.E. Hoover, L.L. Hutchinson, *J. Paint. Tech.,* **44**, 76, (1972).

[7] R.T. Ruggeri, T.R. Beck, *Corrosion*, **39**, 452 (1983).

[8] G.D. Christian, J.E. O' Reilly, *Instrumental Analysis,* 2nd Edition, Allyn and Bacon.

PAGE

NUMBERING

AS ORIGINAL

Chapter 7

Conclusions and Suggestions for Future Work

7.1 Introduction

This thesis has attempted to examine, in detail, the degradation of organic coatings on aluminium and/or steel substrates, brought about by three principle means; mechanical damage, UV degradation and filiform corrosion. It has been shown that Electrochemical Impedance Spectroscopy (EIS) can give detailed information on coating breakdown, and EIS combined with other surface measurement techniques such as SEM is especially informative.

The principle advantage of EIS over other techniques used to measure coating degradation is that it gives relatively accurate *quantitative* information on the total area of pores and cracks in the coating (conducting channels through the coating) and information, in many cases, on the corrosion of the substrate.

It has also been shown that in many cases substantial delamination of the coating occurs around pores, cracks or defects in the coating. This is highly relevant to the understanding of corrosion under organic coatings as the corroding area of metal can be several orders of magnitude larger than the defect area (porosity).

7.2 Mechanical Damage

The mechanical damage analysis of polyester on steel has shown that the delamination measured by EIS is in close agreement with the delamination measured by observation of corrosion products under the coating. This work suggests that in most cases, the equation

$$W = \frac{C_{dl}}{C_{dlo}}$$

gives a reasonably accurate measure of wetted area (delaminated area + pore area).

Analysis of mechanical damage on coated aluminium has shown that the delaminated area around defects appears to decrease with time. This is thought to be due to the low diffusion rate of Al^{3+} from the substrate under the delaminated coating. In addition the measured oxide film capacitance of the aluminium varies with immersion time in 0.1M sulphuric acid. Both these factors make the estimate of delaminated area on aluminium more difficult than on steel, with results probably underestimating the delaminated area. It was found, that for identical size defects, on initial immersion in electrolyte, the delaminated area on coated aluminium was several times greater than on coated steel. However after five days the situation was reversed, because of the apparent decrease in delamination with immersion time already mentioned.

Modelling the delaminated interface with resistances and capacitances using a transmission line model has shown that when the thickness of the electrolyte under the delaminated coating decreases to a point where the electrolyte in this area has a significant resistance. At this point the measured capacitance of the system is less than the actual capacitance of the complete transmission line.

Measurement of delamination around defects of different sizes on coated aluminium, has shown that the extent of delamination (the delamination radius shortly after adding electrolyte) was six times greater on the 1.5 mm diameter defects than on the 0.6 mm diameter defects. This suggests that larger defects have a greater effect on the adhesion of the surrounding, intact polymer than smaller defects.

7.3 UV Degradation

The investigation into the effect of UV light weathering on steel coated with pigmented and non-pigmented coatings has shown that EIS can give quantitative information on the increase in porosity of a coating with UV exposure. As a coating is exposed to UV light the coating starts to crack due to a sharp increase in brittleness of the top exposed layer of the coating overlying a more plastic, less brittle layer. These cracks provide conducting pathways for electrolyte through the film which are measured as porosity. In addition, delamination under the coating could in some cases be measured as wetted metal area. Scanning Electron Microscopy (SEM) and light reflectance (gloss loss) measurements were made and compared with the EIS measurements. Gloss loss measurements measure the degree of surface break-up of the coating.

Two coatings were studied in detail. Both coatings were polyester powder coatings, one a clear coating (none pigmented) and the other pigmented with titanium dioxide which was white in colour. It was found that both SEM and EIS gave a fairly early indication of coating degradation. However the qualitative and surface nature of SEM means it is of less value than EIS. EIS gave a quantitative measure of coating breakdown at a time before gloss measurements suggested that the coating was starting to fail. It would therefore seem likely that EIS could provide a 'fast answer' test of coating degradation for industry, which currently relies almost solely on gloss measurements as a benchmark for coating reliability.

Differences in the way pigmented and non-pigmented coatings fail when exposed to UV weathering are evident. The non-pigmented, clear coating showed a measurable porosity after a relatively short weathering time (90 hours), and then no significant increase in porosity over the increased weathering times. The pigmented coating however shows a far more gradual increase in porosity with weathering time, with the degree of porosity being more closely related to the time of UV weathering. However weathered pigmented coatings had a porosity several orders of magnitude greater than the clear coatings for similar weathering time. This difference is attributed to the way the coatings interact with UV light. The clear coatings are penetrated to a far greater depth by UV light than the pigmented coatings, causing a less distinct brittleness differential through the coating, which would account for the lower levels of coating failure in these coatings compared with the pigmented coatings. When the pigmented coatings are exposed to UV light, the energy is absorbed and concentrated in the top surface levels of the coating, causing a large brittleness differential through the coating, and as a result more serious coating failure.

7.4 Filiform Corrosion I. Effect of Substrate

Filiform corrosion initiated on two different aluminium substrates labelled Q and A aluminium has shown a reproducible difference in filiform corrosion growth rate, under identical coatings. A aluminium exhibited a greater filiform corrosion growth rate than Q aluminium. This has been attributed to two principle factors:

1. *Surface roughness*

The surface roughness of the two substrates was measured using a laser profilometer. This showed that the Q aluminium was more rough than the A aluminium. Surface roughness has an effect on the adhesion of a coating to the substrate. It is possible that one of the causes of the different filiform corrosion growth rate observed on the two substrates is that the rougher Q aluminium had adhered better to the coating than the Q aluminium. As filiform corrosion advance appears to require mechanical delamination and uplifting of the coating it is possible that the greater surface roughness of the Q aluminium inhibited this delamination and as such gave a lower filiform corrosion growth rate. A aluminium, being smoother had poorer adhesion between the coating and the substrate and as such showed a correspondingly greater filiform corrosion rate.

2. *Corrosion rate*

Bare A aluminium had a corrosion rate approximately 2.5 times greater than the Q aluminium when both substrates were tested in 0.1M sulphuric acid. Since the conditions in the active filiform corrosion head are also acidic, it seems likely that a substrate with a higher bare metal corrosion rate will also exhibit a greater filiform corrosion rate.

Overall, it seems likely that it is a combination of the above two factors that are responsible for the difference in filiform corrosion rate on the two substrates.

7.5 Filiform Corrosion II. Effect of Coating

EIS and SEM measurements have all given clear evidence of coating cracking and an increase in porosity of the coating overlying filiform corrosion filaments compared with the bulk coating.

Two coating systems were examined. The first system compared a clear (none pigmented) coating W1 and a pigmented coating G1. Impedance measurements were made on the coating overlying the filiform corrosion, and porosity calculated from these measurements. Porosity measurements were correlated with impedance / porosity measurements. Coating W1 gave a greater filiform corrosion rate and EIS measurements showed a greater porosity of the coating W1 overlying the filiform corrosion. From these results it would appear that coatings that crack more (have greater porosity overlying filiform corrosion) exhibit a greater filiform corrosion rate, probably due to a greater flux of oxygen and water vapour reaching the active filiform corrosion head.

The second coating system studied was two pigmented coatings, with different glass transition temperatures. Coatings D42 and D200 different filiform corrosion growth rates, with D42 having a filiform corrosion growth rate approximately twice that of coating D200. Coating D42 has a higher glass transition temperature than coating D200. This suggests that coating D42 may be more brittle, or susceptible to brittle failure than D200. It would appear that this difference in glass transition temperature may be responsible for the difference in observed filiform corrosion activity. EIS measurements were made on the two coatings overlying filiform corrosion. These results were inconclusive, and (unexpectedly) did not show definite differences in the porosity of the two coatings.

From these two experiments it is clear that the role of the coating in affecting filiform corrosion is highly complex and it seems likely that a number of different properties of the coating all play a part in determining filiform corrosion rate.

Overall it is clear that it is not purely the nature of the coating or purely the nature of the substrate that effects filiform corrosion growth rate but a synergistic combination of the two.

7.6 Suggestions for Future Study

7.6.1 Mechanical Damage Experiments

One of the most interesting things to come out of the work on the mechanically damaged coatings was the effect that defect size appeared to have on the delaminated area surrounding a defect. Whilst it might appear intuitively obvious that there will be a larger delaminated radius around a large defect than a small defect the reasons for this appear unclear. Measurement of the adhesion of a coating around defects of different sizes would be of interest, and measurement of the stresses put on a coating system when mechanically damaged.

7.6.2 UV Weathering

Future work in this area could centre around a more detailed study into the different ways that pigmented and non-pigmented coatings degrade, and to perform both EIS and ESR experiments on the weathered coatings, in order to determine the degree of correlation between radical formation and coating porosity increase. In addition a study of the role of anti-oxidant additives in the paint system would be of considerable interest, in terms of their effect on general coating porosity and prevention of break down of the weathered coating.

7.6.3 Filiform Corrosion

It has been shown in this thesis that both the surface roughness and the corrosion activity of the substrate metal have an effect on the rate of advance of filiform corrosion. Studies in the literature suggest, as has been observed, that both factors are important. Further work could be done to elucidate the relative importance of these two factors.

It appears clear that in the coatings studied here, oxygen and water are both transported to the filiform corrosion head through the coating. This transport mechanism is probably in addition to the transport of water and oxygen through the tail. It might be possible that preventing the transport of water and oxygen through the coating, *i.e.* by using a thicker more plastic coating could inhibit the growth of filiform corrosion.